Aus dem Labor für Molekulare Psychiatrie der Klinik für
Psychiatrie und Psychotherapie
der Medizinischen Fakultät Charité – Universitätsmedizin Berlin

DISSERTATION

Role of inflammatory cells in cerebral ischemia

zur Erlangung des akademischen Grades
Doctor of Philosophy in Medical Neurosciences
(PhD in Medical Neurosciences)

vorgelegt der Medizinischen Fakultät
Charité – Universitätsmedizin Berlin

von

Katja Blazej

aus Wien

Gutachter/in: 1. Prof. Dr. med. J. Priller

2. Prof. Dr. med. I. Bechmann

3. Prof. Dr. med. M. Schwaninger

Datum der Promotion: 1. Februar 2013

TABLE OF CONTENTS

1 ZUSAMMENFASSUNG

Myeloidzellen spielen eine Schlüsselrolle beim ischämischen Schlaganfall. Einerseits wandern Makrophagen und Neutrophile von der Peripherie in das Gehirnparenchym ein, wobei sie die Blut-Hirn-Schranke passieren, welche durch Perizyten reguliert wird. Andererseits werden im Gehirn residente Mikroglia aktiviert, die wiederum periphere Immunzellen rekrutieren. Ob die derart entstehende Neuroinflammation für das Zentrale Nervensystem (ZNS) schädlich oder protektiv ist, ist derzeit noch unklar. Nach zerebraler Ischämie kommt es darüber hinaus zu einer peripheren Immundepression, die zu Apoptose von Lymphozyten und myeloiden Zellen führt. In der Folge kann es zu Sekundärinfektionen kommen, die klinische Komplikationen und den Tod nach sich ziehen können.

Um die Rolle des angeborenen Immunsystems in neurologischen Krankheiten besser verstehen zu können, generierten wir eine Maus, der das *Ikk2*-Gen spezifisch in Myeloidzellen fehlt. Zu diesem Zweck kreuzten wir eine Maus, welche die Cre-Rekombinase (Cre) unter der Kontrolle des Lysozym M-Promoters (LysM) exprimiert, mit einer anderen Maus, deren beide *Ikk2*-Allele von loxP-Sequenzen flankiert (floxed) sind. Die resultierende LysM-Cre Ikk2$^{fl/fl}$-Maus charakterisierten wir *in vitro* um die zellspezifische Deletion des *Ikk2*-Gens zu prüfen. Im Zuge dessen belegten wir, dass IKK2 auf mRNA- und Proteinebene in kultivierten Mikroglia und Makrophagen vermindert produziert wird. Als Kontrolle dienten Mikroglia und Makrophagen aus Mäusen, die kein Cre tragen, sowie Astrozytenkulturen aus LysM-Cre Ikk2$^{fl/fl}$-Mäusen, die dem Neuroektoderm entstammen. Wir überprüften die Kerntranslokation der NF-κB-Untereinheit p65 in diesen Kulturen, sowie die Sekretion von proinflammatorischen Molekülen wie TNF-α, Stickoxid und IL-6 nach Stimulation mit LPS. Tatsächlich war die NF-κB Signalkaskade in LysM-Cre Ikk2$^{fl/fl}$-Mikroglia gehemmt. Weiters zeigten kultivierte LysM-Cre Ikk2$^{fl/fl}$-Mikroglia erhöhte Mortalität aufgrund der *Ikk2*-Deletion. In Makrophagen hingegen waren Vitalität und Zytokinsekretion unverändert, was einen Übergang zu einem alternativen Phenotyp bedeuten könnte. Darüber hinaus entdeckten wir, dass LysM-Cre Ikk2$^{fl/fl}$-Mäuse teils stark vergrößerte Milzen hatten. Genauere Untersuchungen dokumentierten in diesem Zusammenhang erhöhte Werte von Endzündungsmarkern sowie Neutrophilie in der Milz.

In einem weiteren Ansatz verabreichten wir Wildtyp-Mäusen nach zerebraler Ischämie periphere immunkompetente Zellen. Hierfür transplantierten wir Milzzellen in Mäuse, bei denen kurz davor eine MCAo durchgeführt worden war. In diesem Szenario waren weder Effekte auf die periphere Immundepression noch auf das Infarktvolumen zu beobachten. Ebenfalls nach MCAo untersuchten wir das Schicksal der Perizyten, die an der Blut-Hirn-Schranke sitzen, und möglicherweise Einfluss auf die Einwanderung von Immunzellen ins ZNS haben. Wir detektierten sowohl vermehrte Apoptose als auch erhöhte Proliferation in dieser Zellpopulation.

2 ABSTRACT

Myeloid cells are key effector cells in cerebral ischemia. Peripheral macrophages and neutrophils infiltrate from the periphery into the brain parenchyma thereby passing the blood brain barrier that is regulated by pericytes. Resident microglia get activated and enhance attraction of peripheral immune cells. Whether subsequent neuroinflammation is harmful or neuroprotective is unclear. Post-stroke immunodepression leads to apoptosis of lymphocytes and myelocytes causing secondary infections entailing clinical post-stroke complications and mortality.

To better understand the role of innate immune cells in neurological disorders we generated a mouse lacking *Ikk2* specifically in myeloid cells. To this aim, mice expressing Cre recombinase (Cre) under the control of the Lysozyme M (LysM) promoter were crossed with mice carrying two loxP-flanked (floxed) *Ikk2* alleles. We characterized the resulting LysM-Cre Ikk2$^{fl/fl}$ mouse *in vitro* for cell-specific deletion of the *Ikk2* gene. Thereby we confirmed decreased *Ikk2* mRNA and protein levels in microglia and macrophage cultures in comparison to those of littermates, which do not express Cre, and with astroglial cultures, which derive from the neuroectoderm. Analysis of these cell cultures for nuclear translocation of the NF-κB subunit p65 and the secretion of pro-inflammatory molecules like TNF-α, nitric oxide and IL-6 in response to LPS stimulation implicated inhibition of the NF-κB signaling pathway in LysM-Cre Ikk2$^{fl/fl}$ microglia. Cultured LysM-Cre Ikk2$^{fl/fl}$ microglia showed reduced vitality compared to control cells with a switch to apoptosis due to *Ikk2* disruption. In macrophages viability and cytokine secretion seemed to be unaffected suggesting a switch to an alternative phenotype. *In vivo* characterization of the LysM-Cre Ikk2$^{fl/fl}$ mouse revealed the development of splenomegaly accompanied by enhanced expression of inflammatory markers and neutrophilia.

Furthermore we explored the general feasibility of administration of peripheral immuno-competent cells by transplantation of splenocytes into mice after MCAo, which failed to affect post-stroke immunodepression and infarct volume. Since pericytes/mural cells at the blood brain barrier may modulate infiltration of inflammatory cells into the CNS, we investigated the fate of pericytes after MCAo, detecting both apoptosis and proliferation.

3 INTRODUCTION

3.1 Role of innate immunity in cerebral ischemia

3.1.1 Inflammation in the CNS

Inflammation is one of the first responses of the innate immune system to infection or irritation. The cells which represent innate immunity are neutrophils, macrophages, dendritic cells and natural killer cells (NK). Their function is to identify and eliminate invading pathogens that might lead to infection, to recruit immune cells to the site of injury and to activate the adaptive immune system by antigen presentation. In the central nervous system (CNS), which is essential for survival, immune response is tightly regulated: on one hand, the blood brain barrier (BBB) limits the entry of solutes and ions into the brain [1]. Its structure is supported and organized by pericytes representing the first line of immunologic defense of the brain [2]. They are mural cells covering endothelial cells in capillaries. Pericyte density in the brain is correlated with BBB permeability [3]. However, selective passage of compounds and cell migration into the CNS take place, the latter being controlled by adhesion molecules, chemokines and cytokines and their receptors [4]. On the other hand, astrocytes and microglia play an important role in regulation of an immunosuppressive, homeostatic environment inside the brain. Microglia, the brains resident macrophages, take a resting, protective role. They are evenly distributed throughout the CNS and monitor the parenchyma. Astrocytes suppress T cell activation and induce apoptosis in already activated T cells [5]. Of course, despite this immune-privileged environment, innate as well as adaptive immune responses take place in the CNS. Pattern recognition receptors, such as Toll-like receptors (TLRs), on CNS cells bind either pathogen-associated molecular patterns (PAMPs) or endogenous signals from damaged or stressed tissues, called danger-associated molecular patterns (DAMPs). TLRs are up-regulated during CNS disorders in varying constellations on microglia, astrocytes, oligodendrocytes and neurons. When activated, they trigger the secretion of pro-inflammatory cytokines, which might be neurotoxic. Knocking out the universal TLR cytoplasmic signal transducer Myd88 (myeloid differentiation primary response gene 88) leads to reduced secretion of pro-inflammatory cytokines, fewer numbers of invading neutrophils and less severe brain lesions and clinical outcome following traumatic brain injury [6]. Besides,

cytokines activate phagocytic cells to clear up the site of infection thereby eliminating cytotoxic PAMPs and DAMPs.

3.1.2 Immune response after cerebral ischemia

Ischemic stroke is a pathologic condition resulting from transient or permanent reduction in cerebral blood flow caused by cerebral artery occlusion by an embolus or local thrombosis. Impairment of blood flow restricts the delivery of oxygen and nutrients inducing death and dysfunction of brain cells and neurological deficits reflecting the location and size of the ischemic brain area. Tissue damage results from excitotoxicity, peri-infarct depolarizations, inflammation and apoptosis (Fig 3.1) [7].

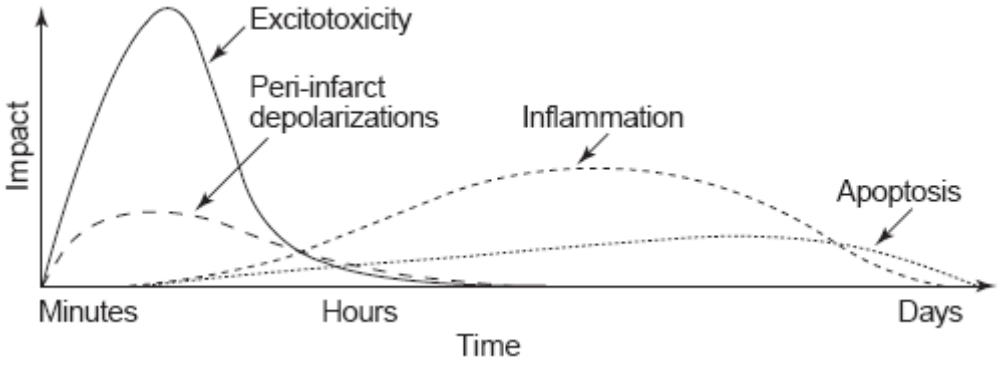

Fig 3. 1 Putative cascade of damaging events in focal cerebral ischemia

Excitotoxic mechanisms damage brain cells very early after stroke. Excitotoxicity triggers peri-infarct depolarization and later inflammation and apoptosis. The x-axis reflects the time scale while the y-axis illustrates the impact of each element of the cascade on final outcome. From Dirnagl et al. 1999, Trends Neurosci [7].

Activation and infiltration of inflammatory cells is a consequence of energy depletion and neuronal cell death. Reperfusion after spontaneous or therapeutic thrombolysis causes generation of reactive oxygen species (ROS) which can stimulate ischemic cells, glia, and neurons to secrete inflammatory cytokines and chemokines. Once activated, microglia remain in an effector state over several months. They accumulate at the lesion site ("gliosis") and in the penumbra and produce a set of pro-inflammatory mediators such as cytokines, chemokines, matrix metallo-proteinases (MMPs), inducible nitric oxide synthase (iNOS), and cyclooxygenase (COX)-2 [8], a consequence of the activation of the transcription factor nuclear factor (NF)-κB [9-12]. These inflammatory molecules entail microglia activation, up-regulation of adhesion molecules on

vascular cells, induction of BBB leakage, and recruitment of peripheral leukocytes, endangering the brain to subsequent brain injury and potentiating neurotoxicity (Fig 3.2) [13].

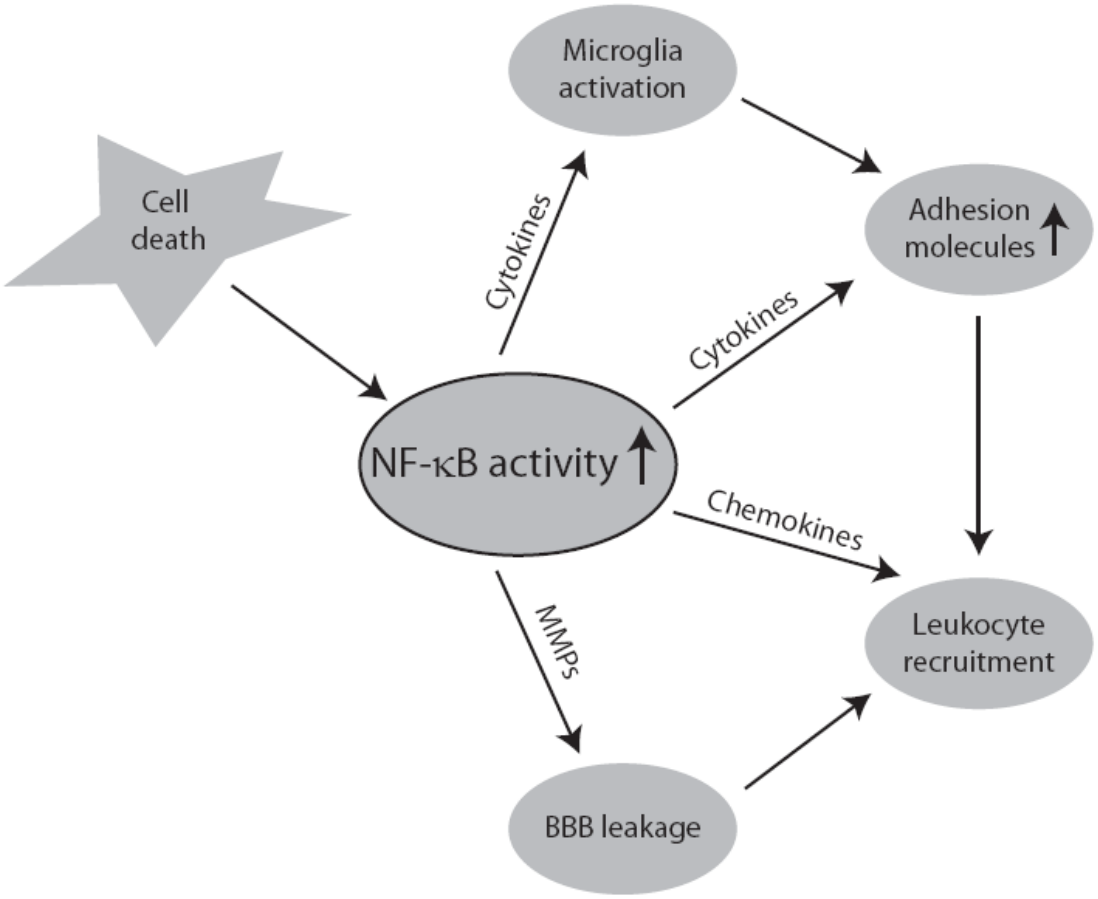

Fig 3. 2 Role of NF-κB in post-ischemic inflammation following brain ischemia

Necrotic cell death after stroke is followed by up-regulation of NF-κB leading to the production of cytokines, chemokines and matrix metalloproteinases (MMPs). These molecules entail microglia activation, up-regulation of adhesion molecules, blood brain barrier (BBB) disruption and successive leukocyte recruitment into the brain parenchyma.

However, microglia also play a neuroprotective role, by producing neurotrophins, growth factors (fibroblast growth factor (FGF), transforming growth factor (TGF) -β1), and neurotransmitters and by cleaning up the brain parenchyma from excitotoxins by phagocytosis. Activated microglia seem to be critical in the clearance of infiltrating neutrophils and potentially neurotoxic substances in the first days after cerebral ischemia. They do so by inducing apoptosis and phagocytic engulfment, important steps in the resolution of inflammation [14]. Whether post-ischemic inflammation is harmful or beneficial to neuroregeneration is an ongoing debate (Fig 3.3).

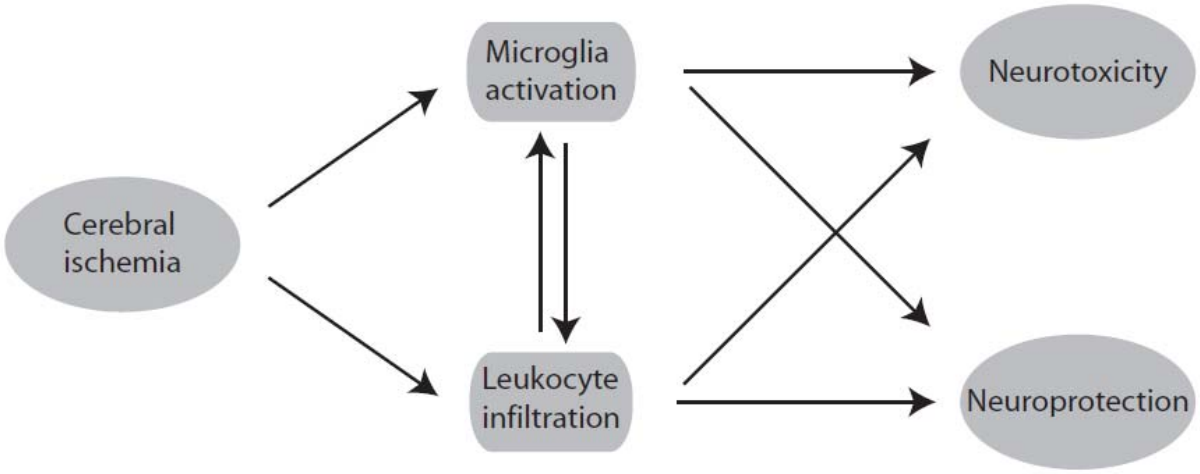

Fig 3. 3 Inflammation following stroke – a double edged sword

Cerebral ischemia triggers activation of microglia and infiltration of leukocytes from the periphery. Once in the brain and activated, these cells carry out several effector functions contributing to both neurotoxic and neuroprotective mechanisms.

3.1.3 Stroke-induced immunosuppression

For the patient, apart from the neurological deficit, stroke outcome is mainly dependent on post-stroke complications. Most frequently, cerebral ischemia entails infections like pneumonia and urinary tract infections causing fever. Aspiration and dysphagia after stroke might be a reason of pneumonia, but is not sufficient alone to cause severe infections, as half of all healthy adults aspirate during sleep without developing pneumonia [15]. Several studies have shown that patients with CNS injury show signs of systemic immunosuppression leading to lymphopenia, T helper cells 1 (T_H1)/T_H2 shift, impaired NK cytotoxicity and monocyte deactivation. In a mouse model of focal cerebral ischemia apoptotic loss of lymphocytes in spleen, thymus and blood was detected already 12 hours after stroke. Decreased secretion of interferon (INF)-γ and tumor necrosis factor (TNF)-α by lymphocytes and monocytes, respectively, after *ex vivo* stimulation revealed cellular dysfunction and adoptive transfer of T and NK cells from healthy mice reduced bacterial burden [16]. An explanation for this phenomenon might be the intention of the CNS to control inflammation and beware the organism from shock or multiple organ failure caused by an overwhelming systemic inflammation [15].

The modulation of the immune system by the CNS takes place via the hypothalamo-pituitary-adrenal (HPA) axis, the sympathetic nervous system (SNS) and the parasympathetic nervous

system (PNS). Recognition of the inflammation by the CNS is triggered by cytokines binding either to receptors at local afferent fibers of the vagal nerve, or to receptors in the CNS after entry from the bloodstream into the brain. Activation of the SNS entails the release of catecholamines (CAs) (i.e. adrenaline, noradrenalin) which - after prolonged exposure - leads to inhibition of T_H1 cells directly and indirectly by suppressing antigen-presenting cells. CAs also repress monocytic production of pro-inflammatory cytokines while enhancing interleukin (IL)-10 secretion. Acetylcholines (ACs), the mediators of the PNS, show similar anti-inflammatory effects on activated macrophages. Gucocorticoids (GCs), released by the HPA axis, suppress production of TNF-α, IL-1β and IL-8, but enhance IL-10 and TGF-β secretion. GCs inhibit differentiation from immature T cells to T_H1 cells and induce apoptosis in both these cell populations. Further, GCs may promote maturation of T_H2 cells and give rise to the development of regulatory, IL-10-producing T cells [15].

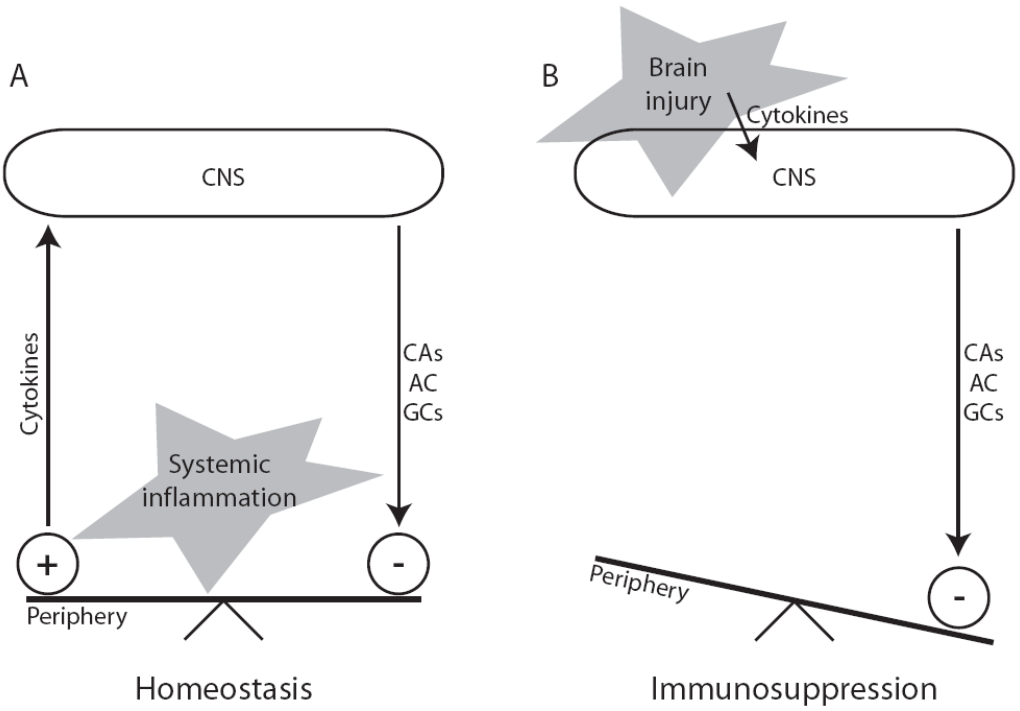

Fig 3. 4 Interactions between the CNS and the peripheral immune system

A. Systemic inflammation is sensed by the central nervous system (CNS) via cytokines. To keep homeostasis catecholamines (CAs), acetylcholine (AC) and glucocorticoids (GCs) are secreted into the periphery leading to anti-inflammatory effects in the periphery.

B. Following brain injury cytokines are released directly inside the brain triggering anti-inflammatory effects in the periphery without systemic inflammation and leading to immunosuppression.

Ideally, pro-inflammatory and anti-inflammatory stimuli are balanced to avoid hyperinflammation and immunosuppression (Fig 3.4A). Systemic anti-inflammatory effects by the CNS are useful to remain homeostasis in case of peripheral infection to avoid septic shock, but it can be detrimental when triggered without systemic inflammation as a consequence of CNS injury (Fig 3.4B) [15].

3.1.4 Experimental stroke – middle cerebral artery occlusion (MCAo)

The most common cause of human stroke is occlusion of the middle cerebral artery (MCA) and thus animal models are mostly designed to target the area supplied by this artery. In general, there are two different approaches to give access to cerebral arteries, even opening the skull to allow direct access to the required cerebral vessels, or to introduce a thread into the extra cranial internal carotid artery (ICA) and advance it until covering the MCA. The latter model, also called "intraluminal suture", avoids surgical injury in the brain and is the most frequently used model in recent stroke analysis (Fig 3.5) [17, 18]. Another advantage is that the filament can either be left in the artery for permanent occlusion or be withdrawn at any time point to allow controlled reperfusion of the ischemic brain area. However, surgery is difficult and susceptible to variance of infarct volumes (20 to 30 %) and post-stroke mortality (10 to 20 %) [19]. Thread thickness and coating seem to be important parameters and have to be adjusted for specific strains or weight categories of animals [20].

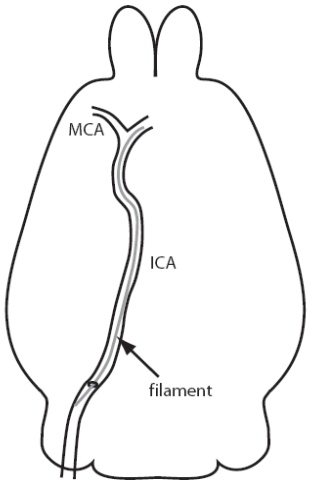

Fig 3. 5 Illustration of intraluminal suture to occlude the middle cerebral artery

The filament is introduced into a small whole cut into the internal carotid artery (ICA) of the mouse and advanced until covering the middle cerebral artery (MCA).

After 60 minutes of MCAo the infarcted area includes parts of the cerebral cortex and the corpus striatum. Since the striatum is more sensitive to ischemia than the cortex, subcortical infarcts without remarkable cortical damage can be produced selectively by shorter occlusion periods down to 30 minutes, excluding the possibility of permanent closure in this context [19].

3.2 NF-κB – a key player of innate immunity

3.2.1 The role of NF-κB in cerebral ischemia

As already mentioned, the major elements of inflammation following cerebral ischemia are activation of resident brain cells, and recruitment and activation of peripheral leukocytes. NF-κB appears to be a key regulator of both these aspects and crucial for regulation of apoptotic cell death. The NF-κB family is a small group of transcription factors consisting of five members in mammals: c-Rel, p65 (RelA), RelB, p105/p50 (NF-κB1) and p100/p52 (NF-κB2). p105 and p100 are large precursor proteins that are post-translationally processed to form the subunits p50 and p52, respectively, which have the ability to bind to the DNA. All NF-κB subunits exhibit a Rel homology domain (RHD) at the N terminus which mediates DNA binding, dimerization and interaction with the inhibitors of κB (IκB) proteins (Fig 3.6). They form numerous homo- and heterodimers which have different roles in gene regulation in response to distinct biological stimuli. c-Rel, p65 and RelB act as transcriptional activators. p50 and p52 do not contain a transcription activation domain hence homodimers formed by these subunits act as repressors. DNA binding occurs at "κB sites" in the DNA strand [21-23].

In unstimulated cells, one of the members of the IκB family binds to homo- or heterodimers of NF-κB in the cytoplasm. Thereby they cover the nuclear localization sequence (NLS) which is located at the C terminus of the RHD. In mammalian cells seven members of the IκB family are known, IκB-α, IκB-β, IκB-γ, IκB-ε, and Bcl-3, as well as NF-κB precursors p105 and p100. The latter two sequester NF-κB dimers in the cytoplasm and thereby block transcriptional regulation. IκBs use a core domain of six to seven ankyrin repeats to bind to the RHD. They are also present in p105 and p100, before their processing to mature p50 and p52 (Fig 3.6). By this auto-inhibitory domain the two precursors and their dimerized partner subunits are trapped in the cytoplasm and function as a pool for mature p50 and p52 subunits and as IκBs.

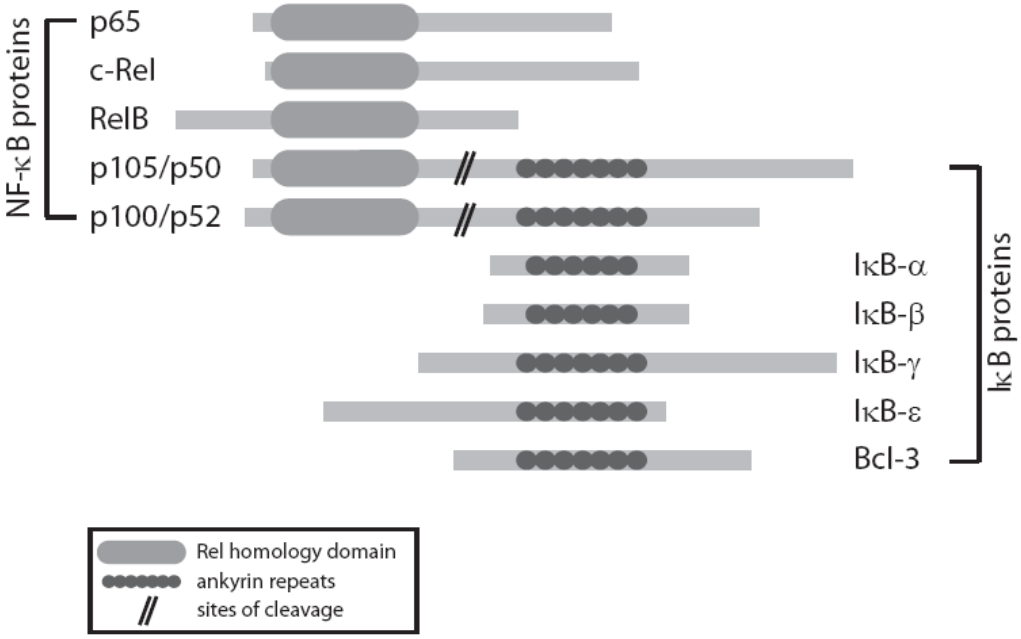

Fig 3. 6 Schematic depiction of NF-κB and IκB proteins

All NF-κB subunits exhibit a Rel homology domain (RHD) at the N terminus which mediates DNA binding, dimerization and interaction with IκB proteins. To bind to the RHD IκBs use a core domain of six to seven ankyrin repeats also present in p105 and p100, before their cleavage to mature p50 and p52.

In human post-mortem tissue p65 was shown to be up-regulated after cerebral ischemia in neurons, astrocytes and macrophages within the infarct area [24-26]. In mice and rats activated p65 was detected in neurons after MCAo, in p50 knockout mice infarcts were significantly smaller after permanent and transient MCAo compared to wild type mice [10, 25, 27]. Coherent, cortical injection of a mutated dominant-negative IκB super-repressor (SR), which lacks serines 32 and 36, and thus cannot be marked for degradation, reduced lesion size after permanent MCAo in rats [28]. Cell specific inhibition of NF-κB by selective neuronal or astrocytic expression of IκB SR, demonstrated a neuroprotective role for NF-κB in neurons, but not in astrocytes after experimental ischemia [29]. Camk2a-Cre $Ikk2^{fl/fl}$ and Nestin-Cre $Ikk2^{fl/fl}$ mice developed smaller infarcts after focal cerebral ischemia, suggesting an NF-κB effect dependent on its activation by IκB kinase (IKK) 2 [30].

3.2.2 The canonical NF-κB pathway and IKK2

Various inflammatory stimuli such as nucleic acids of viruses, several components of bacteria, and pro-inflammatory cytokines bind to members of TNF receptor (TNFR) and TLR-IL-1

receptor superfamilies. These receptors trigger the activation of the IKK complex to phosphorylate IκB proteins at serines 32 and 36. Thereby they get marked for ubiquitination at lysines 21 and 22 and subsequent degradation by the 26S proteasome [31]. As a consequence, NF-κB dimers are free to translocate into the nucleus, to bind the DNA and to switch on gene transcription. Target genes of NF-κB encode cytokines (granulocyte macrophage-colony stimulating factor (GM-CSF), TNF-α, IL-1β, and IL-6), chemokines (IL-8, RANTES, macrophage inflammatory protein (MIP)-1α, and macrophage chemoattractant protein (MCP)-1), adhesion molecules (intercellular adhesion molecule (ICAM)-1, vascular cell adhesion molecule (VCAM)-1, and E- selectin) and enzymes that produce secondary inflammatory messengers (iNOS, COX-2). These molecules are important for migration of inflammatory and phagocytic cells to the area of infection or injury. Since IL-1 and TNF-α are able to activate NF-κB, an autocrine and paracrine amplification loop is created. Additionally, NF-κB regulates gene expression of its own inhibitor IκB-α to provide negative feedback, as well as anti-apoptotic genes like Fas, Fas-ligand, and Bcl-xL [32-34].

The IKK complex contains three subunits: the catalytical subunits IKK1 (IKK-α) and IKK2 (IKK-β) and the regulatory subunit NF-κB essential modulator (NEMO or IKK-γ). IKK1 and IKK2 show 50 % sequence identity both carrying an N terminal kinase domain, a helix-loop-helix (HLH) important for modulating IKK kinase activity, a leucine zipper (LZ) to allow dimerization, and a NEMO-binding domain (NBD) at the C terminus (Fig 3.7).

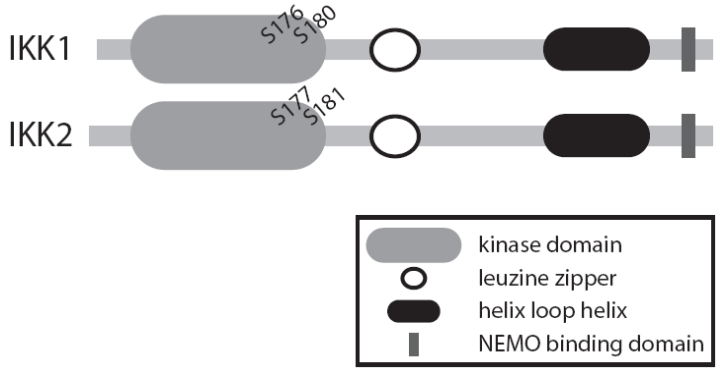

Fig 3. 7 Schematic illustrations of IKK1 and IKK2

IKK1 and IKK2 show 50 % sequence identity both carrying an N terminal kinase domain, a helix-loop-helix important for modulating IKK kinase activity, a leucine zipper to allow dimerization, and a NEMO-binding domain at the C terminus. Phosphorylation sites within the kinase activation loop are serines S176/S180 and S177/S181, respectively.

The similarity between the two catalytic kinase subunits and their presence in the same complex suggested overlapping functions of IKK1 and IKK2. Surprisingly, investigations revealed that they have different substrates and functions. The "canonical" or "classical" NF-κB activation pathway, triggered by pro-inflammatory stimuli, is activated by IKK2 in a NEMO-dependent and IKK1-independent manner. On the other hand, activation of IKK1 is necessary for the "non-canonical" or "alternative" pathway required in lymphoid organ development [32, 35, 36].

In general, in the canonical pathway, binding of ligands (i.e. nucleic acids, bacterial components, cytokines) to their respective receptors guides association of adaptor molecules with cytosolic receptor domains. These adaptor molecules include proteins of the TNF-receptor associated factors (TRAF) family, with TRAF-6 being crucial for IL-1-mediated IKK activation and TRAF-2 or TRAF-5 as essential factors in TNF-α-induced signaling. Several steps of ubiquitination are followed by phosphorylation of serines 177 and 181 in the activation loop of IKK2. Once activated, IKK2 phosphorylates IκB proteins to target them for ubiquitination and degradation and thereby liberating NF-κB dimers to translocate into the nucleus. Further, p65 subunit is phosphorylated itself by IKK2 at serine 536 enhancing its transcriptional activity (Fig 3.8) [37-39].

Many pathways of "canonical" NF-κB activation run together at the level of IKK2, indicating that it might be a potent target for modulation or inhibition to investigate the role of NF-κB-dependent inflammatory response. In mice, deleting *Ikk2* leads to embryonic lethality at E13.5 due to apoptotic liver degeneration as a consequence of defective NF-κB activation [40]. Mice lacking NEMO already die at E12.5 from the same cause, suggesting that IKK1/NEMO-complexes could be able to compensate partially for the loss of IKK2 [41]. In contrast, *Ikk1* knockout mice die at birth and show morphogenetic defects, again underlining the differing roles of IKK1 and IKK2 [33, 42]. The phenotype of mice lacking IKK2 or NEMO is similar to that of p65-deficient mice dying at day E14 to E15 due to massive apoptosis of hepatocytes highlighting the anti-apoptotic role of NF-κB [43, 44]. In this context lethality was rescued by deletion of *Tnf* or *Tnfr1* genes thereby implying an inducing function of TNF-α in this respect [45, 46]. To circumvent embryonic lethality and enable the analysis of *Ikk2* gene function and NF-κB signaling in adult mice, the technique of conditional knockout is used.

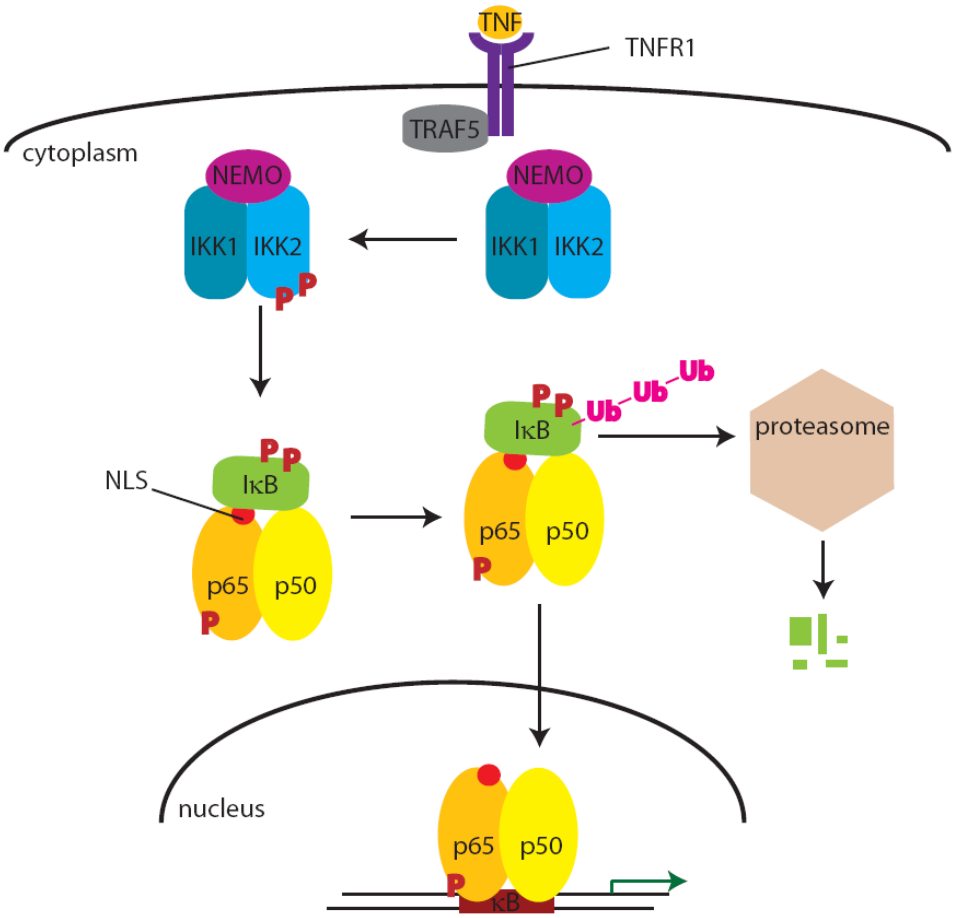

Fig 3. 8 Scheme of the canonical NF-κB pathway by the example of TNF signaling

Tumor necrosis factor (TNF) binds as a ligand to the TNF-receptor 1 (TNFR1). Phosphorylation of the IκB kinase (IKK) complex requires TNF-receptor associated factor (TRAF) 5 interacting with the cytoplasmic domain of the receptor. The thereby activated IKK complex phosphorylates p65 and the inhibitor of κB (IκB) which sequesters the NF-κB dimer, consisting of p50 and p65 subunits, in the cytoplasm covering the nuclear translocation signal (NLS). Consequently, IκB is ubiquitinated and thereafter degraded by the proteasome. NF-κB is freed to translocate into the nucleus, bind to a κB-site, and regulate gene transcription.

3.3 Conditional knockout

Genetic engineering has gained flexibility and importance since the use of site-specific DNA recombinases. Site-specific recombination allows conditional gene modifications and thereby the investigation of tissue- and cell-specific gene effects. As already mentioned, it gives the possibility to study gene knockouts that are embryonic lethal when performed systemically. As a third big advantage a gene of interest can be studied upon induction in a certain developmental stage or from a given time point on [47].

3.3.1 The Cre/loxP system

The Cre/loxP system was first described by Sternberg and Hamilton [48] as a highly efficient site-specific recombination system present in the P1 bacteriophage. The two important components of the system are the loxP site (**l**ocus **o**f crossing (**X**) over **P**1), which is a 34 bp palindromic DNA sequence [49], and the 38 kDa protein called Cre recombinase (Cre for **c**auses **re**combination) promoting recombination [48]. Cre-mediated recombination is independent of loxP orientation thereby enabling both deletion and inversion of a loxP-flanked or "floxed" DNA segment. This P1 recombination system works in yeast and mammalian cells [50, 51] and is therefore routinely used for genetic engineering of embryonic stem (ES) cells and mice.

In a first step loxP sites are introduced into the ES cell genome by homologous recombination. Subsequent transient expression of Cre leads to recombination between two loxP sites. It has to be considered that there is always one loxP site remaining after Cre-driven recombination. The targeting vector can be tested for the functionality of introduced loxP sites in Cre-expressing bacterial strains. The position of those loxP sites has to be chosen carefully to not disturb normal gene expression.

The strategy of conditional knockout implies that the mouse arising from loxP-containing ES cells has to be crossed to a Cre expressing mouse. Cre expressing mice rise from ES cells manipulated by targeted insertion of the Cre gene behind the promoter of an endogenous gene or by targeted transgenesis of a DNA construct consisting of a cell-type-specific promoter and the Cre gene. In the first case it has to be considered that one copy of the endogenous gene is inactivated in the resulting "knock-in" mouse. The expression pattern and the expression level of the used promoter region determines onset, cell type specifity, and efficiency of Cre-mediated genomic rearrangements [47].

3.3.2 The LysM-Cre mouse

The LysM-Cre mouse expresses Cre behind the promoter of the gene encoding Lysozyme M (LysM) [52], a protein which is expressed in the myeloid cell lineage [53, 54]. The targeting vector was constructed to integrate Cre directly behind the translational start codon into the first exon of the endogenous mouse *LysM* gene (Fig 3.9). Consecutive destruction of the *LysM* gene

locus on the Cre-expressing allele is unavoidable in the resulting LysM-Cre$^{+/-}$ knock-in mouse. Thus the consequence of expressing Cre on both alleles inevitably leads to a total knockout of the *LysM* gene in the targeted myeloid cells [55].

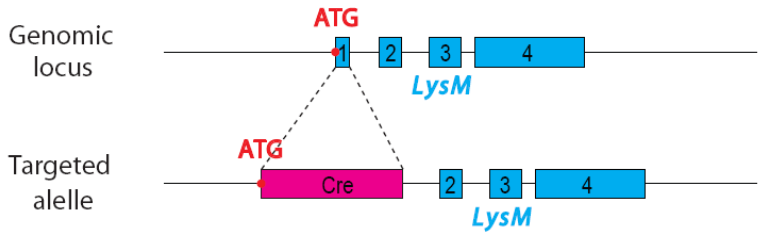

Fig 3. 9 *LysM* locus of the LysM-Cre mouse

The murine *LysM* locus consists of 4 exons. Cre recombinase (Cre) was cloned into the first exon of the endogenous *LysM* gene directly behind the translational start codon (ATG).

Cre-driven recombination efficiency in the LysM-Cre mouse was tested by crossing it to a βT14 mouse homozygous for a loxP-flanked βpol gene [56] and subsequent Southern Blot analysis of different cell populations. Deletion was nearly complete in peritoneal macrophages (95 %) and peritoneal neutrophils (99 %), and hit 16 % of dendritic cells, while B and T cells did not exhibit recombination [52]. LysM-Cre mice were mated with mice carrying a simian diphtheria toxin receptor (DTR) followed by a floxed STOP cassette. Injection of diphtheria toxin on three successive days, lead to ablation of resident liver and skin macrophages, while loss of circulating monocytes was not achieved in this setup. Wound formation and healing was delayed in these mice [57]. Prinz et al. crossed the LysM-Cre mouse to the Ifnar$^{fl/fl}$ mouse carrying floxed alleles of the IFN type I receptor (Ifnar). In these mice clinical outcome of experimental autoimmune encephalomyelitis (EAE) was aggravated, while B- and T-cell-specific ablation of Infar had no effect, hence indicating a unique role for the myeloid-specific receptor [58].

3.3.3 Conditional knockout of Ikk2

To investigate the role of IKK2 in different tissues, Pasparakis et al. generated the Ikk2$^{fl/fl}$ mouse carrying floxed exons 6 and 7 of the *Ikk2* allele (Fig 3.10) [59]. These mice develop normally and express IKK2 regularly.

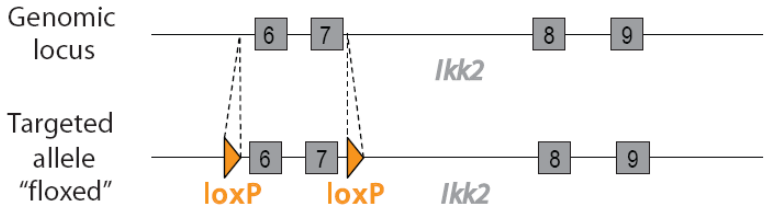

Fig 3. 10 *Ikk2* locus of the Ikk2$^{fl/fl}$ mouse

Exons 6 and 7 of the endogenous *Ikk2* locus are flanked by loxP sites. Recombination at these sites leads to premature stop codons producing *Ikk2* null alleles.

Crossing this mouse to a Cre-deleter mouse [60] produced progeny lacking IKK2 in all cells which, as expected, died *in utero* due to liver degeneration. When crossed to K14-Cre mice, expressing Cre in keratinocytes, IKK2 protein was totally absent in these cells and NF-κB subunit p65 was blocked to translocate into the nucleus after stimulation. K14-Cre Ikk2$^{fl/fl}$ mice developed severe inflammatory skin disease [59]. Further, B cell-specific IKK2 is important for B cell maturation as demonstrated by the absence of mature B cells in the CD19-Cre Ikk2$^{fl/fl}$ mouse [61]. In T cells IKK2 is involved in development of regulatory and memory T cells as shown by a lack of these T cell subpopulations in CD4-Cre Ikk2$^{fl/fl}$ mice [62]. Inducible deletion of *Ikk2* in interferon-responsive cells including myeloid cells (Mx1-Cre Ikk2$^{fl/fl}$ mouse) led to neutrophilia and splenomegaly starting 14 days after Cre-induction [63, 64]. Myeloid-specific deletion of *Ikk2* (LysM-Cre Ikk2$^{fl/fl}$ mouse) entailed elevated plasma levels of IL-1β, released by both macrophages and neutrophils, accompanied with increased mortality due to LPS-induced endotoxic shock [63]. Incubation of bone marrow derived macrophages (BMDM) from LysM-Cre Ikk2$^{fl/fl}$ mice with lipopolysaccharide (LPS) resulted in increased apoptosis [65, 66], confirming a major function of myeloid-specific *Ikk2* in triggering inflammation and tumorigenesis.

To clarify the role of the NF-κB pathway in inflammatory disorders, genetically engineered mice conditionally knocking out *Ikk2* were analyzed in various disease models. Neuroprotective effects of T cell-specific and neuronal *Ikk2* deletion were observed in CD4-Cre Ikk2$^{fl/fl}$ and Nestin-Cre Ikk2$^{fl/fl}$ mice, respectively, regarding disease onset and clinical score of EAE [67, 68]. Conditional knockout of *Ikk2* in neurons (Camk2a-Cre Ikk2$^{fl/fl}$ mouse) led to reduced infarct volume after experimental focal ischemia. Improved stroke outcome is even more pronounced, if *Ikk2* is deleted in both neurons and glial cells (Nestin-Cre Ikk2$^{fl/fl}$ mouse) implicating complex interactions between neurons and glial cells. [30]. Reduced levels of *Ikk2* in microglia and

macrophages (LysM-Cre Ikk2$^{fl/fl}$) mice revealed less damage after kainic acid-induced hippocampal neuronal cell death [69].

In the periphery, deletion of *Ikk2* in intestinal epithelial cells prevented lung inflammation after gut ischemia/reperfusion due to reduced neutrophil migration into the lung and attenuated levels of pulmonary expressed pro-inflammatory cytokines (Villin-Cre Ikk2$^{\Delta/fl}$ mouse). On the other hand, dramatic induction of apoptosis and loss of integrity of the intestinal mucosa was observed in this model hence showing the double edged sword of NF-κB inhibition [70]. In a model of liver infarction ablation of hepatocyte-expressed IKK2 diminished leukocyte infiltration and TNF-α and iNOS expression (Alfp-Cre Ikk2$^{fl/fl}$ mouse) [71]. Tumor incidence in colitis-associated cancer was dramatically decreased in mice lacking *Ikk2* in enterocytes (Villin-Cre Ikk2$^{fl/fl}$ mouse) or myeloid cells (LysM-Cre Ikk2$^{fl/fl}$ mouse) confirming an association between chronic inflammation and cancer, suggesting *Ikk2* to be one critical link [72-74]. While enterocytic IKK2 might prevent induction of apoptosis in tumor cells, myeloid expressed *Ikk2* seems to enhance secretion of tumor-promoting factors [72]. In contrast, loss of *Ikk2* in hepatocytes (Alb-Cre Ikk2$^{fl/fl}$ mouse) increased susceptibility to hepatocellular carcinoma, caused by compensatory proliferation following massive hepatocyte necrosis and apoptosis in these mice [75]. The Mx1-Cre Ikk2$^{fl/fl}$ mouse targets *Ikk2* in Kupffer cells, the resident macrophages of the liver, which are believed to enhance liver cell proliferation. Chemically induced hepatocarcinogenesis in these mice evoked less and smaller tumors, as well as reduced levels of TNF-α and IL-6 mRNA in the liver [75, 76]. Conclusively, all these results underscore the importance of cell-specific gene manipulation to elucidate the specific roles of individual cell populations in disorders.

3.4 Hypothesis

1. Myeloid cells are key effector cells in cerebral ischemia. A major genetic modulator influencing their activation and effector functions is the transcription factor NF-κB. Therefore we addressed the question whether genetic modulation regarding the NF-κB pathway especially in myeloid cells is possible and how this influences their effector functions.

2. Post-stroke immunodepression leads to massive decrease of immune cells including T- and B-lymphocytes as well as myeloid cells and is a major cause of clinical post-stroke complications. Hence we investigated if adoptive transfer of peripheral immunocompetent cells has an effect on stroke-outcome.

3. After cerebral ischemia inflammatory cells infiltrate from the periphery into the brain parenchyma. Thereby they have to pass the BBB that is regulated by pericytes. Thus we explored whether cerebral ischemia affects survival and proliferation of pericytes.

4 MATERIALS AND METHODS

4.1 Materials

4.1.1 Chemicals and reagents

100 bp DNA ladder	New England Biolabs, Frankfurt/Main (Germany)
2-Methylbutane	Roth, Karlsuhe (Germany)
3-(4,5-Dimethylthiazol-2-yl)-2,5-di-phenyltetrazolium bromide (MTT)	Sigma-Aldrich, Taufkirchen (Germany)
Acridine orange	Sigma-Aldrich, Taufkirchen (Germany)
Agar-Agar, bacteriological	Roth, Karlsuhe (Germany)
Agarose NEEO Ultra	Roth, Karlsuhe (Germany)
Bovine serum albumin (BSA), FractionV	Roth, Karlsuhe (Germany)
Ammoniumpersulfate (APS)	Sigma-Aldrich, Taufkirchen (Germany)
AmpliTaq DNA polymerase	Applied Biosystems, Darmstadt (Germany)
β-Mercaptoethanol	Sigma-Aldrich, Taufkirchen (Germany)
Bromophenol blue	New England Biolabs, Frankfurt/Main (Germany)
Chloroform	Sigma-Aldrich, Taufkirchen (Germany)
Complete protease inhibitors, EDTA-free	Roche, Mannheim (Germany)
4′,6-Diamidin-2-phenylindol (DAPI)	Sigma-Aldrich, Taufkirchen (Germany)
Deoxycholate	Sigma-Aldrich, Taufkirchen (Germany)
Diethylpyrocarbonate (DEPC)	Roth, Karlsuhe (Germany)
dNTP Mix, 1.25 mM each	Promega, Mannheim (Germany)
Dithiothreitol (DTT)	Sigma-Aldrich, Taufkirchen (Germany)
Dulbecco´s phosphate buffered saline (PBS)	Sigma-Aldrich, Taufkirchen (Germany)
Ethylenediaminetetraacetic acid (EDTA)	Roth, Karlsuhe (Germany)
Ethanol	J.T. Baker, Deventer (Netherlands)
Ethidium bromide	Sigma-Aldrich, Taufkirchen (Germany)
Fetal calf serum (FCS)	Bichrom AG, Berlin (Germany)
FluorSave Reagent®	Merck, Darmstadt (Germany)

Glacial acetic acid	Merck, Darmstadt (Germany)
Glycerol	Sigma-Aldrich, Taufkirchen (Germany)
Glycine	Roth, Karlsuhe (Germany)
Griess Reagent	Sigma-Aldrich, Taufkirchen (Germany)
Hematoxylin solution acc. to Harris	Roth, Karlsuhe (Germany)
Heparin-Sodium-25000	Ratiopharm, Ulm (Germany)
Histopaque 1038	Sigma-Aldrich, Taufkirchen (Germany)
Hydrochloric acid (HCl), 25 %	Roth, Karlsuhe (Germany)
Isopropanol	Sigma-Aldrich, Taufkirchen (Germany)
Lipopolysaccharide (LPS) from E. coli	Sigma-Aldrich, Taufkirchen (Germany)
Lysing buffer BD Pharm Lyse™	Becton Dickinson, Heidelberg (Germany)
M-MLV Reverse Transcriptase	Promega, Mannheim (Germany)
Methanol	Roth, Karlsuhe (Germany)
Nonidet P-40 (NP-40)	Sigma-Aldrich, Taufkirchen (Germany)
Normal donkey serum (NDS)	Biozol, Eching (Germany)
Normal goat serum (NGS)	Biozol, Eching (Germany)
Paraformaldehyde (PFA)	Roth, Karlsuhe (Germany)
Peptone	Roth, Karlsuhe (Germany)
pHrodo™ BioParticles® Conjugates	Invitrogen, Karlsruhe (Germany)
Ponceau S solution	AppliChem, Darmstadt (Germany)
Primers	Eurofins MWG Operon, Ebersberg (Germany)
Random primers	Promega, Mannheim (Germany)
Roti-Histokitt	Roth, Karlsuhe (Germany)
Roti-Histol	Roth, Karlsuhe (Germany)
Roti-Polyvinylidene fluoride (PVDF)	Roth, Karlsuhe (Germany)
Roti Quant Bradford Reagent	Roth, Karlsuhe (Germany)
Rotiphorese Gel 30	Roth, Karlsuhe (Germany)
RQ1 DNase, RNase free	Promega, Mannheim (Germany)
RQ1 DNase stop solution	Promega, Mannheim (Germany)
Sodium chloride (NaCl)	Roth, Karlsuhe (Germany)
Sodium dodecyl sulfate (SDS) Pellets	Roth, Karlsuhe (Germany)
Sodium hydroxide pellets	Roth, Karlsuhe (Germany)
Sucrose	Sigma-Aldrich, Taufkirchen (Germany)

SuperBlock T20 (TBS) blocking buffer	Pierce, Bonn (Germany)
SYBR Gold	Invitrogen, Karlsruhe (Germany)
Tetramethylethylenediamine (TEMED)	Roth, Karlsuhe (Germany)
Tris hydrochloride (Tris HCl)	Roth, Karlsuhe (Germany)
Triton X-100	Sigma-Aldrich, Taufkirchen (Germany)
Trizma baze	Sigma-Aldrich, Taufkirchen (Germany)
TRIzol reagent	Invitrogen, Karlsruhe (Germany)
Trypan blue 0.5 %	Euroclone, Milan (Italy)
Türk´s solution	Merck, Darmstadt (Germany)
Tween 20	Sigma-Aldrich, Taufkirchen (Germany)
Western Lightning Plus-Electrochemi-luminescence (ECL)	Perkin Elmer, Rodgau (Germany)
Whatman papers	NeoLab, Heidelberg (Germany)
Yeast extract	Roth, Karlsuhe (Germany)
Xantopren Activator NF Optosil	Haereus Kulzer, Hanau (Germany)
Xantopren M Mucosa silicone resin	Haereus Kulzer, Hanau (Germany)

4.1.2 Kits

LightCycler® FastStart DNA Master SYBR Green I Kit	Roche, Mannheim (Germany)
Myelin Removal Beads	Miltenyi Biotec, Bergisch Gladbach, (Germany)
Neural Tissue Dissociation Kit	Miltenyi Biotec, Bergisch Gladbach, (Germany)
REDExtract-N-Amp™ Tissue PCR Kit	Sigma-Aldrich, Taufkirchen (Germany)
Quantikine® Mouse TNF-α Immuno-assay	R&D Systems, Wiesbaden-Nordenstadt (Germany)
Quantikine® Mouse IL-6 Immunoassay	R&D Systems, Wiesbaden-Nordenstadt (Germany)

4.1.3 Anesthetics and analgesia

Isoflurane Forene	Abbott, Baar (Switzerland)
Ketamin 10 %	WDT eG, Garbsen (Germany)

Lidocaine	B. Braun, Melsungen (Germany)
Xylazine Rompun 2 %	Bayer AG, Leverkusen (Germany)

4.1.4 Consumable materials

0.2 µm Filter	GE Healthcare, Solingen (Germany)
0.5-, 1.5-ml Safe-Lock tubes	Eppendorf, Hamburg (Germany)
1-, 5-, 30 ml Syringes	Becton Dickinson, Heidelberg (Germany)
15-, 50-ml Polypropylene tubes	Becton Dickinson, Heidelberg (Germany)
2-, 5-, 10-, 25-ml Serological pipettes	Becton Dickinson, Heidelberg (Germany)
6-, 12-, 24-, 48-, 96- Multiwell plates	Becton Dickinson, Heidelberg (Germany)
75cm²-Tissue culture flasks	Becton Dickinson, Heidelberg (Germany)
Cell scrapers	TPP, Trasadingen (Switzerland)
40-, 100 µm Cell strainer	Becton Dickinson, Heidelberg (Germany)
Combitips plus	Eppendorf, Hamburg (Germany)
Cover slips 24 x 50 mm	Roth, Karlsuhe (Germany)
FACS tubes	Becton Dickinson, Heidelberg (Germany)
GentleMACS C tubes	Miltenyi Biotec, Bergisch Gladbach, (Germany)
Glassware	Schott Duran, Wertheim/Main (Germany)
MACS separation columns (Automacs)	Miltenyi Biotec, Bergisch Gladbach, (Germany)
Microscope cover glasses 12mm	Marienfeld, Lauda Königshofen (Germany)
SuperFrost Ultra plus microscope slides	R. Langenbrinck, Emmendingen (Germany)
MultiGuard barrier tips	Sorenson BioScience, Inc., Utah (US)
PCR softtubes 0.2 ml	Biozym, Hessisch Oldendorf (Germany)
Pipette tips	Sarstedt, Nümbrecht (Germany)
Pistill	Roth, Karlsuhe (Germany)
Sterican hypodermic needles	B. Braun, Melsungen (Germany)

4.1.5 Tools and equipment

Analytical balance LC 620 S	Sartorius, Göttingen (Germany)
AutoMACS	Miltenyi Biotec, Bergisch Gladbach, (Germany)

Bacteria incubator Minitron	Infors AG, Bottmingen (Switzerland)
Balance BL 150	Sartorius, Göttingen (Germany)
Biofuge pico	Heraeus, Hanau (Germany)
BioPhotometer	Eppendorf, Hamburg (Germany)
Bunsen burner Gasprofi 2	W_LD-TEC, Göttingen (Germany)
Cell culture shaker K50 – 500	Incutec, Mössingen (Germany)
Centrifuge 5804 R	Eppendorf, Hamburg (Germany)
Centrifuge Universal 32	Hettich, Oberhausen (Germany)
CO_2 Incubator MCO-18AIC(UV)	Sanyo, München (Germany)
Cryostat HM 560	Microm International GmbH, Walldorf (Germany)
CytoFluor Multi-well Plate Reader 4000	PerSeptive Bioscience, Massachusetts (US)
Western Blot Bio-Rad Mini-Protean 3 Cell	BioRad, München (Germany)
Electrophoresis Sub-Cell GT	BioRad, München (Germany)
Elisa Reader MRX_ctc	Dynex Technologies GmbH, Denkendorf (Ger.)
LSRII flow cytometer	Becton Dickinson, Heidelberg (Germany)
Homeothermic blanket control unit	Harvard Apparatus, March-Hugstetten (Germany)
Cooled CCD camera	Finger Lakes Instrumentation, New York (US)
GentleMACS Dissociator	Miltenyi Biotec, Bergisch Gladbach, (Germany)
Heating cage MediHEAT™	Peco Services Ltd., Brough (UK)
Hemocytometer Neubauer Improved	Laboroptik, Bad Homburg (Germany)
Imager Typhoon 8600	Amersham Biotec, California (US)
Laminar Flow Box Biowizard	Kojair, Nideggen (Germany)
LightCycler 1.5	Roche, Mannheim (Germany)
MACSQuant® Analyzer flow cytometer	Miltenyi Biotec, Bergisch Gladbach, (Germany)
Magnetic stirrer VMS-A	VWR, Darmstadt (Germany)
Microwave MW 736	Clatronic, Kempen (Germany)
Microscope Confocal DM 2500	Leica, Solms (Germany)
Microscope DMRA	Leica, Solms (Germany)
Microscope (inverse) DMI 30000B	Leica, Solms (Germany)
Microscope Zoom 2000	Leica, Solms (Germany)
MRI Pharmascan 70／16	Bruker BioSpin, Ettlingen (Germany)
Multipette	Eppendorf, Hamburg (Germany)

Mastercycler Gradient poly chain reaction (PCR) machine	Eppendorf, Hamburg (Germany)
pH meter pH100	VWR International, Darmstadt (Germany)
Pipette boy Accu-Jet pro	Brand, Wertheim (Germany)
Pipettes	Eppendorf, Hamburg (Germany)
Pipettes	Gilson, Limburg-Offheim (Germany)
Power supply Power Pac 200	BioRad, München (Germany)
Trans-Blot® SD Cell semi-dry blotter	BioRad, München (Germany)
Small Animal Monitoring & Gating System	SA Instruments, New York (US)
Sonicator Sonorex Super 10 P Digital	Bandelin electronic, Berlin (Germany)
Vortex MS2 minishaker	IKA, Staufen (Germany)
Vertical shaker SM-30	Edmund Bühler Lab Tec, Hechingen (Germany)

4.1.6 Primer sequences

Genotyping

Cre8	5′-CCC AGA AAT GCC AGA TTA CG-3′
NLSCre	5′-CCC AAG AAG AAG AGG AAG GTG TCC-3′
LysM-for	5′-CCA TTA TTT CAC AGC AGC ATT GC-3′
LysM-rev	5′-GCT GAC TCC ATA GTA GCC AG-3′
IKK2-rev	5′-GAC TAG CCT GCA AGA GAC AAT ACG-3′
IKK2-for	5′CCT ATT CCA AGA AGG CCA CAC CTC C-3′

Realtime PCR

GAPDH+	5′-AGA TTG TCA GCA ATG CAT CCT GC-3′
GAPDH-	5′-CCT TCT TGA TGT CAT CAT ACT TGG-3′
IKK2-RT-fw	5′-GTT CGA GAA CTG CTG TGG C-3′
IKK2-RT-rev	5′-GAT TAT TGG GGA AGG GTA GCG-3′

4.1.7 Antibodies

Western Blot

Monoclonal mouse-anti-human IKK2 (10AG2) (1:125)	Imgenex, California (US)
Polyclonal goat-anti-mouse Actin (I-19) (1:1000)	Santa Cruz, California (US)
Polyclonal rabbit-anti-mouse IKKα (M-110) (1:3000)	Santa Cruz, California (US)
Polyclonal rabbit-anti-mouse IKKγ (FL-419) (1:3000)	Santa Cruz, California (US)
Donkey-anti-rabbit IgG, HRP-linked (1:1000)	GE Healthcare, Solingen (Germany)
Sheep-anti-mouse IgG, HRP-linked (1:5000)	GE Healthcare, Solingen (Germany)
Donkey anti-goat IgG, HRP-linked (1:10000)	Santa Cruz, California (US)

Immunocytochemistry (ICC)

Monoclonal rat-anti-mouse Cd11b (M1/70.15) Microglia (1:250), Macrophages (1:500)	Serotec, Martinsried (Germany)
Polyclonal rabbit-anti-mouse p65 (C-20) (1:500)	Santa Cruz, California (US)
Monoclonal rat-anti-mouse-GFAP (2.2B10) (1:1000)	Zymed Laboratories, California (US)
Polyclonal rabbit-anti-mouse-GFAP (1:1000)	Zymed Laboratories, California (US)
Polyclonal rabbit-anti-active Caspase 3 (1:1000)	BD, Heidelberg (Germany)
Alexa Fluor 488-donkey-anti-rabbit IgG (1:2000)	Invitrogen, Karlsruhe (Germany)
Alexa Fluor 594-goat-anti-rat IgG (1:2000)	Invitrogen, Karlsruhe (Germany)

Immunohistochemistry (IHC)

Polyclonal rabbit-anti-active Caspase 3 (1:500)	BD, Heidelberg (Germany)
Polyclonal rabbit-anti- Ki67 (1:500)	Abcam, Cambridge (UK)
Monoclonal rat-anti-CD13 (1:200)	Acris, Herford (Germany)
Alexa Fluor 594-donkey-anti-rabbit IgG (1:1000)	Invitrogen, Karlsruhe (Germany)
Alexa Fluor 488-donkey-anti-rat IgG (1:1000)	Invitrogen, Karlsruhe (Germany)

Fluorescence-activated cell sorting (FACS)

FITC-anti-mouse CD45 (30-F11) (1:500)	BioLegend, Uithoorn (Netherlands)
PE/Cy 7-anti-mouse CD8a (53-6.7) (1:400)	BioLegend, Uithoorn (Netherlands)
APC-anti-mouse CD4 (GK1.5) (1:200)	BioLegend, Uithoorn (Netherlands)

PE/Cy 5-anti-mouse CD3ε(145-2C11) (1:400)	BioLegend, Uithoorn (Netherlands)
Pacific Blue-anti-mouse Ly-6G (Gr-1) (1A8) (1:200)	BioLegend, Uithoorn (Netherlands)
PE-anti-mouse CD11b (M1/70) (1:800)	BioLegend, Uithoorn (Netherlands)
FITC-anti-mouse Ly-6C (AL-21)(1:500)	BioLegend, Uithoorn (Netherlands)
PerCP-anti-mouse CD19 (6D5) (1:200)	BioLegend, Uithoorn (Netherlands)
PerCP/Cy 5.5-anti-mouse/human CD44 (IM7) (1:200)	BioLegend, Uithoorn (Netherlands)

4.1.8 Mice

LysM-Cre (C57BL/6 J) and Ikk2$^{fl/fl}$ (C57BL/6 J) breeder pairs were kindly provided by Marco Prinz, Institut für Neuropathologie, Universitätsmedizin Göttingen. Mice were bred, raised and housed until delivery for experiments at the "Forschungseinrichtungen für experimentelle Medizin" (FEM) Charité, Berlin Steglitz.

4.1.9 Buffers and solutions

DEPC-treated water

1 ml/l DEPC in dH_2O, stirred 3 hours, autoclaved

Lysogeny broth (LB) medium

10 g/l peptone, 5 g/l yeast extract, 10 g/l NaCl in dH_2O, pH 7, autoclaved

LB-agar-plates

LB medium, 15 g/l agar, autoclaved, at 60°C poured into Petri dishes

50x Tris-acetate-EDTA (TAE) buffer

242 g/l Tris HCl, 100 ml/l 0.5 M EDTA (pH 8), 57.1 ml/l glacial acetic acid in dH_2O

Tris-buffered saline (TBS)

10 ml/l 1 M Tris HCl (pH 8), 30 ml/l 5M NaCl in dH_2O

Tris-buffered saline-Tween 20 (TBS-t)

0.5 ml/l Tween 20 in TBS

PBS

9.6 g/l PBS powder in dH_2O

10 % Polyacrylamide resolving gel (0.75 mm)

2 ml Rotiphorese Gel 30, 1.2 ml 1.88 M Tris HCl pH 8.8), 1.2 ml 0.5 % SDS, 1.6 ml dH_2O, 5 µl TEMED, 30 µl 10 % APS

Polyacrylamide stacking gel (0.75 mm)

0.33 ml Rotiphorese Gel 30, 0.4 ml 0.625 M Tris HCl (pH 6.8), 0.4 ml 0.5 % SDS, 0.87 ml dH_2O, 2 µl TEMED, 10 µl APS

Radioimmunoprecipitation assay (RIPA) buffer

50 mM Tris (pH 8), 150 mM NaCl, 1 % NP-40, 50.5 % deoxycholate, 0.1 % SDS, 1x Complete protease inhibitors in dH_2O

5x Lämmli´s buffer

28 g/l Glycin, 6 g/l Trizma base, 1 g/l SDS in dH_2O

Western blot transfer buffer

200 ml/l 5x Lämmli´s buffer, 200 ml/l methanol in dH_2O

4% PFA/PBS

40 g/l PFA, 2 pellets of NaOH in PBS solution at 60°C dissolved, cooled down, pH 7.4

FACS buffer

2 % FCS in PBS

MACS buffer

0.5 % BSA, 2 mM EDTA in PBS

4x SDS sample buffer

200 mM Tris HCl (pH 6.8), 8 % SDS, 0.4 % Bromphenol blue, 40 % glycerol, 400 mM DTT

ICC blocking solution

10 % NGS, 0.3 % Triton X-100, 1 % BSA in PBS

ICC 1st antibody solution

3 % NGS, 0.3 % Triton X-100, 0.3 % BSA in PBS

ICC 2nd antibody solution

3 % NGS in PBS

IHC blocking solution

10 % NDS, 0.3 % Triton X-100, 1 % BSA in TBS

IHC 1st antibody solution

3 % NDS, 0.3 % Triton X-100, 0.3 % BSA in TBS

IHC 2nd antibody solution

3 % NDS in TBS

2 % Agarose gel

2 % Agarose in TAE buffer, cooked and poured into electrophoresis mold, cooled until polymerization

4.1.10 Cell culture supplements and media

Dulbecco´s modified Eagle's medium (DMEM) high glucose	Biochrom AG, Berlin (Germany)
Very Low Endotoxin Roswell Park Memorial Institute medium (VLE RPMI) 1640	Biochrom AG, Berlin (Germany)
Penicillin/Streptomycin (Pen/Strep)	Biochrom AG, Berlin (Germany)
FCS	Biochrom AG, Berlin (Germany)
FCS South American CE, Charge 41F7284K, tested for primary microglia cultures	Invitrogen, Karlsruhe (Germany)
Trypsin/EDTA	Biochrom AG, Berlin (Germany)

Microglia culture medium

20 % FCS South American CE, 1 % Pen/Strep in DMEM high glucose

Macrophage culture medium

20 % FCS, 1 % Pen/Strep in VLE RPMI 1640

Cell culture medium (Astrocytes, L929 cells)

20 % FCS, 1 % Pen/Strep in DMEM high glucose

4.1.11 Software

FlowJo	TreeStar Inc., Oregon (US)
GraphPad Prism 5	GraphPad Software, Inc., California (US)
MATLAB	The MathWorks, Ismaning (Germany)
SigmaScan Pro 5	Jandel Scientific, Erkrath (Germany)
TINA 2.0	Raytest GmbH, Straubenhardt (Germany)
Stereo Investigator	MicroBrightField, Magdeburg (Germany)
Paravision 4	Bruker BioSpin, Ettlingen (Germany)
Analyze 5.0	AnalyzeDirect, Inc.; Lenexa (US)
ImageJ	National Institutes of Health, Maryland (US)

4.2 Methods

4.2.1 Genotyping of the conditional knockout of Ikk2

Cloning strategy and primer design

LysM-Cre mouse

LysM-Cre mice were generated by Clausen et al. by inserting the Cre recombinase (Cre), including the nuclear localization signal, from bacteriophage P1 directly behind the ATG start codon of the *LysM* gene. Primers were chosen as described ("NLSCre" and "Cre8") to produce a 512 bp DNA fragment implicating Cre insertion [52]. For detection of the intact *LysM* gene "LysM-for" positioned in the 3´UTR (untranslated region) and "LysM-rev" located in the first exon of the *LysM* locus were designed, synthesizing a 436 bp PCR fragment. Genotyping was performed by multiplex PCR including all four primers.

$Ikk2^{fl/fl}$ mouse

The cloning strategy was described by Pasparakis et al. [59]. In brief, exons 6 and 7 of the murine *Ikk2* gene were placed between a loxP-flanked PGKneo cassette and a third loxP site. After selection for homologous recombinant clones, the PGKneo cassette was excised by transient expression of Cre recombinase, leaving the floxed exons of *Ikk2*. For genotyping primers "IKK2-for" and "IKK2-rev" were placed within intron 5, flanking the first loxP site and producing a 346 bp-fragment of the loxP-flanked sequence, and a 244 bp-fragment of the wild type gene. Deletion of *Ikk2* exons 6 and 7 leads to premature stop codons producing *Ikk2* null alleles.

DNA extraction from mouse tail cuts

DNA extraction was performed using the REDExtract-N-Amp™ Tissue PCR Kit according to the manufacturer's protocol.

PCR conditions

PCR reactions were carried out with a Mastercycler Gradient under the following conditions:

Detection of *LysM* and *Cre*

3 minutes at 94°C
30 cycles: 30 seconds at 94°C - 30 seconds at 58°C - 1 minute at 72°C
10 minutes at 72°C

Detection of *Ikk2*

3 minutes at 94°C
30 cycles: 30 seconds at 94°C - 30 seconds at 64°C - 40 seconds at 72°C
10 minutes at 72°C

Agarose gel electrophoresis

DNA fragments were separated on a 2 % agarose gel inside an electrophoresis chamber filled with 1x TAE buffer at 100 V. Gels were stained shaking in a bath of SYBR Gold (1:10000) in TAE buffer for 30 minutes. DNA was visualized using a Typhoon scanner.

4.2.2 Primary microglia and astrocyte cultures

Preparation of L929-conditioned medium

L929 mouse fibroblasts conditioned media was described to contain macrophage colony stimulating factor (M-CSF) [77], which enhances proliferation and survival of microglia, macrophages and granulocytes. To increase cell numbers, microglial primary cells and peritoneal macrophages were supplied with fresh culture medium containing 33 % of L929-conditioned medium when indicated.

L929 cells were cultured in cell culture medium at 37°C, 0.5 % CO_2 in 75 cm²-flasks until confluency. Medium was exchanged for 30 ml of microglia culture medium per flask and incubated for conditioning. After 3 to 4 days the medium was harvested, filtered with a 0.2 µm filter and aliquoted for freezing at -20°C. L929 cells were washed with PBS, trypsinized for 5 minutes at 37°C and split 1:10 into new 75 cm²-flasks to let them grow again until confluency. After 15 passages cells were eliminated. Remaining L929 medium already thawed had to be discarded.

Preparation of astrocyte/microglia co-cultures

New born mice were decapitated at days 1 to 3 after birth. Brains were isolated and meninges were removed carefully under a Zoom 2000 microscope. Mouse heads and isolated brains were stored in ice-cold PBS during the whole preparation procedure. Afterwards PBS was aspirated, and each mouse brain was covered with 1 ml of microglia culture medium and shredded slowly with a 5 ml-pipette, and subsequent with a pasteur glass pipette (previously narrowed by scorching). Mashed brains were transferred to 75 cm²-cell culture flasks - one brain per flask -, supplied with 10 ml of microglia culture medium and incubated at 37°C/0.5 % CO_2. After two days, a few astrocyte islands had adhered to the bottom of the flask. They were washed twice with PBS to remove cell debris and fed with 10 ml of fresh medium. After 9 to 12 days *in vitro*, when the astrocyte layer was confluent, medium was exchanged for 10 ml fresh microglia culture medium and 5 ml L929-conditioned medium, to enhance growth of microglia.

Harvest of microglia

Within 3 days after L929-conditioning, microglia were grown on top of the astrocyte layer and ready to be shaken off on a cell culture shaker inside the CO_2-Incubator for 30 to 60 minutes at 200 rpm. The medium containing microglial cells was collected, pooled in 50 ml-polypropylene tubes and centrifuged for 10 minutes at 300 g and 4°C, to concentrate the cells. They were kept on ice while resuspending the cell pellet in microglia culture medium. Cells were counted with a hemocytometer and plated immediately into well-plates. After 30 minutes, when microglia had already adhered to the bottom of the plate, medium was exchanged to remove non-microglial cells and thereby increase culture purity. Purity was confirmed by immunocytochemistry using antibodies against CD11b as a microglia marker and GFAP as a marker for astrocytes. Purity of microglia cultures was 90 %. After microglia shake-of, astrocytes were again supplied with a mix of L929-conditioned and normal microglia culture medium, as described, to grow up more microglia. Shake-off of microglia was performed three times per flask every 3 to 4 days.

Since viability of microglia differed in cells of different genotypes, cell vitality was tested by MTT assay after experiments, to be able to relate the measured values.

Harvest of astrocytes

After the last microglia shake-off, astrocytes were washed with PBS and trypsinized for 5 minutes at 37°C. Detached cells were harvested and washed once by adding 10 ml of cell culture

medium followed by centrifugation at 300 g and 4°C for 10 minutes. Cells were counted with a hemocytometer and seeded into well-plates. Purity of astrocyte cultures, confirmed by immunocytochemistry using antibodies against GFAP as marker for astrocytes and CD11b as microglia marker, was 80%.

4.2.3 Peritoneal macrophage lavage

8 to 12 weeks old mice were anesthetized shortly with isoflurane and killed by cervical dislocation. Subsequently, 5 ml of ice-cold macrophage culture medium were injected into the peritoneum. After 5 minutes of massage, the peritoneum was opened and the medium was recollected using a 2 ml-pipette. The cell solution was diluted 1:1 with sterile dH_2O to lyse erythrocytes for 5 seconds. The lysis reaction was stopped by addition of 30 ml PBS containing 2 % BSA. Cells were centrifuged at 300 g and 4°C for 10 minutes and resuspended in macrophage culture medium to seed them into well-plates. After 2 hours, when macrophages had adhered to the plate bottom, medium was changed to increase culture purity. By immunocytochemistry using an antibody against CD11b as a macrophage marker and counterstaining with DAPI purity was proven to be 97 %.

Since cell solutions gained from the peritoneum contained other cells than macrophages (e.g. lymphocytes), it was not possible to count the macrophages before seeding. Hence, cells were quantified after experiments by MTT assay.

4.2.4 Determination of IKK2 protein levels

Cell culture

Microglia and macrophages were obtained and seeded into well-plates as described in 4.2.2 and 4.2.3. Microglial cells from 3 to 4 75 cm²-cell culture flasks, and whole macrophages amounts derived from one mouse, respectively, were split into 4 wells of a 6-well-plate. After 30 minutes or 2 hours, respectively, medium was changed for 2 ml of fresh culture medium and 1 ml of L929-conditioned medium. After 2 additional days of proliferation at 37°C/0.5 % CO_2, cells were harvested and pooled from all 4 wells, respectively. Astrocytes were grown as described and one confluent 75 cm²-cell culture flask was used after shaking off the microglia fraction.

Cell harvest and sample preparation

Cells were harvested in ice-cold PBS using a cell scraper and collected in a 15 ml-polypropylene tube. After centrifugation at 300 g and 4°C for 10 minutes, PBS was aspirated and cells were lysed with RIPA-buffer for 10 minutes on ice. Lysates were centrifuged sharply at 22000 g and 4°C for 5 minutes and supernatants containing the soluble protein fraction were transferred into a fresh 1.5 ml-tube. Protein concentration was measured by Bradford protein assay. 2 µl of protein sample or standards (containing 5 to 40 µg/ml BSA) were mixed with 398µl PBS and 100µl of 5x Roti Quant Bradford Reagent. After 10 minutes of incubation at room temperature absorption was measured at 595 nm. After determination of protein concentration, samples were mixed with 4x SDS sample buffer, heated up for 5 minutes at 95°C and stored at -20°C.

SDS-polyacrylamide gel electrophoresis (PAGE) and Western blot

Protein lysates were loaded in triplets onto an SDS-polyacrylamide gel (20µg per slot) inside a vertical electrophoresis chamber filled with 1x Lämmli´s buffer. Proteins were concentrated for 10 minutes at 80 V in the stacking gel and then separated in a 10 % polyacrylamide resolving gel for 90 minutes at 120 V. Separated proteins were then blotted for 1 hour at 15 V onto a Roti-PVDF membrane using Western blot transfer buffer and a Trans-Blot® SD Cell semi-dry blotter. Successful protein transfer was proven by incubating the membrane for 5 minutes in Ponceau S solution. The membranes was washed with dH_2O, blocked with SuperBlock T20 (TBS) blocking buffer for 1 hour at room temperature, and then incubated with the first antibody diluted in SuperBlock T20 (TBS) blocking buffer over night and shaking at 4°C. After 24 hours the membrane was washed three times for 10 minutes in TBS-t and incubated with a secondary horse radish peroxidase (HRP)-conjugated antibody in SuperBlock T20 (TBS) blocking buffer for 2 hours and shaking at room temperature. The membrane was washed three times, and immunoreactive bands were visualized with a cooled CCD camera after one minute of incubation with Western Lightning Plus-ECL.

Standard curves and quantification

Before quantification, standard curves for IKK1, IKK2, NEMO, and actin antibodies were generated by serially diluting a protein lysate from 40 to 5 µg. The linear area was determined within 5 and 20 µg of protein (Fig 4.1). Consequently, 20 µg of protein were used for Western Blot analysis of the IKK subunits. Quantification of protein expression was performed by density plot analysis using the software TINA 2.0.

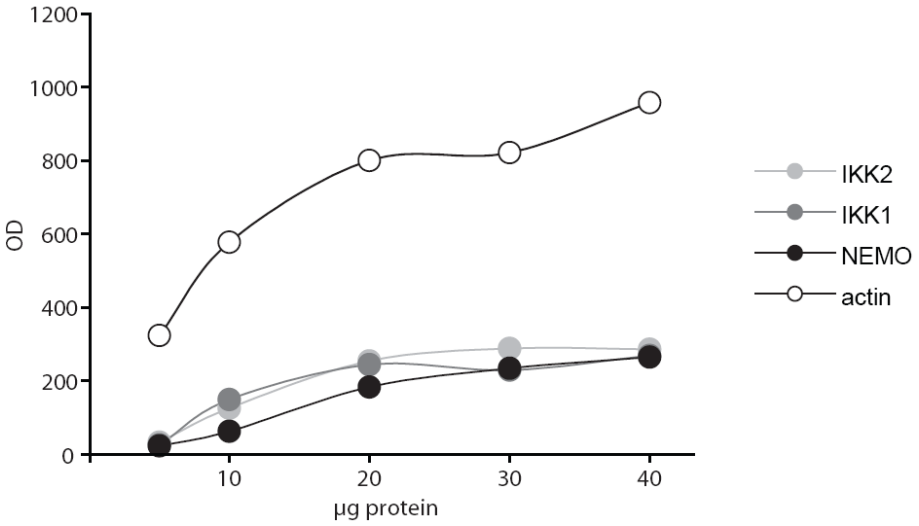

Fig 4. 1 Standard curves for protein quantification

Protein lysates serially diluted from 40 to 5 µg were analyzed by Western Blot. All four primary antibodies to be used in the study (IKK1, IKK2, NEMO and actin) were tested and immunoreactive bands were quantified. The linear area was determined between 5 and 20 µg of protein. OD, optical density

4.2.5 Measurement of Ikk2 mRNA expression

Cell culture

Microglia and macrophages were seeded into 6-well-plates as described in 4.2.2 and 4.2.3. After 30 minutes or 2 hours, respectively, medium was exchanged for 2 ml of fresh culture medium and 1 ml of L929-conditioned medium and cells were incubated to proliferate for 2 additional days at 37°C/0.5 % CO_2. Astrocytes were washed with PBS and trypsinized, seeded into 6-well plates (200000 per well) and grown in culture for 2 days.

After incubation, the medium was aspirated and cells were supplied with 500 µl TRIzol reagent per well and incubated for 5 minutes at room temperature to ensure complete dissociation of nucleoprotein complexes. Samples were resuspended by pipetting, transferred to a 1.5 ml-tube and then stored at -80°C.

RNA purification

For RNA purification TRIzol samples were thawed on ice and 100 µl Chloroform were added. Samples were shaken over-head for 15 seconds and incubated for 10 minutes at room temperature. After centrifugation at 12000 g and 4°C for 15 minutes the upper aqueous phase

containing the RNA fraction was harvested carefully and transferred to a fresh tube. 250 µl of isopropyl alcohol were added for RNA precipitation. Tubes were shaken over-head for 15 seconds, incubated for 10 minutes at room temperature and centrifuged at 12000 g and 4°C for 15 minutes. Supernatants were discarded and RNA pellets were washed with 1 ml of 75 % ethanol in DEPC-treated dH_2O. Samples were centrifuged at 12000 g and 4°C for 5 minutes, ethanol was decanted carefully and pellets were left to dry for 5 to 10 minutes at room temperature. RNA was dissolved in 30 µl of DEPC-treated dH_2O by shaking at 55 °C for 20 to 30 minutes and repeated pipetting in between. RNA concentration and purity was measured with a BioPhotometer (absorption at 260 and 280 nm). If not used immediately RNA was stored at -80°C.

DNA digestion and reverse transcription

2 µg of RNA were digested with 2 units of RQ1 DNase in an end volume of 20 µl DNase reaction buffer for 30 minutes at 37°C. Reaction was stopped by adding 2 µl RQ1 DNase stop solution and heating up the samples to 65°C for 10 minutes. 2 µl of DNA-digested RNA were stored as negative control to check for genomic DNA (gDNA) contamination. The remaining 20 µl of RNA were supplied with 4 µl of 25 mM Random Primers, heated up for 10 minutes at 70°C to denature RNA secondary structures and placed on ice immediately for ideal primer annealing. In the next step a mix of dNTPs (0.5 mM each) and 10 units M-MLV Reverse Transcriptase in M-MLV reaction buffer was added to a total volume of 40 µl. Reverse transcription was performed by the following incubation steps:

10 minutes	21°C
50 minutes	37°C
15 minutes	70°C

Transcribed samples were tested for successful cDNA synthesis and earlier stored DNA-digested RNA samples for absence of gDNA contamination. To this end PCR was performed on a Mastercycler Gradient to amplify a 348 bp DNA band of the glyceraldehyde 3-phosphate dehydrogenase (Gapdh) housekeeping gene using primers “GAPDH+” and “GAPDH-“. Therefore 2 µl cDNA or RNA were mixed with 0.2 mM dNTPs each, 1.5 mM $MgCl_2$, 0.5µM of each primer and 1.25 units AmpliTaq DNA polymerase in a total volume of 50 µl reaction buffer. The reaction was performed under the following cycling conditions:

2 minutes at 94°C
30 cycles: 30 seconds at 94°C - 30 seconds at 63°C – 30 seconds at 72°C
5 minutes at 72°C

Successfully generated cDNA leads to creation of a Gapdh PCR product. Untranscribed control samples - free from gDNA contamination – do just contain RNA which cannot be recognized for transcription by the DNA-dependent Taq-polymerase. Thus a PCR product in the control samples would prove the presence of gDNA contamination. To test this, samples were separated by agarose gel electrophoresis as described in 4.2.1. cDNA sample free from gDNA were used for quantitative analysis by Realtime PCR.

Quantitative real-time PCR (qPCR)

qPCR was performed by LightCycler® FastStart DNA Master SYBR Green I Kit according to the manufacturer's protocol on a LightCycler 1.5.

SYBR Green I is a cyanine dye that binds preferentially to double-stranded DNA. The resulting DNA-SYBR Green I-complex emits green light (λ_{max} = 522 nm). Thus the amount of double-stranded DNA generated during PCR is proportional to the increase of fluorescent signal emitted when SYBR Green I intercalates to the DNA double helix. Fluorescence was measured at the end of the elongation step of every cycle.

Melting curve analysis was performed by continuously heating up the sample to 95°C. DNA duplexes dissociate during heating and SYBR Green I fluorescence decreases. The first derivation of the melting curve shows a peak for each PCR product generated in the reaction. Fluorescence can just be representative for the amount of a transcribed gene, if only one specific PCR product is amplified. If this was the case, subsequent gel electrophoresis of the samples proved the amplification of the desired PCR product.

Samples were analyzed for their amount of the housekeeping gene *Gapdh* cDNA as a reference. The outcome parameter was the Crossing point (CP) describing the cycle revealing a statistically significant fluorescence signal generated by the sample above background. Efficiencies of both

PCR panels were determined by titration. For relative quantification the expression of *Ikk2* was related to the expression of *Gapdh*. The ratio was calculated as follows:

$$\text{Ratio } Ikk2 : Gapdh = \text{Efficiency}_{Ikk2}^{-CP} : \text{Efficiency}_{Gapdh}^{-CP}$$

Ratio values were expressed in % and related to the LysM-$Cre^{-/-}$ $Ikk2^{fl/fl}$ wild type control (100 %).

qPCR conditions:

Gapdh:
With primers "GAPDH+" and "GAPDH–" a 348 bp fragment was amplified under the following conditions:

10 minutes at 95°C
50 cycles: 15 seconds at 95°C - 10 seconds at 61°C - 12 seconds at 72°C
Fluorescence was measured at 87°C.

Ikk2:
With primers "IKK2-RT-fw" and "IKK2-RT-rev" a 463 bp fragment was amplified under the following conditions:

10 minutes at 95°C
50 cycles: 10 seconds at 95°C - 5 seconds at 68°C - 16 seconds at 72°C
Fluorescence was measured at 87°C.

4.2.6 Nuclear translocation of the NF-κB subunit p65

Cell culture

Microglia

200000 cells per well were seeded onto glass disks of 12mm diameter inside of 24-well-plates. After one day of culture, medium was aspirated and fresh medium with and without 1µg/ml LPS (triplicates), respectively, was added for 30 minutes of stimulation at 37°C/0.5 % CO_2. After

stimulation, cells were washed once with PBS, fixed with 4% PFA/PBS for 10 minutes and washed twice with PBS. Fixed cells were stored at 4°C or stained immediately.

Astrocytes

50000 cells per well were seeded onto glass disks of 12mm diameter inside of 24-well-plates. Cells were kept in culture for additional 2 days to proliferate. Medium was removed and fresh medium with and without 1 µg/ml LPS (triplicates), respectively, was added for 30 minutes of stimulation at 37°C/0.5 % CO_2. After stimulation, cells were washed once with PBS, fixed with 4% PFA/PBS for 10 minutes and washed twice with PBS. Fixed cells were stored at 4°C or stained immediately.

Immunocytochemistry

Cells were blocked for 1 hour in ICC blocking solution. Incubation with the primary antibodies (Tab 4.1) was performed in ICC 1st antibody solution over night and shaking at 4°C. After washing three times with PBS for 10 minutes, fluorochrome-coupled secondary antibodies (Tab 4.1) were added in ICC 2nd antibody solution for 2 hours at room temperature. Cells were washed three times with PBS and counterstained with DAPI diluted 1:10000 in PBS for 30 minutes. After additional three wash steps, glass plates were mounted with FlourSave™ Reagent and stored at 4°C for microscopy.

Staining	Primary antibodies	Secondary antibodies
Microglia	rabbit-anti-mouse p65 rat-anti-mouse CD11b	Alexa 488-conjugated donkey-anti rabbit Alexa 594-conjugated goat-anti-rat
Astrocytes	rabbit-anti-mouse p65 rat-anti-mouse GFAP	Alexa 488-conjugated donkey-anti rabbit Alexa 594-conjugated goat-anti-rat

Tab 4. 1 Combination of antibodies for immunocytochemistry

Quantification of p65 in microglia

Using a confocal DM 2500 microscope pictures of 400-fold magnification were taken of at least 500 cells per genotype and condition. Ratios of co-localizing p65 with CD11b as a microglial

surface marker or DAPI as a nucleic marker were measured and calculated by Francisco Fernández-Klett using the software MATLAB.

4.2.7 Secretion of inflammatory molecules

Cell culture

Macrophages

First, a time and concentration curve was established to test for the best condition of LPS stimulation for TNF-α secretion. Therefore, macrophages harvested from one mouse were split into 24 wells of a 48-well-plate. Next day, different concentrations of LPS (from 0.1 to 10 µg/ml) were added in fresh culture medium and supernatants were harvested at 1, 2, 3 or 6 hours, respectively after stimulation. TNF-α levels were examined by Immunoassay as described below. For experiments examining TNF-α and IL-6 levels stimulation with 10µg/ml LPS for 6 hours was chosen. The stimulation paradigm for NO release had been former established in the lab with 0.1 µg/ml LPS for 24 hours.

For one experiment, macrophages obtained from one mouse were split into 6 wells of a 24-well-plate. Next day the medium was removed and wells were supplied with either 500 µl fresh medium (unstimulated control) or medium containing LPS as indicated above, respectively. Experiments were carried out in triplicates. Cells were stimulated for the indicated time, respectively, at 37°C/0.5 % CO_2. After stimulation, 300 µl of the supernatant were collected and stored at -80°C for immunoassays or Griess reaction. In the end, cell vitality was determined by MTT assay (described below).

Microglia

Stimulation paradigms for microglia had been former established in the lab with 0.1 µg/ml LPS for 3 hours (TNF-α and IL-6) or 24 hours (NO). 100000 microglia per well were seeded into 96-well-plates. After one day in culture, medium was removed and 100 µl of fresh medium with or without 0.1 µg/ml LPS, respectively, was added for the indicated time, respectively, at 37°C/0.5% CO_2. Experiments were carried out in triplicates. Supernatants were harvested and stored at -80°C for immunoassays or Griess reaction and cell vitality was analyzed by MTT assay (described below).

TNF-α and IL-6 levels

TNF-α and IL-6 levels were measured by Quantikine® Mouse TNF-α Immunoassay and Quantikine® Mouse IL-6 Immunoassay, respectively, according to the manufacturer's protocol.

Nitric oxide (NO)

By Griess reaction, nitrite - one of the stable breakdown products of NO - was measured in cell culture supernatants. Dilutions of nitrite were prepared within a range of 0.3 to 80 µM to create a standard curve. 50 µl of supernatant or standards were pipetted into a 96-well-plate. 100 µl of Griess Reagent (0.2 % naphthylenediamine dihydrochloride, 2 % sulphanilamide in 5% phosphoric acid) were added to the samples, and incubated for 10 minutes at room temperature to develop a pink color. Absorption was measured by an MRX_ctc Elisa Reader at 550 nm.

MTT assay

Cell viability was measured by MTT assay, which is based on reduction of yellow MTT to purple formazan in mitochondria of living cells [78].

MTT was added directly to the wells containing cells and normal culture medium to a final concentration of 0.5 mg/ml. After incubation of 90 minutes at 37°C/0.5 % CO_2, 10 % SDS in 0.01 M HCl was added in a ratio of 1:1, to lyse cells and formazan crystals. After 24 hours, absorption was measured by an MRX_ctc Elisa Reader at 550 nm to serve as a representative value of cell vitality.

4.2.8 Mortality of microglia

Cell culture

32000 and 200000 microglia per well were seeded into 96-well- and 24-well-plates, respectively - 3 plates, each for three different time points (0 hours, 24 hours, 48 hours). 30 minutes later, medium was removed and fresh culture medium was added. In 96-well-plates numbers of vital cells were determined either immediately (time point 0 hours as a reference value) or after cultivation of 24 and 48 hours, respectively, by MTT assay (described in 4.2.7).

Cleaved caspase 3 (CC3)-staining and quantification

For immunofluorescent CC3-staining microglia were fixed in 24-well-plates with 4 % PFA/PBS and stained as described in 4.2.6 using a polyclonal rabbit-anti-mouse active caspase 3 primary antibody and an Alexa 488-conjugated donkey-anti-rabbit as a secondary antibody. The whole glass slide was analyzed for CC3-positive cells by using a DMRA microscope and the Stereo Investigator Software.

Acridine orange (AO)/ethidium bromide (EB) staining

At designated time points (0, 24 and 48 hours) after seeding cells in 24-well-plates were supplied with 2 µg/ml AO and 2 µg/ml EB in 10 µl of PBS for 5 minutes. 500 to 1500 cells per condition were photographed immediately with a 200-fold magnification by inverse microscopy on a DMI 3000B microscope. Cells were counted using the software Image J after classification into the following two groups:

1. AO positive small fragmented nucleus and/or EB positive nucleus
2. AO positive normal size nucleus

To show microglia morphology, phase-contrast pictures of representative cultures were taken with a 200-fold magnification by on a DMI 3000B microscope.

LPS stimulation

Microglia, cultured in 96-well-plates, were supplied with fresh medium with or without 0.1 µg/ml LPS, respectively. Cell viability was determined after 24 hours by MTT assay (described in 4.2.7).

4.2.9 Phagocytosis assay

Cell culture

Microglia

100000 microglia per well were seeded into 96-well-plates. 30 minutes later, medium was changed and cells were incubated over night at 37°C/0.5 % CO_2. Next day, negative controls

were incubated with 10 µM Cytochalasin D, an inhibitor of actin polymerization, for 30 minutes before and during the phagocytosis assay.

Macrophages

Macrophages obtained from one mouse were split into 47 wells of a 96-well-plate and cells were incubated over night at 37°C/0.5 % CO_2. Next day, 7 wells were used for the phagocytosis assay. Medium was changed and negative controls were incubated with 10 µM Cytochalasin D for 30 minutes before and during the phagocytosis assay.

Phagocytosis assay

pHrodo™ BioParticles® Conjugates for Phagocytosis were resuspended in 6 ml of microglia culture medium. To separate particle aggregates, they were sonicated inside a glass tube on an ice-cold water bath five times for one second at full power. 100 µl per well of this suspension were added to the 96-well plates containing cells. Phagocytosis was performed at 37°C/0.5 % CO_2 for 1 hour. Fluorescent emissions at 590 nm were measured with a CytoFluor Multi-well Plate Reader 4000 after excitation at 530 nm. Cell viability was measured by MTT assay as described in 4.2.7.

4.2.10 Intracardial perfusion and organ removal

Mice were anesthetized with 4 % isoflurane in 10 % oxygen and subsequent injection of 20 mg/kg Xylazin and 100 mg/kg Ketamine into the peritoneum. After ascertained deep anesthesia, thoracotomy was performed and mice were perfused intracardially with PBS. Organs were collected and stored in cold PBS until further processing. In case of histological analysis mice were perfused additionally with fresh 4 % PFA/PBS. Organs were post-fixed in 4 % PFA/PBS over night at 4°C and embedded in 30 % sucrose in PBS, until they were sunk to the bottom of the tube. For storage samples were frozen at -80°C.

4.2.11 Fluorescence-activated cell sorting (FACS)

FACS is a special type of flow cytometry. A heterogeneous suspension of cells can be sorted due to cell size, granularity and fluorescent characteristics. Therefore the cell suspension is applied

into a narrow, rapidly flowing stream of liquid leading to a large separation of the cells. One cell after the other passes through a fluorescent scanner to determine its fluorescent composition. Fluorescence of cells is achieved by previous labeling of cell markers with determined fluorescent antibodies as described below.

Sample preparation of spleens

Harvested spleens were squeezed in 5 ml of PBS through a 100 µm cell strainer. The cell solution was resuspended by pipetting several times and further filtrated with a 40 µm cell strainer to receive a single cell suspension. Cells were centrifuged at 300 g and 4°C for 10 minutes and then resuspended in 5 ml of PBS. Cell suspension was loaded onto 3 ml of Histopaque density gradient medium and centrifuged at 400g for 25 minutes at room temperature. The white interphase containing mononuclear splenocytes was collected carefully and washed with PBS. The cell pellet was contained in 5 ml of FACS buffer and leukocytes were counted in Türk´s solution using a hemocytometer. 10^6 cells per staining were transferred into FACS tubes and stained as described below.

Sample preparation of lymph nodes

Axillary, iliac, inguinal, mediastinal, brachial, pancreatic, mesenteric, lumbar and renal lymph nodes were squeezed gently through a 100 µm cell strainer in 5 ml of PBS. The cell suspension was homogenized by pipetting several times and further filtrated with 40 µm cell strainers to receive a single cell suspension. Cells were centrifuged at 300 g and 4°C for 10 minutes and resuspended in 5 ml of FACS buffer. Leukocytes were counted in Türk´s solution using a hemocytometer. 10^6 cells per staining were transferred into FACS tubes and stained as described below.

Sample preparation of blood

Mouse blood was collected into heparin or citrate supplied syringes by puncture of the inferior vena cava and diluted 1:1 with PBS. Blood samples were loaded onto 1.5 ml of Histopaque density gradient medium and centrifuged at 400g for 25 minutes at room temperature. The white interphase containing peripheral blood mononuclear cells (PBMC) was collected carefully and washed with PBS. The cell pellet was contained in 5 ml of FACS buffer and leukocytes were counted in Türk´s Solution using a hemocytometer. Due to cell numbers less than 2 x 10^6, the whole samples were distributed to two FACS tubes, respectively, and stained as described below.

Sample preparation of brain

A single cell suspension was generated from mouse brains using a Neural Tissue Dissociation Kit and a GentleMACS Dissociator according to the manufacturer's protocol. Myelin Removal by Magnetic Cells Sorting (MACS) was performed using an AutoMACS and the Myelin Removal Beads according to the manufacturer's protocol. Sorted cell fractions were not countable due to remainders of myelin, so the complete cell fraction was used for FACS staining.

Fluorescent labeling and cell gating

Cell samples were transferred to FACS tubes and washed with FACS buffer (centrifugation at 300 g and 4°C for 10 minutes). Cells were incubated with 100 µl of FACS buffer containing FACS antibodies for 20 minutes at 4°C, then washed again with FACS buffer and fixed in 100 µl of 1 % PFA/PBS for 10 minutes at 4°C. After another washing step, cells were resuspended in 250 µl FACS buffer and stored at 4°C.

For analysis on splenomegaly splenocytes were stained for CD11b, Ly-6C, Ly-6G, and, CD44. The gating strategy is shown in Fig. 4.2. For determination of the immune status, cell suspensions of spleens, lymph nodes and blood were stained for CD45, CD3, CD4, CD8, CD11b and CD19. The gating strategy is shown in Fig. 4.3. Brain samples were stained for CD11b. The gating strategy is shown in Fig. 4.4.

Brain suspensions were analysed using a LSRII flow cytometer. Spleen, lymph node and blood samples were analyzed using a MACSQuant® Analyzer flow cytometer. Data analysis was performed by means of the software FlowJo. Both FACS measurement and data analysis was performed by Dr. Juliane Ladhoff.

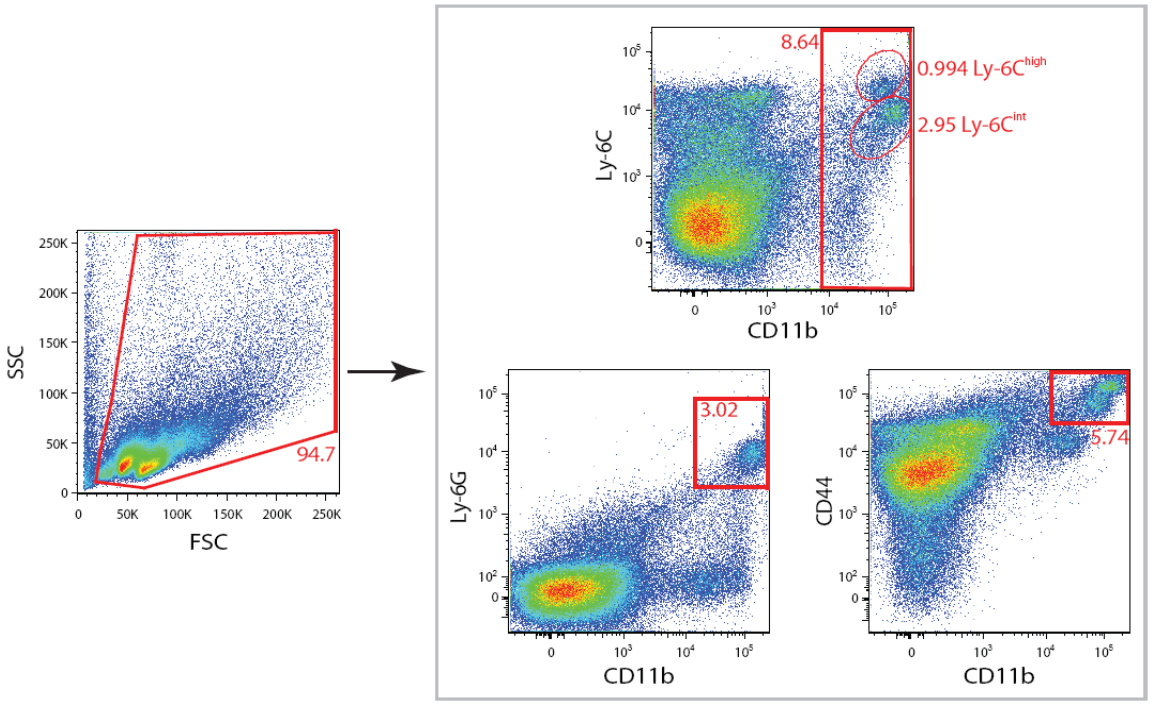

Fig 4. 2 Gating strategy for splenocytes

Living cells (left plot) were gated for CD11b^{+} Ly-6C^{high} and CD11b^{+} Ly-6C^{int} (right upper plot), CD11b^{+} Ly-6G^{+}, and CD11b^{+} CD44^{high} (right lower plots). SSC, side scatter; FSC, forward scatter

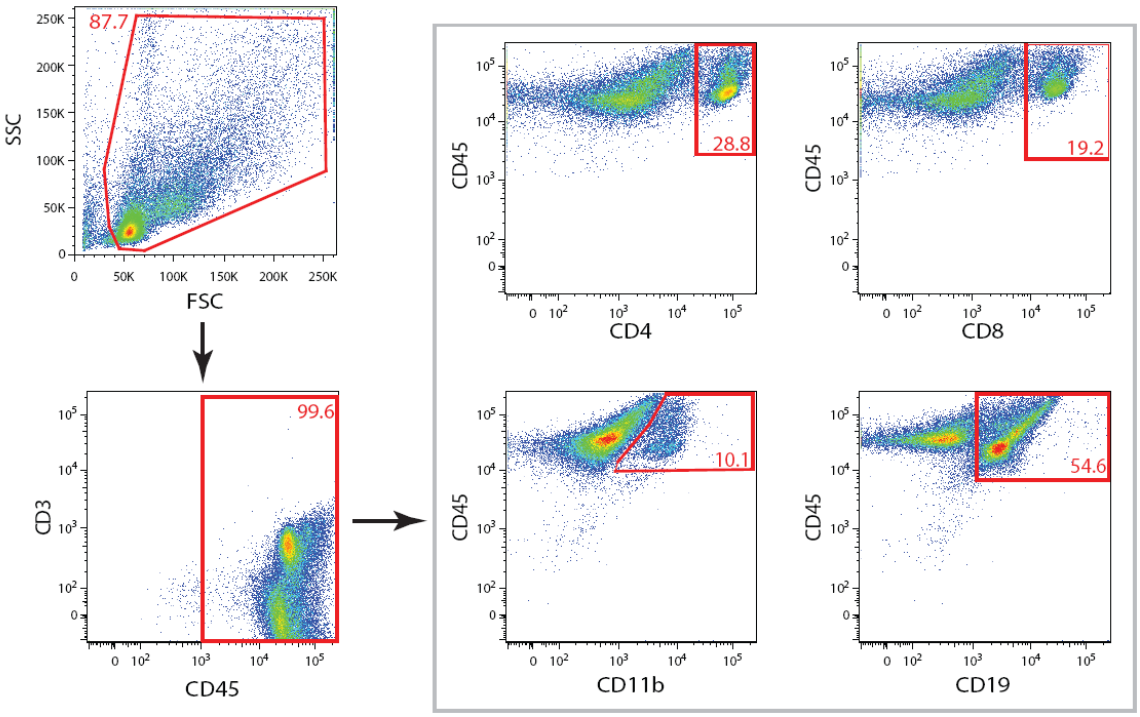

Fig 4. 3 Gating strategy for spleen, lymph nodes and blood samples

Living cells (upper plot left) were gated for CD45 (lower plot left) and then further as depicted for CD4, CD8, CD11b and CD19 (right plots). SSC, side scatter; FSC, forward scatter

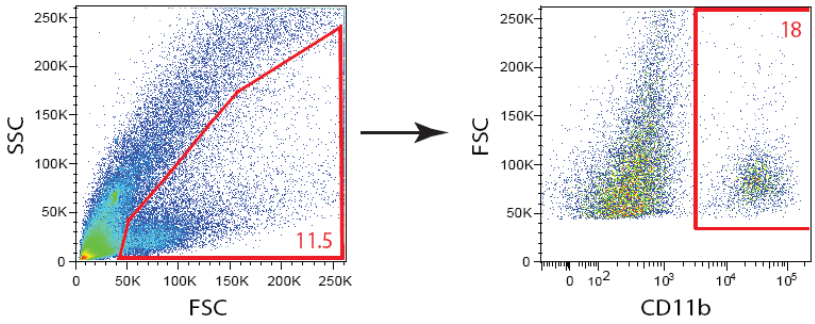

Fig 4. 4 Gating strategy for FACS analysis of brain samples

Brain samples were still contaminated with myelin even after myelin removal by MACS. Myelin was excluded from the live gate (left plot). CD11b positive cells were gated as depicted (right plot). SSC, side scatter; FSC, forward scatter

4.2.12 Middle cerebral artery occlusion (MCAo)

Animal experiments were performed by Peggy Mex according to institutional, national and international guidelines and standard operating procedures [79].

Mice anesthesia was induced with 2 % isoflurane in 70 % N_2O/30 % oxygen and maintained during operation with 1 % isoflurane in 70 % N_2O/30 % oxygen using a vaporizer. Ischemia experiments were performed as described [19, 79-81]. In brief, cerebral ischemia was induced with an 8.0 nylon filament coated with a Xantopren silicone resin/activator mixture. The filament was introduced into the left internal carotid artery up to the anterior cerebral artery. Thereby, the middle cerebral artery and anterior choroidal arteries were occluded. Lidocaine was applied as a local anesthetic for pain relieve. Filaments were withdrawn after 60 minutes to allow reperfusion of the infracted area and the cut was sutured with 2 stitches. Core temperature during the experiment was maintained at 36.5 °C ± 0.5 °C with a Homeothermic blanket Control Unit. After surgery animals were allowed to recover for 2 hours in a heating cage.

In the case of sham-operated animals, the filament was inserted as described and withdrawn immediately to allow prompt reperfusion. The subsequent operation procedure was identical to the MCAo.

Stroked and sham-operated animals were supplied with soaked food directly inside the cage. Weight loss and state of health were checked daily. If necessary, mice were euthanized according to ethical guidelines of the Landesamt für Gesundheit und Soziales (LAGeSo) Berlin.

4.2.13 Transplantation of splenocytes

Donor spleens were harvested from C57BL/6 mice and suspensions of mononuclear splenocytes were prepared as described in 4.2.11. The cells were washed with PBS and counted in Türk´s solution using a hemocytometer. 2.5 million cells per ml PBS were supplied with 5 µl of Heparin. 400 µl of this cell suspension were injected into the tail vein of recipient mice 6 hours after MCAo. For vehicle controls 400 µl of PBS containing 5 µl Heparin per ml were intravenously injected. Tail vein injection was performed by Peggy Mex.

4.2.14 Infarct volumetry

Hematoxylin staining

Mice were shortly anesthetized with 4 % isoflurane in 10 % oxygen and killed by cervical dislocation. After craniotomy, brains were removed from the skull and snap-frozen in 2-methylbutane in liquid nitrogen for cryostat sectioning. Brain sections of 20 µm were collected serially at 600 µm-intervals, mounted on glass slides and stained with hematoxylin by the following protocol: Slides were treated with 100 %, 80 % and 70 % ethanol, shortly rinsed with tap water and stained with hematoxylin solution for 4 minutes. They were again rinsed shortly in tap water and then in 0.25 % HCl in 96 % ethanol. After another short rinsing step in dH_2O they were stained in 1 % $NaHCO_3$ for 3-4 minutes, shortly washed in dH_2O and dehydrated in 70 %, 80 % and 100 % ethanol before mounting them in Roti-Histol and Roti-Histokitt.

Calculation of lesion size

Slides were scanned and infarct volumes were determined blinded using the image analysis software SigmaScan Pro 5. Volumes were corrected for post-ischemic edema by calculating the indirect infarct volume as the difference of volume of the contralateral hemisphere and the volume of the healthy area in the ipsilateral hemisphere.

MRI

MRI was performed using a 7 Tesla rodent scanner equipped with a 16 cm horizontal bore magnet and a 9 cm (inner diameter) shielded gradient with H-resonance-frequency of 300 MHz and a maximum gradient strength of 300 mT/m. For imaging a ^{1}H-RF quadratur-volume resonator with an inner diameter of 20 mm was used. Data acquisition and image processing were carried out with the software Paravision 4.0.

During imaging, animals were fixed to a heated blanket to ensure constant body temperature of 37°C. Anesthesia was induced with 3 % isoflurane and maintained with 1.5 % delivered in 0.5 l/minute of 100 % oxygen via facemask. The respiration rate was constantly controlled by a monitoring unit.

The ischemic lesion area in the mouse brain was visualized with a T2-weighted, 2D turbo spin-echo sequence (imaging parameters TR / TE = 4059 / 36 ms, rare factor 8, 4 averages). 20 axial slices with a slice thickness of 0.5 mm, a field of view of 2.85 x 2.85 cm and a matrix of 256 x 256 were positioned over the brain from olfactory bulb to cerebellum.

Image analysis

Calculation of lesion volume was carried out with the program Analyze 5.0. The hyper intense ischemic area visualized on a stack of T2-weighted images was assigned with threshold based segmentation resulting in a 3D map of the whole stroke region (Fig 4.5). The total volume of the whole object map was automatically calculated.

4.2.15 Immunohistochemistry

Mouse brains were fixed with 4 % PFA/PBS as described in 4.2.10 and cryo-protected in 30 % sucrose in PBS before freezing. 30 µm cryosections were sliced in a cryostat and collected in PBS to stain them free-floating. Slices were blocked with IHC blocking solution for 1 hour at room temperature and then incubated with primary antibodies (Tab 4.2) in IHC 1st antibody solution over night and shaking at 4°C. After washing three times with TBS containing 0.3 % Triton-X, secondary antibodies (Tab 4.2) were applied in IHC 2nd antibody solution for 2 hours at room temperature. Slices were counterstained for 10 minutes with DAPI (1:5000). After additional three washing steps, objects were mounted onto glass slides and covered with

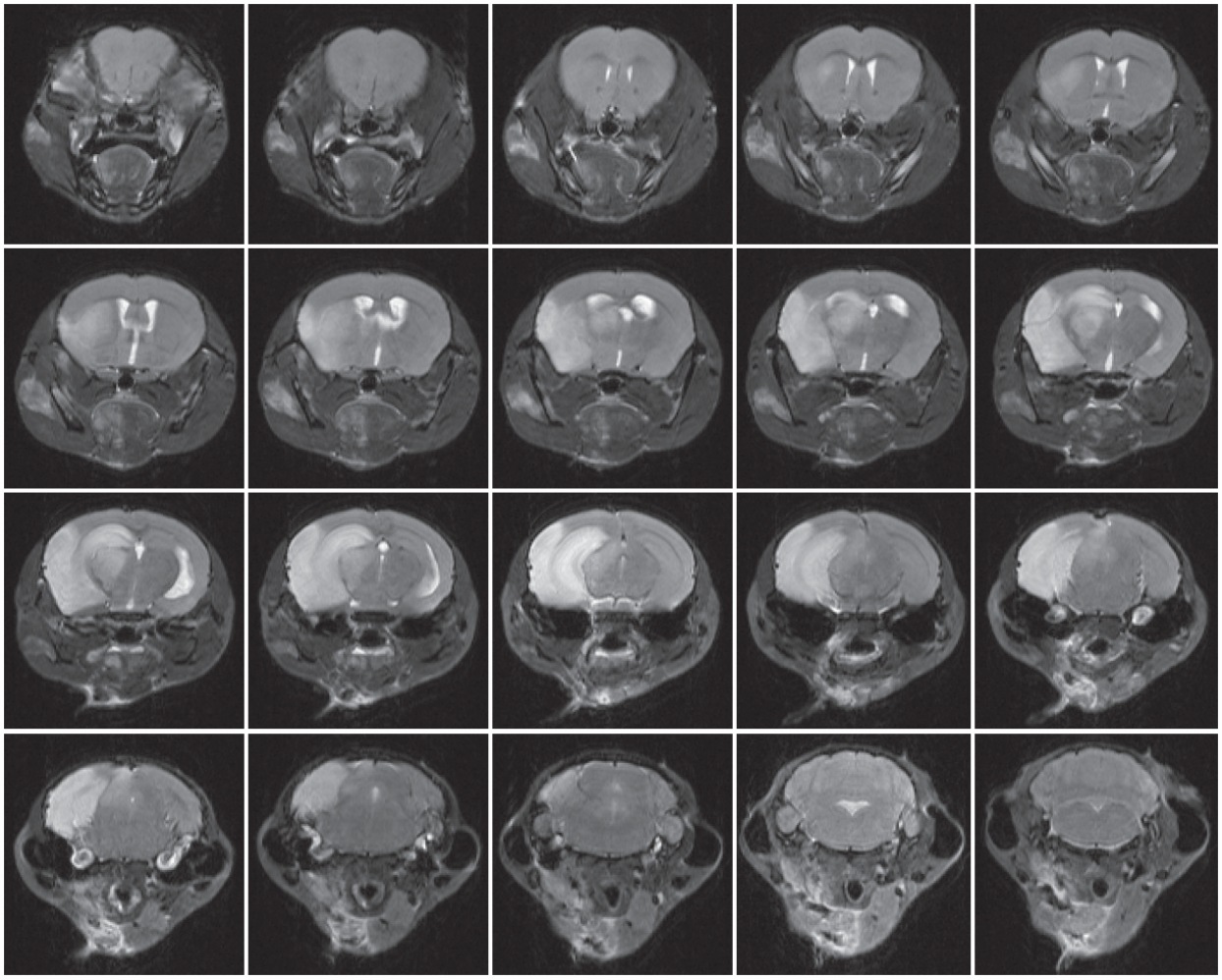

Fig 4. 5 Infarct volumetry by MRI

An exemplary stack of 20 images from one mouse brain: The bright areas (except the ventricles) represent the infarct zone. By using the software Analyze 5.0 this area was measured in each picture to calculate the infarct volume.

FlourSave™ Reagent. Slides were stored at 4°C. Photos were taken using a confocal DM 2500 microscope.

$CC3^+$ $CD13^+$ and $Ki67^+$ $CD13^+$ pericytes were counted by Francisco Fernández-Klett.

Staining	Primary antibodies	Secondary antibodies
Proliferation	rabbit-anti-mouse Ki67 rat-anti-mouse CD13	Alexa 594-conjugated donkey-anti rabbit Alexa 488-conjugated donkey-anti-rat
Apoptosis	rabbit-anti-mouse CC3 rat-anti-mouse CD13	Alexa 594-conjugated donkey-anti rabbit Alexa 488-conjugated donkey-anti-rat

Tab 4. 2 Combination of antibodies for immunohistochemistry

4.2.16 Statistical analysis

Statistical analysis was performed by using Graph Pad Prism 5. Means and Standard deviations (SD) were determined. To test for significance, one-way analysis of variance (ANOVA) or two-way ANOVA followed by Bonferroni´s Multiple comparison test were performed as indicated, since normal distribution was assumed. Differences between groups were considered to be significant when * $p < 0.05$, ** $p < 0.01$, or *** p as indicated.

5 RESULTS

5.1 Conditional knockout of *Ikk2* in the myeloid cell lineage

To achieve a deletion of *Ikk2* specifically in myeloid cells, the LysM-Cre mouse expressing Cre recombinase (Cre) under the promoter of Lysozyme M (LysM) [52] was crossed with the Ikk2$^{fl/fl}$ mouse [59]. Progeny carrying one copy of Cre and one floxed *Ikk2* allele were inbred for a second generation to receive amongst others the four genotypes of interest to our study, the LysM-Cre$^{-/-}$ Ikk2$^{fl/fl}$, LysM-Cre$^{+/-}$ Ikk2$^{fl/fl}$, LysM-Cre$^{+/+}$ Ikk2$^{fl/fl}$ and the LysM-Cre$^{+/+}$ (Ikk2$^{+/+}$) mouse. LysM-Cre$^{+/-}$ Ikk2$^{fl/fl}$ and LysM-Cre$^{+/+}$ Ikk2$^{fl/fl}$ mice delete *Ikk2* in the myeloid lineage due to Cre recombination. "LysM-Cre Ikk2$^{fl/fl}$" was used as an umbrella term for both of them (Fig 5.1). LysM-Cre$^{-/-}$ Ikk2$^{fl/fl}$ animals do not express Cre and serve as wild type controls. It has to be considered, that LysM-Cre$^{+/+}$ Ikk2$^{fl/fl}$ knock-in mice have lost both alleles of *LysM*. Thus LysM-Cre$^{+/+}$ mice carrying unfloxed *Ikk2* alleles served as an additional control in functional assays, enabling the identification of effects caused by the knockout of *LysM* and not *Ikk2*.

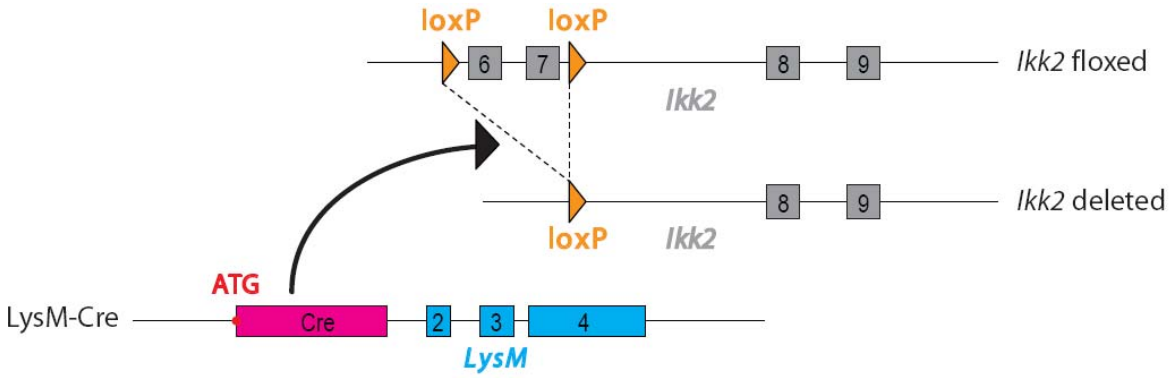

Fig 5. 1 Scheme of the genetic situation in myeloid cells from the LysM-Cre Ikk2$^{fl/fl}$ mouse

In myeloid cells, Cre recombinase (Cre) is expressed and recognizes specifically loxP DNA sequences flanking exons 6 and 7 of the *Ikk2* gene. Thus recombination takes place between loxP sites with high efficiency to excise the flanked exons. The *Ikk2* gene product is missing in the targeted cell population as the *Ikk2* locus cannot be transcribed correctly anymore. ATG, translational start codon

Mice were identified by genotyping revealing PCR fragments specific for *Cre* (512 bp), *LysM* (436 bp), the unfloxed *Ikk2* allele (Ikk2^{+}) (244 bp) and the floxed *Ikk2* exons (Ikk2^{fl}) (346 bp) (Fig 5.2).

A

Genotype	PCR fragments			
	Cre	LysM	Ikk2^{+}	Ikk2^{fl}
LysM-Cre$^{-/-}$ Ikk2$^{fl/fl}$		x		x
LysM-Cre$^{+/-}$ Ikk2$^{fl/fl}$	x	x		x
LysM-Cre$^{+/+}$ Ikk2$^{fl/fl}$	x			x
LysM-Cre$^{+/+}$ Ikk2$^{+/+}$	x		x	

B

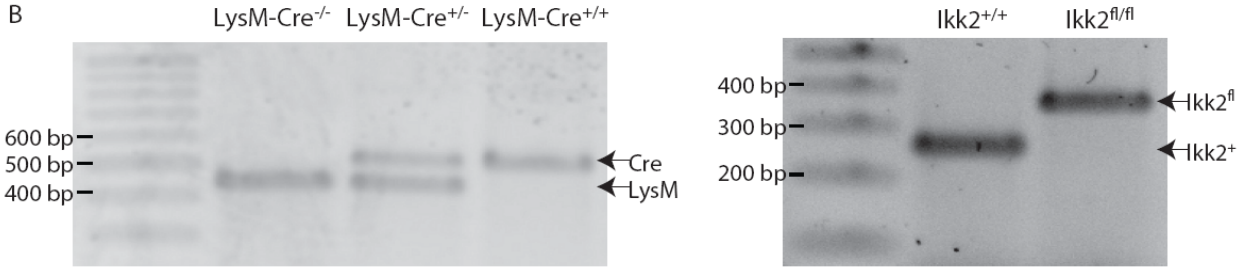

Fig 5. 2 Identification of different LysM-Cre Ikk2$^{fl/fl}$ genotypes by PCR

A. Insertion of Cre recombinase into none, one or both alleles of the *LysM* locus was proven by the presence of PCR products for the *LysM* and *Cre* genes. An additional PCR reaction determined whether the *Ikk2* alleles were floxed or unfloxed.

B. PCR products were separated on agarose gels. A DNA band of 512 bp proved presence of *Cre*, a band of 436 bp indicated at least one remaining intact *LysM* allele. The wild type *Ikk2* gene was assessed by a PCR product of 244 bp, while *Ikk2* carrying loxP flanks resulted in a 346 bp PCR product.

5.2.1 Reduced Ikk2 expression in microglia and macrophages

LysM-Cre Ikk2$^{fl/fl}$ mice were characterized *in vitro* for cell-specific deletion of the *Ikk2* gene. To this aim primary microglia and peritoneal macrophage cultures were prepared and protein as well as mRNA expression levels of IKK2 were measured. The results were compared with microglia and macrophage cultures from littermates, which do not express Cre (LysM-Cre$^{-/-}$ Ikk2$^{fl/fl}$), and with astroglial cultures, which derive from the neuroectoderm as a control for tissue-specifity. A decrease of *Ikk2* mRNA was detected in peritoneal macrophages of both LysM-Cre$^{+/-}$ Ikk2$^{fl/fl}$ and LysM-Cre$^{+/+}$ Ikk2$^{fl/fl}$ mice to 6 % and 11 % of wild type levels, respectively. In microglia a trend to less *Ikk2* mRNA was shown (48 % and 51 %), compared to the LysM-Cre$^{-/-}$ Ikk2$^{fl/fl}$ littermates. Astrocytic *Ikk2* mRNA expression levels were found to be unchanged in all three genotypes (Fig 5.3A).

Protein lysates were generated from primary astrocytes, microglia and macrophages, and IKK2 expression levels were examined by Western Blot analysis. As a reference, cultures derived from LysM-Cre$^{-/-}$ Ikk2$^{fl/fl}$ mice were set to 100 % of IKK2 protein expression. Microglia-specific IKK2 from LysM-Cre$^{+/+}$ Ikk2$^{fl/fl}$ mice and macrophage-specific IKK2 from both *Ikk2* mutant mice were significantly reduced. As expected, in astrocytes IKK2 protein expression was unchanged (Fig 5.3B and Tab 5.1). Protein levels of IKK1 and NEMO were shown to be not significantly affected by *Ikk2* deletion (Tab. 5.1).

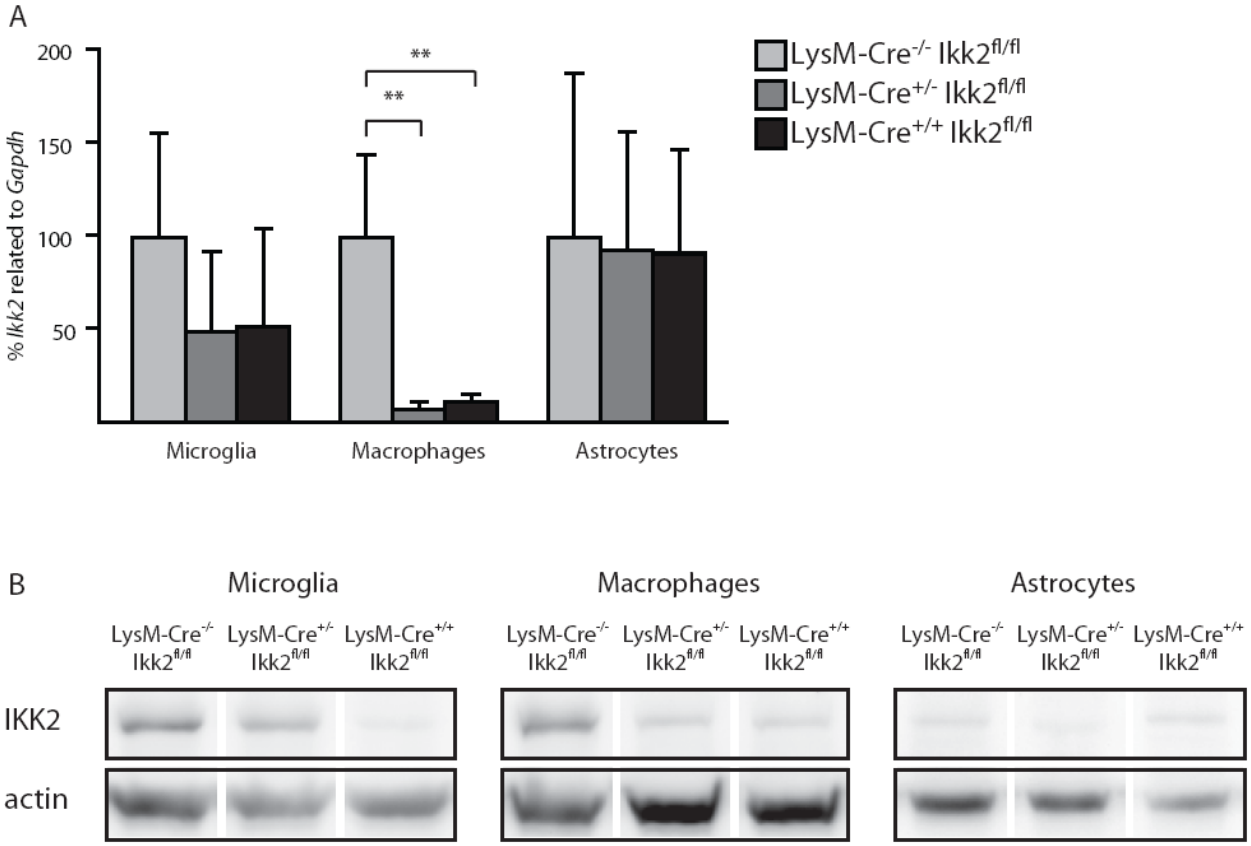

Fig 5. 3 Reduced IKK2 mRNA and protein levels in microglia and macrophages

A. *Ikk2* mRNA levels in primary cell cultures were examined by quantitative real-time PCR using the housekeeping gene glyceraldehyde 3-phosphate dehydrogenase (Gapdh) as a reference. Microglia and macrophages from LysM-Cre Ikk2$^{fl/fl}$ mice exhibited a reduction of *Ikk2* mRNA compared with wild type littermates. microglia n = 6; macrophages n = 3; astrocytes n = 2-3; ** $p < 0.01$ (One-way ANOVA)

B. Protein levels of IKK2 were analyzed by Western Blot. A reduction of IKK2 protein expression in microglia and macrophages was detected in *Ikk2* mutant mice. Actin served as loading control. n=3

	IKK subunit	LysM-Cre$^{-/-}$ Ikk2$^{fl/fl}$	LysM-Cre$^{+/-}$ Ikk2$^{fl/fl}$	LysM-Cre$^{+/+}$ Ikk2$^{fl/fl}$
Microglia	IKK2	100 ± 14	83 ± 41	22 ± 19 *
	IKK1	100 ± 11	133 ± 45	100 ± 70
	NEMO	100 ± 21	128 ± 45	62 ± 29
Macrophages	IKK2	100 ± 40	33 ± 1 *	37 ± 15 *
	IKK1	100 ± 14	78 ± 3	88 ± 21
	NEMO	100 ± 64	58 ± 38	62 ± 25
Astrocytes	IKK2	100 ± 44	76 ± 15	105 ± 9
	IKK1	100 ± 35	106 ± 32	132 ± 7
	NEMO	100 ± 15	108 ± 22	157 ± 93

Tab 5. 1 Protein expression levels of IKK subunits

Protein expression of IKK2, IKK1 and NEMO in microglia, astrocytes and macrophages were analyzed by Western Blot. Protein levels determined in cells derived from LysM-Cre$^{-/-}$ Ikk2$^{fl/fl}$ mice were set to 100 % as a reference. Values represent means ± SD. n=3; * $p < 0.05$ compared to LysM-Cre$^{-/-}$ Ikk2$^{fl/fl}$ (One-way ANOVA)

5.2.2 Disruption of Ikk2 inhibits nuclear translocation of p65 in microglia

To assess the effect of *Ikk2* disruption on NF-κB signaling, nuclear translocation of the NF-κB subunit p65 was visualized by immunocytochemistry after stimulation with 1 µg/ml LPS for 30 minutes. Indeed, the ability of p65 to translocate into the nucleus after stimulation was diminished in microglial cells, but not in astrocytes, derived from *Ikk2* mutant mice (Fig 5.4A, B). Both cytoplasmic and nuclear p65 fractions were quantified to illustrate the significantly attenuated translocation in LysM-Cre$^{+/+}$ Ikk2$^{fl/fl}$ microglia (Fig 5.4C).

5.2.3 Ikk2-mutant microglia secrete decreased levels of inflammatory molecules

Inhibited nuclear translocation of the NF-κB subunit p65 in cultured LysM-Cre Ikk2$^{fl/fl}$ microglia suggested that p65-regulated gene transcription would also be affected in these cells. Hence secretion of tumor necrosis factor (TNF)-α, representing a crucial pro-inflammatory candidate regulated by p65, was measured by Immunoassay after LPS stimulation of microglial and macrophage cultures. TNF-α production by Cre-expressing microglia was strongly reduced (Fig 5.5A). Also microglial release of interleukin (IL)-6 had decreased to 59 % after 3 hours of LPS stimulation in LysM-Cre Ikk2$^{fl/fl}$ microglia (Fig 5.5E). Furthermore, nitric oxide (NO) production was examined. NO is a side product of oxidative conversion of arginine to citrulline

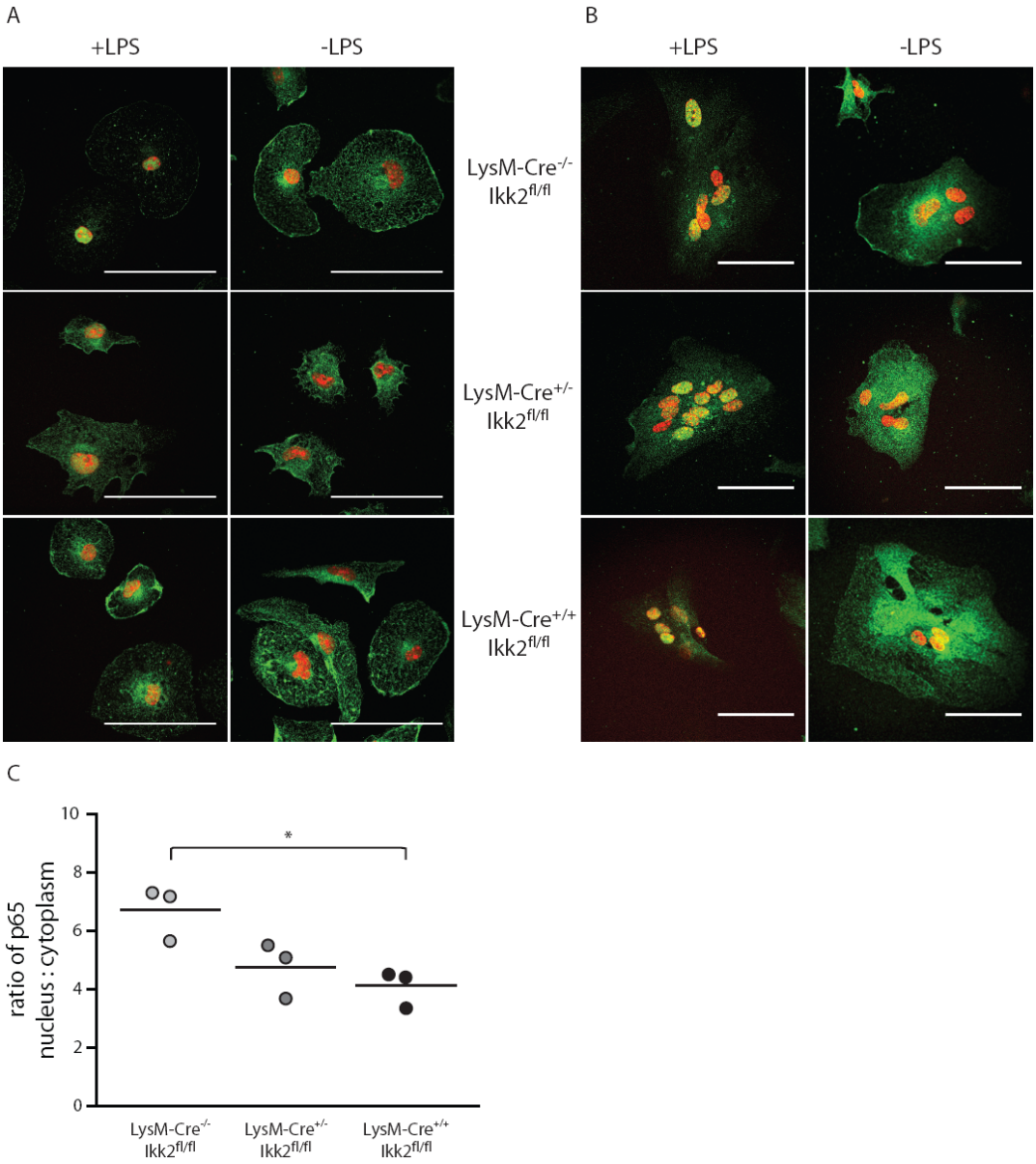

Fig 5. 4 Impaired nuclear translocation of NF-κB subunit p65 in primary microglia

A. Upon stimulation with 1 µg/ml LPS for 30 minutes, the NF-κB subunit p65 (green) translocated from the cytoplasm into the nucleus in wild type microglia. In *Ikk2* mutant cells a certain amount of p65 was detected in the cytoplasm similar to unstimulated cells. Microglia were identified by staining for CD11b (not shown), nuclei were counterstained with DAPI (red). Pictures were taken by confocal microscopy. 360-fold magnification; scale bars = 50 µm

B. In astrocytes, stimulation with 1 µg/ml LPS for 30 minutes provoked efficient p65 (green) nuclear translocation in wild type and *Ikk2* mutant cells, while in unstimulated cells p65 was detected predominantly in the cytoplasm. Astrocytes were identified by staining for Glial fibrillary acidic protein (GFAP) (not shown), nuclei were counterstained with DAPI (red). Pictures were taken by confocal microscopy. 360-fold magnification; scale bars = 50 µm

C. Using MATLAB, simulated microglia were quantified for cytoplasmic and nuclear fractions of p65. The ratio of nuclear to cytoplasmic signal of p65 was significantly decreased in LysM-Cre$^{+/+}$ Ikk2$^{fl/fl}$ microglia cultures compared to LysM-Cre$^{-/-}$ Ikk2$^{fl/fl}$ cells. n=3; * $p < 0.05$ (One-way ANOVA)

performed by the NF-κB-regulated inducible nitric oxide synthase (iNOS) and is transformed to nitrite and nitrate by auto-oxidation. Amounts of nitrite, indicative for cumulative NO production, were measured in cell culture supernatants of microglia and macrophages 24 hours after stimulation with LPS by Griess assay. As for TNF-α and IL-6 declining levels of NO to 35 % were measured in supernatants from LysM-Cre knock-in microglia (Fig 5.5C). TNF-α and NOsecretion by peritoneal macrophages was very variable. No significantly altered production of these inflammatory molecules by cultured macrophages could be measured (Fig 5.5B, D).

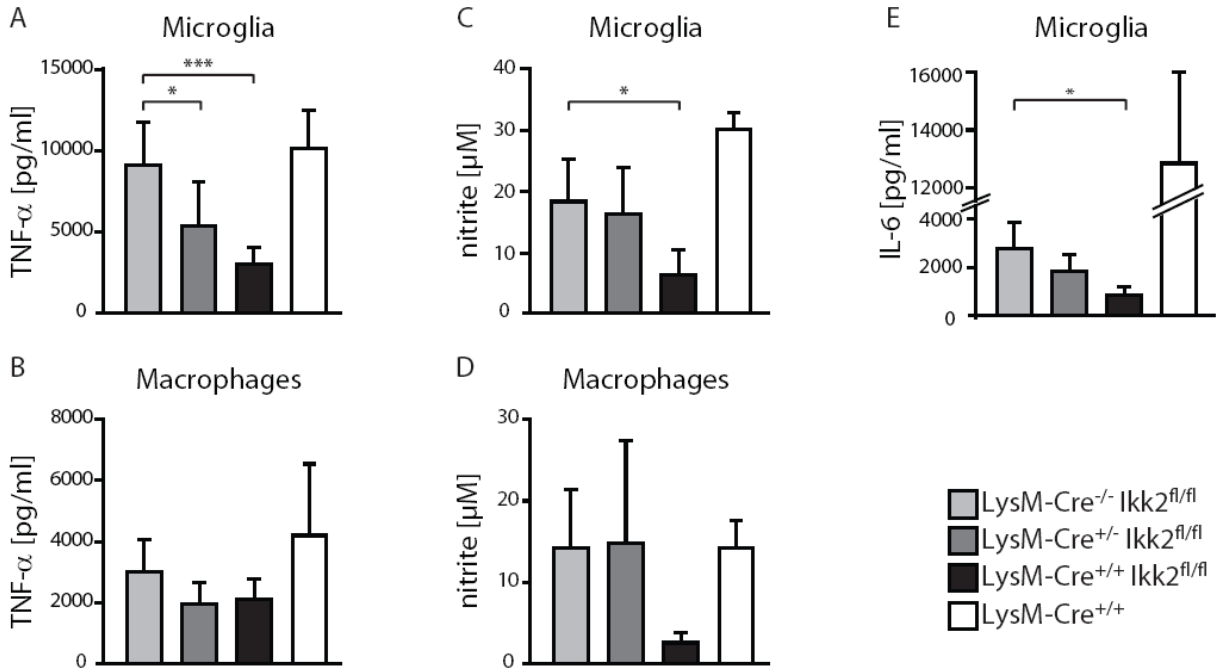

Fig 5. 5 Reduced release of inflammatory molecules by microglia

A-E. Microglia and macrophage cultures were stimulated with LPS, and supernatants were collected and analyzed for secretion of TNF-α and IL-6 by Immunoassay, as well as for accumulation of nitrite by Griess assay. TNF-α, IL-6 and nitrite levels were reduced in cultures of LysM-Cre$^{+/-}$ Ikk2$^{fl/fl}$ and LysM-Cre$^{+/+}$ Ikk2$^{fl/fl}$ microglia. TNF-α and NO secretion by macrophage cultures was very variable and not significantly affected in *Ikk2* mutant mice. Secretion of TNF-α, IL-6 and NO was further unchanged in cells derived from the LysM-Cre$^{+/+}$ mouse. A, C, E: n = 3-6; B: n = 4-9, D: n = 2-6; * $p < 0.05$, ** $p < 0.01$, *** $p < 0.0005$ (One-way ANOVA)

5.2.4 Increased mortality of Ikk2-depleted cultured microglia

Rising death rate and morphological changes were observed in LysM-Cre Ikk2$^{fl/fl}$ primary microglia cultures compared to wild type cells (Fig 5.6A). Cell viability was quantified by MTT assay at 24 hours and 48 hours in culture. Cultured cells of LysM-Cre$^{-/-}$ Ikk2$^{fl/fl}$ and LysM-Cre$^{+/+}$

control mice showed vitality of 86 % and 81 %, respectively, after 48 hours in culture, relative to the amount of vital cells directly after seeding. In contrast, survival was diminished to 53 % in LysM-Cre$^{+/-}$ Ikk2$^{fl/fl}$-derived microglia and to 43 % in cultures prepared from LysM-Cre$^{+/+}$ Ikk2$^{fl/fl}$ mice. After 24 hours *in vitro* no significantly different mortality was measured (Fig 5.6B). Since death rate of LysM-Cre$^{+/+}$ control cultures was not raised after 48 hours, the lack of *LysM* could be excluded as a cause for diminished survival in LysM-Cre$^{+/+}$ Ikk2$^{fl/fl}$ microglia.

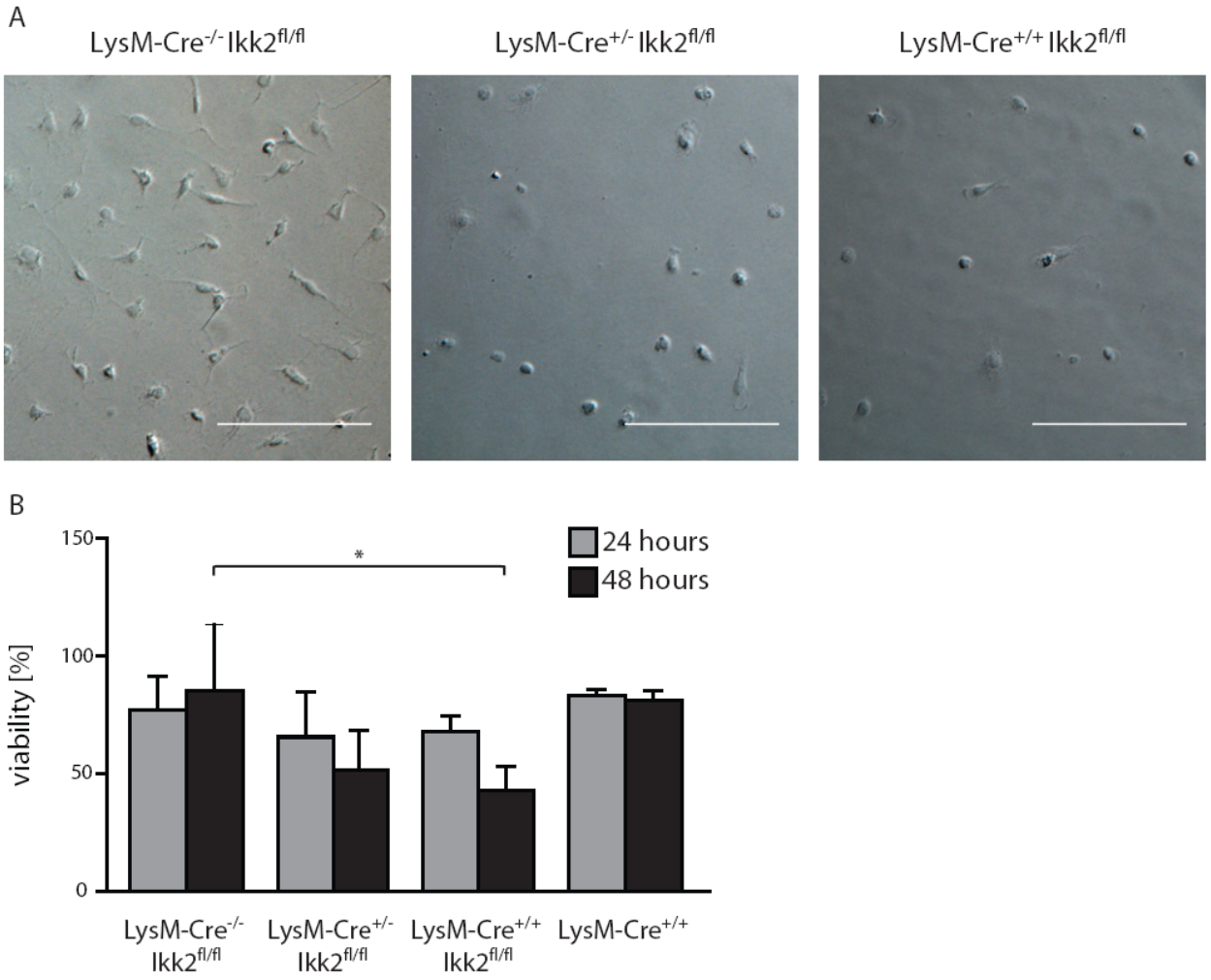

Fig 5. 6 Increased mortality of *Ikk2*-mutant microglia cultures

A. LysM-Cre Ikk2$^{fl/fl}$ microglia displayed morphological changes and low density after 48 hours in culture compared to cells prepared from wild type littermates. Phase-contrast pictures of representative microglia cultures were taken at a 200-fold magnification by inverse microscopy. scale bar = 100 µm

B. After 24 and 48 hours in culture, respectively, cell vitality was analyzed by MTT assay. Cultures from LysM-Cre$^{+/+}$ Ikk2$^{fl/fl}$ cells revealed significantly reduced viability after 48 hours *in vitro*, while vitality of LysM-Cre$^{+/+}$ control cells was unchanged compared to LysM-Cre$^{-/-}$ Ikk2$^{fl/fl}$ microglia. n = 3-5; ** $p < 0.01$ (One-way ANOVA)

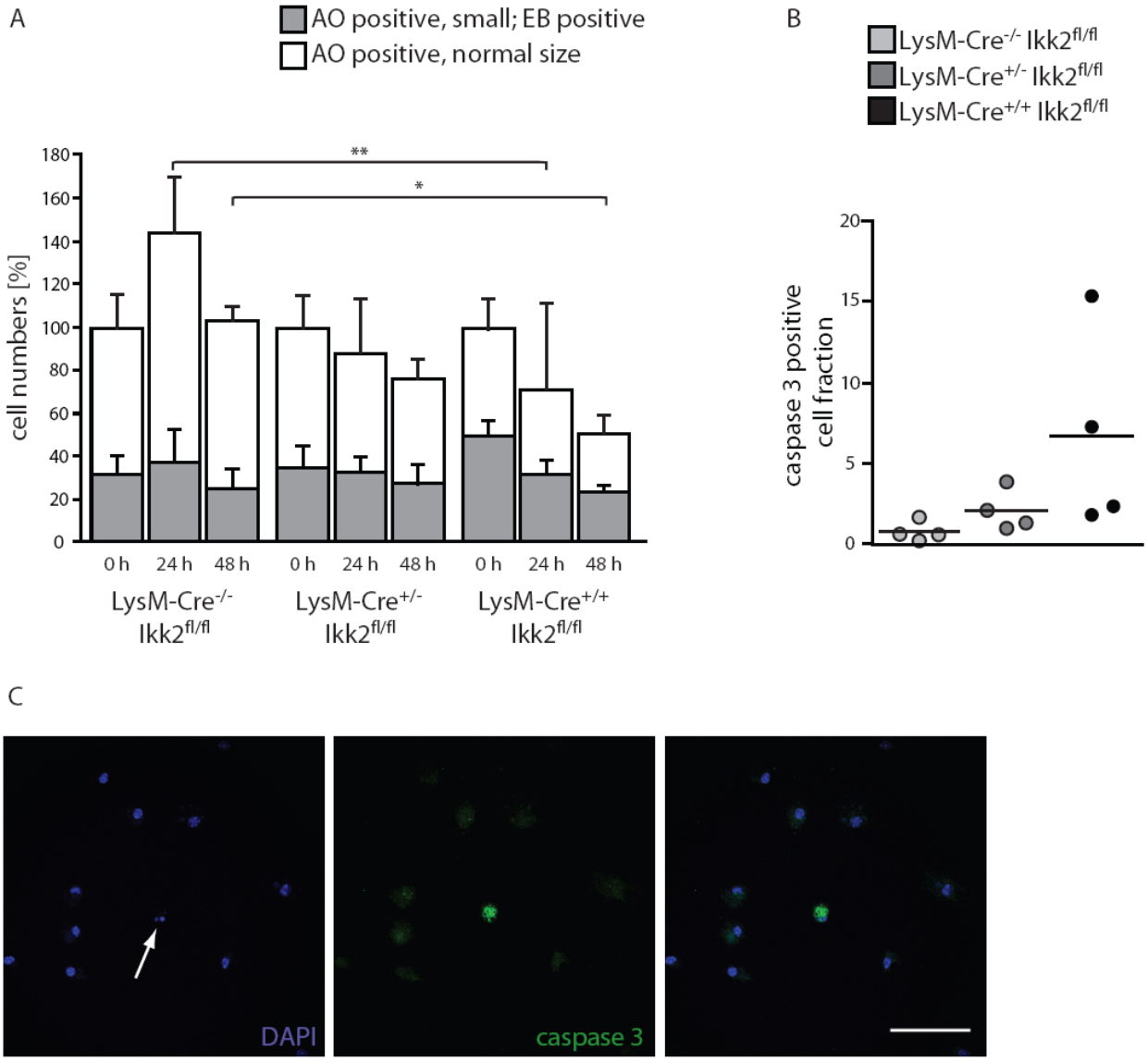

Fig 5. 7 Cell fate of cultured microglia

A. 0, 24 and 48 hours after seeding, respectively, cells were supplied with 2 µg/ml acridine orange (AO) and 2 µg/ml ethidium bromide (EB) for 5 minutes. Pictures were taken with a fluorescent microscope and stained cells were counted. While fractions of dying cells (fragmented AO positive nuclei and/or EB positive) did not change significantly, numbers of vital cells (AO positive, intact nuclei) diminished with time in cultures of *Ikk2*-mutant microglia. n=3; * $p < 0.05$, ** $p < 0.01$ (Two-way ANOVA)

B. After 48 hours in culture, cells were fixed on glass slides and stained for cleaved Caspase 3 (CC3) by immunofluorescence. Total numbers of CC3-positive cells were assessed and related to the MTT value of the same cultures accounting for cell density. The proportion of CC3-positive cells was increased by trend in LysM-Cre Ikk2$^{fl/fl}$ microglia compared to control cultures. n = 4; (One-way ANOVA)

C. Example of CC3 staining (green). Nuclei of CC3-positive cells showed fragmentation and apoptotic bodies visualized by DAPI-staining (blue, arrow). The overlay picture merging green and blue channels is shown on the right. scale bar = 50 µm

To get further information about cell fate, microglia were stained with the DNA-intercalating agents acridine orange (AO) and ethidium bromide (EB) directly after seeding, after 24 hours and after 48 hours in culture, respectively, and stained cells were counted. Green fluorescent AO is membrane permeable and therefore staining nuclei of vital cells and fragmented nuclei of early apoptotic cells. Red fluorescent EB penetrates dying cells with already damaged cell membrane. After 48 hours in culture *Ikk2*-mutant microglia showed reduced numbers of vital cells (AO positive, intact nuclei). However, changes in the fractions of dying or apoptotic cells (fragmented AO positive nuclei and/or EB positive) over time could not be detected by this method (Fig 5.7A). In a second approach microglia were fixed after 48 hours and stained for cleaved caspase 3 (CC3) by immunofluorescence (Fig 5.7C). The numbers of CC3-positive cells were related to MTT values of the same cultures. The proportion of CC3-positive cells related to cell density was increased in LysM-Cre$^{+/+}$ Ikk2$^{fl/fl}$-microglia 48 hours after seeding (Fig 5.7B).

We supposed a relation between increased mortality of *Ikk2*-mutant microglia and stress due to slight cell activation during preparation procedure and culture conditions. To test this hypothesis, microglia were stimulated with 0.1 µg/ml LPS for 24 hours and cell density was assessed by MTT assay. Indeed, LPS stimulation seemed to lower viability of LysM-Cre$^{+/+}$ Ikk2$^{fl/fl}$-derived microglia compared to control cells (Fig. 5.8).

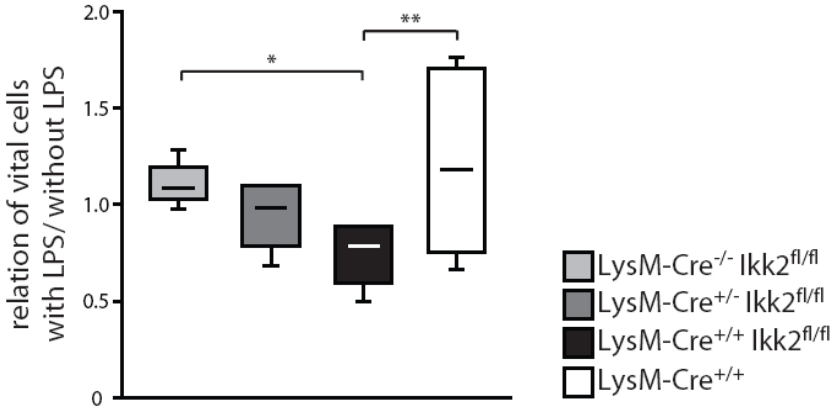

Fig 5. 8 Mortality of *Ikk2*-deficient microglia after LPS stimulation

Microglia cultures were treated with 0.1 µg/ml LPS for 24 hours, cell viability was tested by MTT assay and results were related to the MTT values of untreated control cells, respectively. n=6-9; * $p < 0.05$, ** $p < 0.01$ (One-way ANOVA)

5.2.5 No effect of Ikk2 on phagocytosis

Phagocytic activity of cultured microglia and macrophages was measured using the pHrodo™ BioParticles® Conjugates for Phagocytosis. This method is based on a fluorogenic dye (pHrodo) that increases fluorescence emission as the pH of its environment decreases. The dye is coupled to E. coli particles which are added to the cells to be phagocytised. Fluorescence values thus account for the uptake of particles into the acidic phagolysosome. As a negative control Cytochalasin D, a cytoskeleton inhibitor, was added for 30 minutes before and during the phagocytosis assay. No difference in particle uptake by LysM-Cre Ikk2$^{fl/fl}$ microglia and macrophages was detected compared to controls (Fig 5.9).

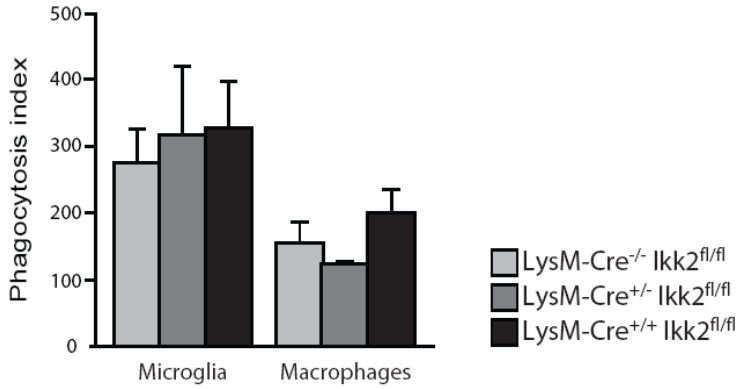

Fig 5. 9 Unchanged phagocytic activity of cultured microglia and macrophages

Fluorescent pHrodo-coupled E. coli were added to cultured microglia and macrophages, respectively, for 1 hour. Emitted fluorescence accounts for the ingestion of the particles into the acidic phagolysosome. No significant difference of phagocytic activity was detectable in LysM-Cre Ikk2$^{fl/fl}$ cells compared to wild type controls. n = 3-4; (One-way ANOVA)

5.2.6 Numbers of CD11b^{+} cells in the naive brain of LysM-Cre Ikk2$^{fl/fl}$ mice

To examine the numbers of microglia and perivascular macrophages in brains of LysM-Cre Ikk2$^{fl/fl}$ mice, we prepared cell suspensions from brain tissue and measured CD11b^{+} cells by FACS. No change of the CD11b^{+} cell compartment was detected in LysM-Cre Ikk2$^{fl/fl}$ mice, compared to control animals (Fig 5.10).

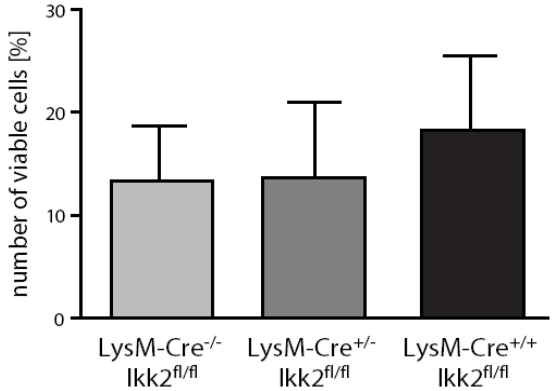

Fig 5. 10 CD11b^{+} cells in the naive brain of the LysM-Cre Ikk2$^{fl/fl}$ mouse

Brain suspensions were depleted for myelin by magnetic cell sorting (MACS), stained for CD11b and analyzed by FACS technology. No significant differences were detected in LysM-Cre Ikk2$^{fl/fl}$ mice compared to control littermates. n = 8-9; (One-way ANOVA)

5.2.7 Splenomegaly

LysM-Cre Ikk2$^{fl/fl}$ mice exhibit splenomegaly especially with aging. Detailed analysis revealed significantly enlarged spleens in young (8-11 weeks), and even more prominent in aged (26-32 weeks) LysM-Cre$^{+/+}$ Ikk2$^{fl/fl}$ mice compared to control littermates (Fig 5.11). There was little variation in spleen weight among wild type controls, but especially older knock-in mice exhibited a large variance. In animals with splenomegaly also lymph nodes, especially mesenteric ones, were observed to be dramatically swollen.

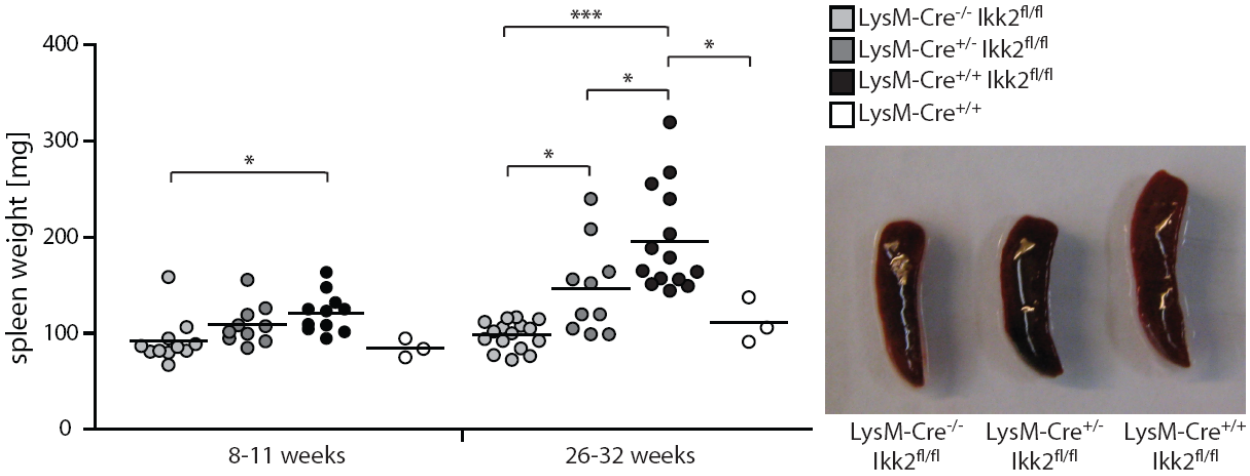

Fig 5. 11 Splenomegaly in LysM-Cre Ikk2$^{fl/fl}$ mice

Spleens were harvested from mice of different age groups. Splenomegaly was observed in young and even more prominent in aged LysM-Cre Ikk2$^{fl/fl}$ mice compared to LysM-Cre$^{-/-}$ Ikk2$^{fl/fl}$ and LysM-Cre$^{+/+}$ controls. n = 3-16; * $p < 0.05$, ** $p < 0.01$, *** $p < 0.0001$ (One-way ANOVA)

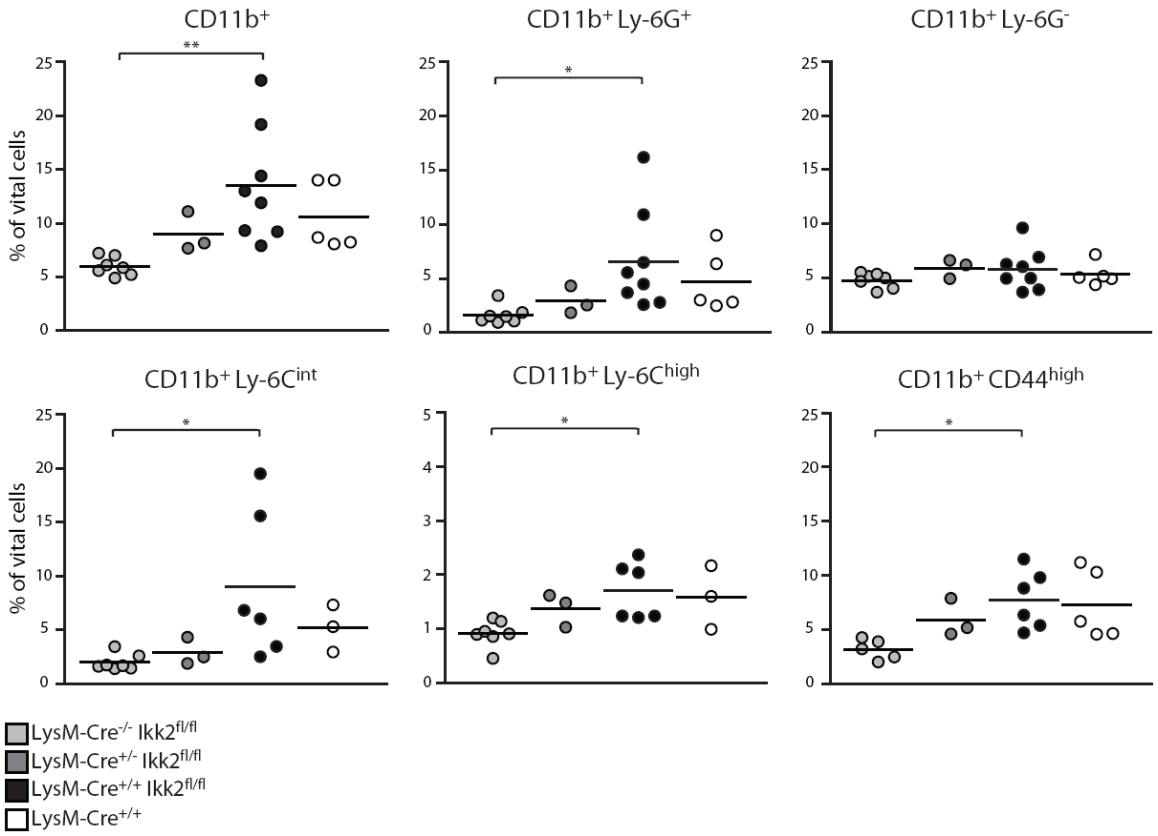

Fig 5. 12 Cellular compositions in spleens from aged LysM-Cre Ikk2$^{fl/fl}$ mice

Cell suspensions from spleens of LysM-Cre Ikk2$^{fl/fl}$ mice were analyzed by flow cytometry. Several cell populations were increased in aged LysM-Cre Ikk2$^{fl/fl}$ animals (26-32 weeks). n = 3-8; * $p < 0.05$ (One-way ANOVA)

Spleens harvested from mice of two age groups (8-11 weeks and 26-32 weeks) were analyzed by flow cytometry. While there were no differences in the splenic cellular composition of young LysM-Cre Ikk2$^{fl/fl}$ mice (data not shown), spleens of aged LysM-Cre$^{+/+}$ Ikk2$^{fl/fl}$ mice revealed significantly higher numbers of CD11b^{+} Ly-6C^{high}, CD11b^{+} Ly-6C^{int}, CD11b^{+} Ly-6G^{+}, and CD11b^{+} CD44^{high} splenocytes compared to wild type controls (Fig 5.12).

5.2 Adoptive transfer of immunocompetent cells after MCAo

5.2.1 Transplantation of splenocytes has no impact on infarct size

Experimental stroke was induced in adult C57BL/6 mice by 60 minutes of MCAo and 1 million splenocytes from donor mice, or the vehicle PBS alone, were transplanted by tail vein injection. The infarct volume was analyzed after 24 hours and 72 hours, describing the area of necrotic

tissue in the brain due to reduction of cerebral blood flow. After 24 hours and 72 hours of reperfusion, respectively, both splenocytes-transplanted and control mice revealed comparable infarct sizes as determined by histology (Fig 5.13) and MRI (data not shown).

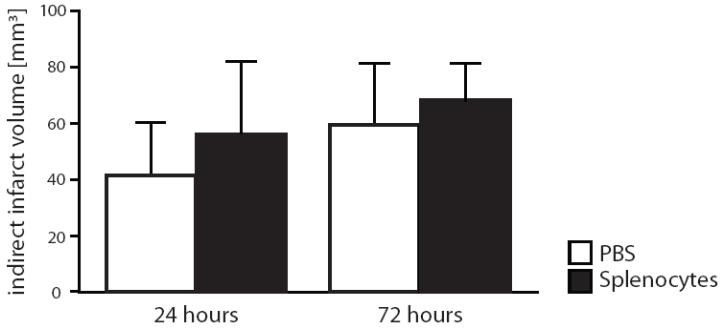

Fig 5. 13 Unchanged infarct volume after transplantation of splenocytes

C57BL/6 mice were subjected to 60 minutes of MCAo and successive tail vein injection of 1 million splenocytes from donor mice, or PBS alone, after 6 hours of reperfusion. Edema-corrected infarct volume was analyzed by histology 24 hours and 72 hours after reperfusion, respectively. n = 6-10; (One-way ANOVA)

5.2.2 Splenocytes do not affect stroke-induced immunosuppression

Analyzing blood, lymph nodes and spleens, an immune status was retrieved from C57BL/6 mice that had been subjected to 60 minutes MCAo and intravenous injection of splenocytes, or PBS alone. Sham-operated and naïve mice served as controls. Composition of different leukocyte subpopulations was analyzed by FACS.

At 3 days after MCAo an impressive 2 to 3-fold reduction of $CD11b^+$ monocytic cells, B and T cells (both $CD4^+$ and $CD8^+$) was detected in blood. Even more pronounced (5 to 15-fold) was the decrease of monocytes and lymphocytes in lymph nodes and spleen compared to untreated controls (Fig 5.14 and 5.15). Also sham-operated animals showed a slight decline of this cell population. Notably, transplantation of splenocytes did not reveal any changes in cellular composition, neither in the MCAo nor in the sham- or control group.

To test whether splenocytes rather have a long-term effect on post-stroke immunosuppression, we examined the immune status at 14 days after MCAo. While the extent of lymphopenia and depletion of $CD11b^+$ cells remained in blood, lymph nodes exhibited rising amounts of these

cells. In spleen, cell numbers were nearly recovered to control levels after 14 days. However, transplanted splenocytes had no impact on cell recovery (Fig 5.14 and 5.15).

In summary, stroke-induced immunosuppression was not influenced by transplantation of splenocytes. Mild lymphopenia and reduction of monocytic cells were also observed in sham-operated animals, but in an attenuated extend.

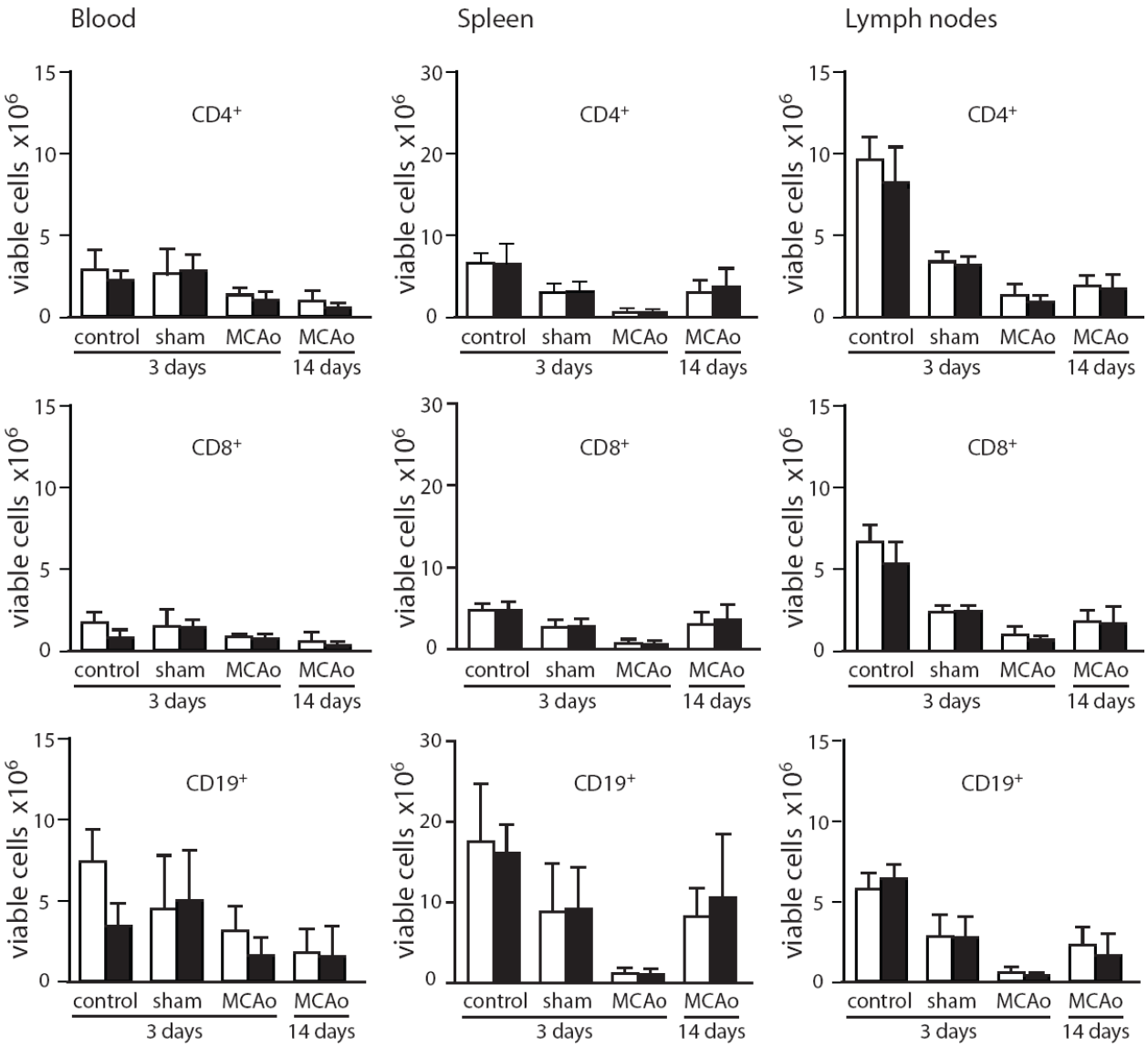

Fig 5. 14 Transplantation of splenocytes has no impact on stroke-induced lymphopenia

3 and 14 days after MCAo entailing splenocytes transplantation, respectively, cell suspensions from blood, spleen and lymph nodes were analyzed by FACS to retrieve an immune status. No different numbers of T ($CD4^+$ and $CD8^+$) and B lymphocytes ($CD19b^+$) were detected between the splenocytes-transplanted (black bars) and the PBS-control (white bars) groups. n = 5-8; (One-way ANOVA)

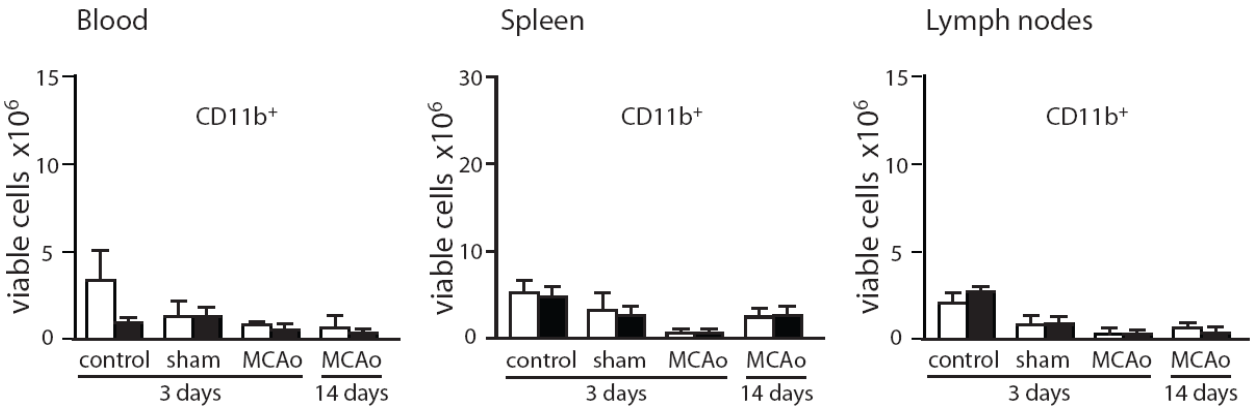

Fig 5. 15 Unaltered post-stroke levels of CD11b$^+$ cells after splenocytes transplantation

Cell suspensions from blood, spleen and lymph nodes were analyzed by FACS to retrieve an immune status 3 and 14 days after MCAo entailing splenocytes transplantation, respectively. No different numbers of CD11b$^+$ cells were measured between the splenocytes- (black bars) and the PBS-injected (white bars) groups. n = 5-8; (One-way ANOVA)

5.3 Fate of pericytes after cerebral ischemia

5.3.1 CC3-positive pericytes peak at day 3 after MCAo

Infiltration of immune cells into the central nervous system (CNS) enhancing neuroinflammation occurs via migration through the blood brain barrier (BBB). Macrophage recruitment into the ischemic brain tissue starts at day 3 after injury, marking the onset of CNS inflammation. As pericyte density is correlated with BBB leakage we were interested in their fate after cerebral ischemia.

C57BL/6 mice were subjected to 60 minutes MCAo and brains were harvested for immunohistochemical analysis after 1, 3, 5, 7, 14 and 28 days of reperfusion, respectively. Cryostat sections were prepared and stained for pericytes (CD13) and CC3. Consistently with the start of stroke-induced neuroinflammation numbers of CC3-positive pericytes were highly increased 3 days after ischemia (Fig 5.16). At days 14 and 28 after ischemia, the presence of massive CD13-immunfluorescence in the ischemic area impeded assessment of egg-shaped pericyte cell bodies.

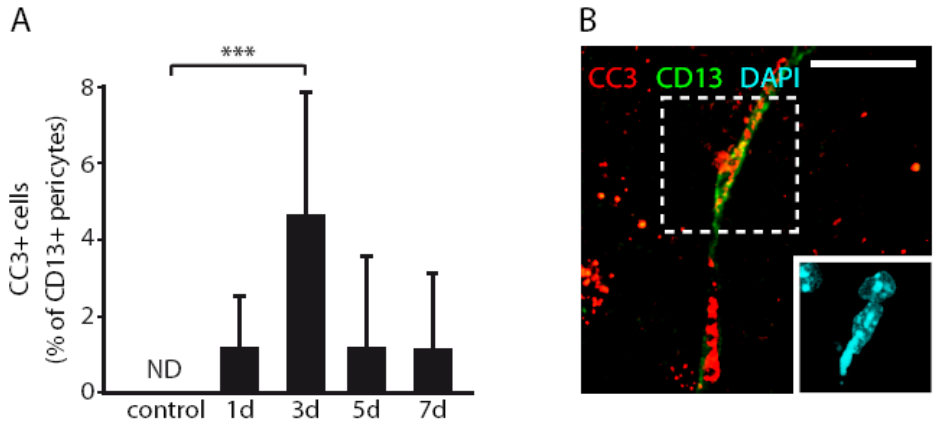

Fig 5. 16 Burst of cleaved caspase 3 (CC3)$^+$ CD13$^+$ pericytes at day 3 after MCAo

A. Quantification of the frequency of CC3$^+$ CD13$^+$ pericytes revealed a peak 3 days after MCAo. n = 3-5; *** p <0.005 (One-way ANOVA); ND, not detected

B. CC3/CD13-double-positive pericytes in the ischemic tissue at day 3 after reperfusion. The DAPI signal (shown in the inset) revealed condensed nuclear apoptotic bodies. scale bar = 20 µm

5.3.2 Increased levels of proliferating pericytes after MCAo

C57BL/6 mice were subjected to 60 minutes MCAo and cryostat sections were prepared from brains after 1, 3, 5, 7, 14 and 28 days of reperfusion, respectively, and stained for pericytes (CD13) and Ki67, a marker of mitotic cells to determine proliferation. As for CC3, again at day 3 after MCAo a significant increase of Ki67$^+$ CD13$^+$ cells was detected (Fig 5.17).

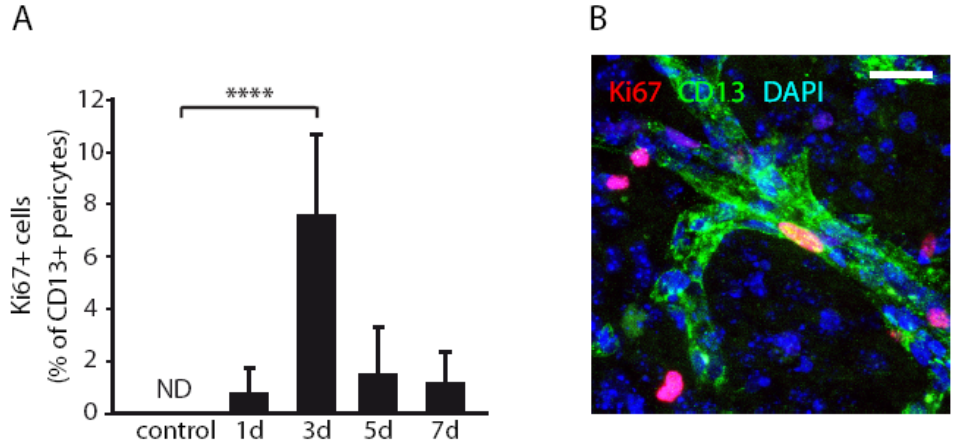

Fig 5. 17 Peak of proliferation of CD13$^+$ pericytes at day 3 after MCAo

A. Quantification of the frequency of Ki67$^+$ CD13$^+$ pericytes revealed a significant increase of proliferation 3 days after MCAo. n = 3-5; *** p < 0.0001 (One-way ANOVA); ND, not detected

B. Ki67/CD13-double-positive pericytes in a larger vessel in the ischemic tissue at day 3 after reperfusion. scale bar = 20 µm

6 DISCUSSION

Myeloid cells are the effector cells in cerebral ischemia. Resident microglia get activated inside the brain and peripheral macrophages and neutrophils are recruited to the central nervous system (CNS) after ischemic damage. A key role in these processes, and thereby modulating neuroinflammation, plays the nuclear factor (NF)-κB pathway. It is activated by the "inhibitor of κB (IκB) kinase" (IKK) via phosphorylation of IκB proteins, and moreover examines direct phosphorylation of p65 [30]. Transgenic and pharmacological approaches aim to inhibit the IKK2 subunit to block NF-κB activation. Hence we aimed to characterize a transgenic mouse model inactivating *Ikk2* specifically in the myeloid lineage. This mouse model could serve as a potent tool for investigating the role of microglia and macrophages in neurological disorders such as cerebral ischemia.

Cells infiltrating from the periphery into the brain parenchyma have to pass the blood brain barrier (BBB) that is regulated by pericytes encircling vascular endothelium. Enhanced secretion of chemokines and cytokines by microglia, up-regulation of adhesion molecules by endothelial cells, as well as migration of pericytes into the ischemic tissue contribute to the modulation of the BBB after stroke and may influence leukocyte migration into the CNS. Thus we investigated the fate of pericytes after cerebral ischemia.

Besides inflammation in the brain, immunologic depression in the periphery is a result of stroke, leading to massive decrease of lymphocytes and myeloid cells. It is a major cause of clinical post-stroke complications and mortality due to infections. We tried to reconstitute the debilitated peripheral immunity by transplanting immunocompetent cells into mice shortly after middle cerebral artery occlusion (MCAo). We tested the feasibility of splenocytes administration by tail vein injection into recipients and analyzed their impact on stroke outcome.

6.1 Conditional knockout of *Ikk2* in the myeloid cell lineage

To investigate the role of *Ikk2* in myeloid cells we chose the Cre/loxP system. We used the $Ikk2^{fl/fl}$ mouse in combination with a Cre recombinase (Cre) expressing mouse. This is the most

frequently analyzed and therefore best described mouse model in the scientific society for targeting *Ikk2* [59, 61-64, 70-72, 75]. Cell-specific gene targeting by utilizing the Cre/loxP system prevents embryonic lethality occurring in mice with conventional knockout of *Ikk2* or *Nemo*. Further, it has advantages compared to pharmacological compounds, which are mostly unspecific for the NF-κB pathway hence enforcing the requirement of high doses and entailing side effects. Non-steroidal anti-inflammatory drugs (NSAIDs) including aspirin and salicylates are known to be unspecific IKK inhibitors [22], and in the case of aspirin gastrointestinal side effects are well described [82]. Secondly, drug application can be a problem as for IKK2 inhibitor BMS-345541. Schwaninger et al. stated that this agent induces neuroprotective effects when injected intracerebroventricular, but not after intraperitoneal administration [83]. This would obligate physical injury of the brain during therapy. Further, conditional knockout enables to dissect the roles of NF-κB signaling in different cell types and developmental stages. An insight into the examinations using mouse models deleting *Ikk2* specifically in several cell lines, including B cells, T cells, keratinocytes, epithelial cells, neurons, glia, and myeloid cells was already given in chapter 3.3.3. There are numerous studies using different strategies of conditional gene manipulation of IKK subunits. Scientific setups targeting NEMO for conditional knockout demonstrated complete blockage of NF-κB activation suggesting a compensative role of IKK1/NEMO-consisting kinase complex in the absence of IKK2 [61, 62]. In other settings expression of a dominant-negative mutant or a constitutively active form of IKK2 specifically in neurons was achieved. These mice were both useful tools to investigate the role of *Ikk2*, underlining its neurotoxic contribution after cerebral ischemia [30, 83]. Alternative, expression of a competitive IκBα-super-repressor, mutated for its phosphorylation sites, under the control of several promoters revealed different levels of NF-κB blockade. In this system a strong promoter is of high importance to assure expression levels of the mutant IκBα overshooting the endogenous one [29, 84, 85].

To direct *Ikk2* deletion to the myeloid cell lineage we crossed the $Ikk2^{fl/fl}$ mouse with the Lysozyme M (LysM)-Cre mouse. In earlier studies, the population of myeloid cells has been targeted by several Cre-expressing mouse lines with differing recombination efficiency. The hunt for the ideal promoter to target myeloid cells specifically is still ongoing. CD11b-Cre mice showed a deletion rate of just 25 % in microglia and 50 % in macrophages in a model of amyotrophic lateral sclerosis (ALS) [86]. The CX_3CR1-Cre mouse is dealt to be a promising tool, but CX_3CR1-driven GFP expression was shown to be expressed on natural killer cells (NK) besides microglia and peripheral blood monocytes [87]. In our lab we tried to generate an Iba1-

Cre mouse without success to raise germ line chimera. Due to other reports the LysM-Cre mouse recombines about 75 % of bone marrow derived macrophages (BMDM) and peritoneal macrophages, but is less efficient in microglia (discussed below) [58, 69, 72]. To efficiently target Kupffer cells, the resident macrophages in the liver, Maeda et al. considered the inducible Mx1-Cre mouse to be useful, even though all cells in spleen and liver are hit by induction [75].

In summary, to get an insight into the role of NF-κB signaling in myeloid cells, and respecting issues of availability, the LysM-Cre Ikk2$^{fl/fl}$ mouse was the most adequate model for this study. Conversely to other groups we could not observe significant blockage of NF-κB when Cre was expressed heterozygously. Actually, in our model a significant loss of *Ikk2* at mRNA, protein and functional level was just detected when Cre was expressed on both alleles. It was described earlier that Cre recombination efficiency is proportional to the promoter activity [88], suggesting to be dependent on Cre expression levels. Thus, in our study, a gene dose effect was proposed and therefore a distinction was made between the LysM-Cre$^{+/-}$ Ikk2$^{fl/fl}$ and the LysM-Cre$^{+/+}$ Ikk2$^{fl/fl}$ mouse. "LysM-Cre Ikk2$^{fl/fl}$" was used as an umbrella term for both of them. Our *in vitro* results reveal nearly persistently intermediate levels of *Ikk2*-deficiency-dependent effects due to one copy of Cre compared to the non-Cre expressing control and the LysM-Cre$^{+/+}$ Ikk2$^{fl/fl}$ mouse.

As already mentioned in chapter 3.3.2, expression of two copies of Cre implicates a homozygous loss of the functional *LysM* gene (see also [55]). LysM is an enzyme with bactericidal activity. Akinbi et al. associated increased expression of LysM by transgenic mice with enhanced bacterial killing after microbial infection [89]. Others stated that LysM-deficient mice appeared healthy when normally housed, but that application of *Micrococcus luteus* resulted in increased inflammation in those mice [90]. Another *LysM* knockout study showed defects in bacterial clearance of *Pseudomonas aeruginosa* infections in *LysM*$^{-/-}$ mice but not *LysM*$^{+/-}$ mice [91]. Shimada et al. reported increased susceptibility to middle ear infection with *Streptococcus pneumoniae* in *LysM* knockout mice [92]. However, our results indicate the LysM-Cre$^{+/+}$ Ikk2$^{fl/fl}$ mouse to be more suitable for further research on the role of myeloid expressed *Ikk2*. To be able to exclude that in this mouse functional modifications in myeloid cells are provoked by the lack of LysM we analyzed an additional control, the LysM-Cre$^{+/+}$ (Ikk2$^{+/+}$) mouse, for selected aspects. This control mouse lacks LysM due to Cre expression on both alleles, but carries an unfloxed *Ikk2* gene. Effects in this mouse should therefore account for a *LysM*$^{-/-}$ but not an *Ikk2*$^{-/-}$ phenotype.

6.1.1 Ikk2 knockout efficiency in microglia and macrophages

We characterized the LysM-Cre Ikk2$^{fl/fl}$ mouse for *Ikk2* deletion in primary microglia cultures from neonatal mice and in cultured peritoneal macrophages from adult mice. Consistent with previous results [69], *Ikk2* mRNA levels in cultured microglia from LysM-Cre$^{+/-}$ Ikk2$^{fl/fl}$ mice were reduced to approx. 50 %, while in peritoneal macrophages a deletion efficiency of more than 90 % was detected. This is within the scope of *Ikk2* mRNA reduction in BMDM of about 75 % described by Greten et al. [72]. Again at the protein level we measured a stronger IKK2 depletion in macrophages than in microglia. Also in other scenarios differing recombination rates within various cell populations were observed: LysM-Cre-mediated deletion of the floxed *β polymerase* gene was demonstrated to take place in 79 % of BMDM, in 99 % of Gr-1 positive neutrophils, and in 30 % of CD11c-positive dendritic cells (DC) [52]. After diphtheria toxin (DTox)-mediated myeloid cell lineage ablation using the LysM-Cre/DTR mouse, macrophages, but not neutrophils were depleted successfully in wounds as well as in healthy tissue [57].

Promoter strength and gene expression is besides cell type specifity dependent on epigenetic regulation of transcription. Cho et al. suggested that LysM might be up-regulated in cultured and thereby basally activated microglia, considering stronger reduction of *Ikk2* mRNA levels in cultured microglia than in microglia directly isolated from neonatal mouse brains. They affirmed this theory by assessing increased recombination levels in microglia after LPS and kainic acid stimulation. Additionally they proposed a decrease of microglial *LysM* expression with aging, as microglia prepared from adult mice nearly did not display any *Ikk2* deletion [69]. Regarding these findings, it has to be considered that Cre recombination in CNS-resident microglia is less powerful than in peripheral macrophages in the LysM-Cre Ikk2$^{fl/fl}$ mouse *in vivo*, at least in the naïve state.

Aside from promoter strength and expression levels of Cre, knockout efficiency in the Cre/loxP system seems to be dependent on target gene accessibility. Clausen et al. achieved varying recombination rates of different floxed DNA sections: While LysM-dependent Cre-expression deleted the floxed *β polymerase* gene to 95 % in peritoneal macrophages, recombination of the floxed *Rfx5* did not exceed 84 % in the same cell population [52]. Additionally, incomplete deletion of *Ikk2* in the myeloid cell population of LysM-Cre Ikk2$^{fl/fl}$ mice might be a consequence of counterselection for *Ikk2*-deficient cells [93]. Limited gene knockout is often a

disadvantage of utilizing the Cre/loxP system. This drawback has to be accepted in order to examine cell type-specific functions of a distinct gene product.

As discussed above, the chase for the ideal promoter targeting myeloid cells is still ongoing. It is of use to find a possibility to target CNS-resident microglia and peripheral macrophages separately to clarify the pathogenic role of these populations, respectively. For successful therapeutic treatment it is crucial to define whether a distinct drug has to be facilitated or restrained to pass the BBB. Unfortunately, until present no definite marker was discovered to differentiate between microglia and macrophages. Hence, bone marrow chimera should be used to investigate the differing roles of these cell populations. Transplanting wild type bone marrow into lethally irradiated LysM-Cre $Ikk2^{fl/fl}$ mice would produce mice bearing *Ikk2*-mutant microglia/macrophages in the CNS. Inversely, LysM-Cre $Ikk2^{fl/fl}$ bone marrow transplanted into wild type mice would generate mice with *Ikk2*-depleted peripheral macrophages.

6.1.2 Impact on NF-κB signaling

To ascertain impaired kinase activity of IKK2 in LysM-Cre $Ikk2^{fl/fl}$ cells, we assessed nuclear translocation of NF-κB subunit p65 after LPS stimulation of microglia cultures, as LPS triggers the activation of the IKK complex. Most prominent in LysM-$Cre^{+/+}$ $Ikk2^{fl/fl}$ microglia we discovered a change in the ratio of cytoplasmic and nuclear fractions of p65. This confirms a potent disruption of the NF-κB signaling pathway in these cells. Equivalent, Cho et al. proved attenuated kinase activity of IKK2 in LysM-Cre $Ikk2^{fl/fl}$ mice by exhibition of decreased degradation of IκB after LPS stimulation [69]. Others detected diminished DNA binding of NF-κB, but not complete shutdown, in BMDMs from LysM-Cre $Ikk2^{fl/fl}$ mice by Electrophoretic Mobility Shift Assay (EMSA) [65, 72].

Levels of pro-inflammatory cytokines regulated by NF-κB, such as TNF-α and IL-1β, were shown to be down-regulated in microglia derived from LysM-Cre $Ikk2^{fl/fl}$ mice [69]. According to this, in our study attenuated secretion levels of TNF-α, IL-6 and NO were measured in microglia. While the effect is well-defined and gene-dose dependent in microglia, surprisingly cultures from peritoneal macrophages seem to behave highly variable and do not manifest inhibition of NF-κB-regulated gene expression. This is in contrast to the fact that ablation of IKK2 mRNA and protein levels is more prominent in macrophages than in microglia. *In vivo*

studies of other investigators revealed reduced mRNA levels of pro-inflammatory mediators including TNF-α, IL-6 and iNOS in injured tissue of LysM-Cre Ikk2$^{fl/fl}$ mice [69, 72]. Macrophages are believed to be the main sources of these molecules, suggesting that the behavior of cultured LysM-Cre Ikk2$^{fl/fl}$ macrophages does not fully reflect the situation *in vivo*. However, due to Greten et al. especially IL-1β plasma levels were elevated after LPS-induced endotoxic shock in LysM-Cre Ikk2$^{fl/fl}$ mice, proposing an *Ikk2*-driven regulation rather for IL-1β than TNF-α or IL-6 [63].

It was mentioned that in our analysis a strong variance was observed in the behavior of cultured macrophages. This possibly accounts for the variability in Cre expression and recombination efficiency in individual mice, an effect that might be balanced in microglia cultures pooled from several neonatal brains. This is underscored by enormous variations we obtained in spleen size in LysM-Cre Ikk2$^{fl/fl}$ mice and correlating increased proportions of splenic CD11b^{+} cells (discussed below). To prove and normalize for Cre variance, analysis of Cre expression levels by histology or FACS is imaginable. To avoid this time- and money-consuming characterization in each mouse, alternatively normalization to individual spleen weight would be a feasible possibility in future experiments.

Unchanged expression profiles of pro-inflammatory molecules in *Ikk2*-deficient macrophages suggest a switch from the so termed “classically activated” macrophages to M2 or “regulatory” macrophages in our *in vitro* assay. Research by Mosser and coworkers revealed that the latter population of macrophages is generated by activation of the Fc receptor for IgG (FcγR) additionally to stimulation of Toll-like receptors (TLRs) [94]. By these combined stimuli macrophages are reprogrammed to secrete high levels of IL-10 and down-regulate IL-12 production. As IL-10 can inhibit the production of several pro-inflammatory cytokines, these regulatory macrophages are suppressors of inflammation [95]. They retain the ability to produce pro-inflammatory cytokines and TNF-α secretion is not affected by FcγR-ligation [94, 96]. Since in our assay macrophages were cultured in the presence of fetal calf serum, FcγR-activation can be assumed. However, Hagemann et al. suggested a controversial role for IKK2 in macrophages co-cultured with tumor cells *in vitro*. In their experimental setup IL-10 was down-regulated and increased levels of IL-12 were measured after *Ikk2* deletion in the macrophage population, suggesting a switch from a M2 to a classically activated M1 phenotype [97].

In our examinations microscope observations revealed no visible changes of cultured macrophages due to IKK2 deletion. However, IKK2-depleted microglia displayed morphological changes and increased mortality after 2 days in culture compared to wild type cells. Thereby a behavioral discrepancy of microglia and macrophages is again manifested in our mouse model analogous to the pro-inflammatory secretion profile. As demonstrated in LysM-Cre$^{+/+}$ microglia, mortality was independent of *LysM*-deficiency. In further experiments applying the DNA-intercalating dyes acridine orange (AO) and ethidium bromide (EB) to cultured microglia, we did not discover any change in the kinetics of the dying cell fraction. However, total cell counts were reduced in *Ikk2*-mutant cultures. This is explained by the presence of cellular leftovers that could not be stained neither by AO nor EB staining at 24 and 48 hours after seeding. To estimate the kinetics of dying cells, shorter time periods between measuring points would have been required. However, in a second approach we noticed raised immune reactivity for cleaved caspase 3 (CC3) in cultured LysM-Cre Ikk2$^{fl/fl}$ microglia related to mitochondrial active cells as measured by MTT. We suggest that microglial mortality is caused by culture-induced stress and consequent basal cell activation. This is supported by our observation that cell death of cultured *Ikk2*-mutant microglia was even enhanced after stimulation with LPS, affirming the anti-apoptotic role of NF-κB activation.

Greten and coworkers made comparable observations in *Ikk2*-depleted macrophages. They measured increased levels of CC3 and caspase 1 in BMDM of the Mx1-Cre Ikk2$^{fl/fl}$ mouse. Increased caspase 1 expression seems to be responsible for elevated cleavage of pro-IL-1β and resulting increased IL-1β plasma levels leading to endotoxic shock in this mouse model [63]. In another study they further indicated that activation with LPS induces apoptosis in BMDMs lacking nuclear p65 due to IKK2-deficiency [65]. NF-κB- and p38-dependent anti-apoptotic genes such as PAI-2 and Bfl-1/A1 were shown to be responsible for inhibition of LPS-induced apoptosis in macrophages. Blocking the expression of these genes might be the mechanism used by the anthrax bacterium *Bacillus anthracis* to evade immune response [66]. Reintroduction of PAI-2 into *Ikk2*-depleted BMDM inhibited LPS-induced apoptosis as well as elevated plasma levels of IL-1β after LPS-injection in mice [63]. Bruey et al. described the NF-κB-regulated anti-apoptotic gene Bcl-X^{L} to suppress caspase-1 activation and to negatively regulate IL-1β production in macrophages and neutrophils [98]. In addition, an anti-apoptotic role for *Ikk2* was observed in other cell types than macrophages and microglia. Enterocytes lacking *Ikk2* underwent massive apoptosis in the model of colitis-associated cancer caused by attenuated

induction of Bcl-X^L [72]. *Ikk2*-depletion in intestinal epithelial cells lead to apoptosis and loss of integrity of the intestinal mucosa after gut ischemia-reperfusion [70].

6.1.3 Unchanged phagocytosis

Macrophages have an important role in clearance of senescent apoptotic neutrophils [14, 57]. We hypothesized that the phagocytic potential of *Ikk2*-depleted microglia and macrophages could be impaired, since we found elevated levels of Ly-$6G^+$ neutrophils in spleens from LysM-Cre $Ikk2^{fl/fl}$ mice. However, we measured unchanged phagocytic activity by *Ikk2*-mutant microglia and macrophages after 1 hour compared to control cells. Consistently with our results, another group could neither detect abnormalities in the potential of bacterial ingestion by LysM-Cre $Ikk2^{fl/fl}$ BMDM [93]. Greenberg and Grinstein reviewed several signaling events involved in phagocytosis independent of the NF-κB pathway, including Fc receptors, phosphatidylinositol 3 (PI3) kinase, protein kinase C, MEK1 and ERK [99]. Other phagocytic mechanisms are dependent on the complement system including complement receptors 1, 3 and 4 or on mannose receptors. GTPases of the Rho family are thought to be involved in regulation of the actin cytoskeleton and the GTPases rab5 and rab7 seem to trigger maturation of the phagosome and the fusion of the latter with endosomes [100]. Underhill et al. discovered the expression of TLR2 in the phagolysosome after ingestion of the yeast cell-wall particle zymosan, which is accompanied by NF-κB activation and TNF-α secretion. However, further experiments in this study, using a mutant form of TLR2, disproved a correlation between particle internalization and the induction of NF-κB [101]. In summary and corresponding with the literature, our results suggest that NF-κB signaling is not responsible for regulation of phagocytosis. Thus neutrophilia in LysM-Cre $Ikk2^{fl/fl}$ mice is not caused by impaired phagocytic activity of macrophages.

6.1.4 Splenomegaly

We noticed that LysM-Cre $Ikk2^{fl/fl}$ mice exhibit splenomegaly and their lymph nodes are enlarged aggravating over age. We further measured elevated numbers of myeloid cells ($CD11b^+$) in spleens from aged LysM-Cre $Ikk2^{fl/fl}$ mice, the group exhibiting extensively higher spleen weights. Splenomegaly was also observed in *RelB*-deficient mice by Weih et al. In agreement with our data they determined increased hematopoiesis and myeloid hyperplasia in spleen as a

reason for enlargement of this organ [102]. In our mouse model counts of the myeloid population could be directly correlated to individual spleen weights. As discussed above, this could be explained by variance in Cre expression in examined individuals. Expansion of myeloid cells is thought to compensate for a loss of function in this population due to *Ikk2* deletion. This would also explain enlarged spleens detected in the Mx1-Cre Ikk2$^{fl/fl}$ mouse by Greten and coworkers [63].

Having a closer look to myeloid subpopulations we found CD11b^{+} Ly-6C^{high}, CD11b^{+} Ly-6C^{int}, CD11b^{+} Ly-6G^{+}, and CD11b^{+} CD44^{+} splenocytes to be expanded. CD11b^{+} Ly-6C^{high} cells were defined by Geissmann et al. to be "inflammatory" monocytes originating from bone marrow and giving rise to CD11b^{+} Ly-6C^{low} "circulating" monocytes/macrophages [103, 104]. Others stated that under inflammatory conditions Ly-6C^{high} monocytes infiltrate the injured tissue without maturating into the Ly-6C^{low} population. They identified the spleen to be a reservoir of these monocytes, which exit in the case of injury [105]. In our model, IKK2 ablation may lead to functional insufficiency of Ly-6C^{high} monocytes and/or switch to "regulatory" monocytes and macrophages (M2). Compensatory proliferation of the CD11b^{+} Ly-6C^{high} cell population would be a logical consequence and an explanation for their raised cell numbers.

Neutrophilia, as characterized by increased numbers of Ly-6G^{+} or Ly-6C^{int} neutrophilic cells, was observed earlier in transgenic mice without functional macrophages. The cause might be an impaired role of macrophages in clearing short-lived neutrophils to resolve inflammation [57]. Our *in vitro* results disprove that reduced phagocytic abilities are responsible for this effect. Consistently with our discoveries, other models characterized by impaired or absent macrophages exhibited neutrophilia: In the LysM-Cre/DTR mouse macrophages were depleted in wounds and healthy tissue accompanied with elevated expression of Ly-6G in skin lesions. [57]. Moreover, a novel genetic model lacking splenic marginal zone, bone marrow, and thioglycollate-elicited peritoneal macrophages (LysM-Cre c-FLIP$^{fl/fl}$ mouse) entailed splenomegaly accompanied by increased numbers of Ly-6C^{int} neutrophils and Ly-6C^{high} monocytes in spleens and blood. Ly-6C^{low} counts were reported to be normal as in our setting [106].

Lastly, we detected increased levels of CD11b^{+} CD44^{+} cells in enlarged spleens. CD44 is a transmembrane glycoprotein binding hyaluronan (HA) and is expressed on the cell-surface of almost every cell type. HA is a major component of the extracellular matrix and is highly

expressed during tissue injury and wound healing. It regulates several mechanisms of tissue repair, such as activating inflammatory cells and regulating the response of epithelial cells and fibroblasts. HA-CD44 interactions are important for various processes, such as development, induction and resolution of inflammation, T cell activation and tumor growth. [107]. CD44 was described to play an important role in resolution of inflammation and to be induced in infarcted myocardium localized on infiltrating leukocytes, fibroblasts and vascular cells [107-109]. Hence we believe that increased expression of CD44 in spleens of *Ikk2*-mutant animals stands for an inflammatory condition caused by attenuated innate immunity provoked by *Ikk2* disruption. Finally, considering the cellular constellation detected in the LysM-Cre$^{+/+}$ controls, a contributing effect of the *LysM* knockout cannot totally be excluded. Values of examined CD11b^{+} populations are increased by trend in this animal group, especially affecting Ly-6C^{high} and CD44^{+} populations. Consequently, these markers might be a sign of a subsymptomatic infection provoked by loss of *Ikk2* and/or *LysM* function.

6.2 Splenocytes transplantation

Cell-based therapy for neurological disorders can be categorized into two strategies. One is the introduction of exogenous cells into the injured brain to replace lost cells or support the remaining ones. Another strategy is to affect the peripheral effector cells participating in CNS damage and, regarding cerebral ischemia, in post-stroke immunosuppression. Walker et al. suggested that injected stem cells might exert their neuroprotective effects by modulating the systemic inflammatory response, since the percentage of transplanted cells indeed reaching the CNS is vanishing small [110]. We injected splenocytes after MCAo to test the feasibility of future gene therapeutic approaches, including transplantation of genetic engineered cell populations as stroke therapy. The site of action of the transferred splenocytes could be in the CNS and/or in the periphery. We used splenocytes instead of bone marrow cells - as used for example in autologous stem cell therapy - to avoid that not only mature “inflammatory” monocytes but also their precursors are transferred. Ly-6C^{high} monocytic precursors present in bone marrow were shown to give also rise to Ly-6C^{low} “patrolling” or “wound healing” monocytes besides mature Ly-6C^{high} “inflammatory” ones as present in spleen [104].

We injected the splenocytes intravenously taking into account the possibility of transplanted cells being trapped in the lung as first pass effect [111, 112]. It has to be assumed that accumulation of mononuclear splenocytes in the lung could account for induced immune response in pulmonary tissue. It was shown for mesenchymal stromal cells (MSCs) embolized in the lungs that they could still exert their anti-inflammatory role [113]. If the impact of transplanted cells is caused by a local effect in the CNS, intra-arterial injection might be an alternative method in terms of cellular survival and engraftment [114], to circumvent the risk of transplanted cells getting trapped in filtering organs like the lung.

In our experimental setup we could not replenish the loss of peripheral immune cells reported by Prass et al. [16]. Leukocyte composition of spleen, lymph nodes and blood was not different compared to vehicle transplanted mice. Additional *ex vivo* experiments in our lab revealed that immunologic functionality was not changed in spleen, lymph node, and blood cells [115]. It would be of further interest, if bacterial burden in the lungs is affected by splenocytes transplantation.

Besides the potential role in the periphery, injected splenocytes could also have a direct neuroprotective effect [116-118] by production of specific neurotrophic factors (e.g. brain-derived neurotrophic factor) by T cells, and by the proper activation of microglia/macrophages. On the other hand transient elimination of naturally occurring regulatory $CD4^+$ $CD25^+$ T cells showed a benefit for the recovery from CNS injury [119]. In our setting we could not detect an impact on infarct size due to an effect of the transplanted splenocytes, although spleen atrophy was shown earlier to be correlated to the extent of the brain damage [120] and Ajmo et al. could demonstrate that splenectomy was neuroprotective in stroke [121]. However, we showed that post-stroke transplantation of splenocytes per se does not induce detrimental effects in the recipient mice. This represents an important observation for future gene therapeutic approaches including transplantation of genetic engineered splenocytes or cellular subpopulations.

6.3 Fate of pericytes after stroke

After cerebral ischemia massive infiltration of immune cells by crossing the BBB contributes to inflammation in the brain. The importance of brain pericytes presenting a fundamental element

of the neurovascular unit and affecting the function of the BBB is emerging. They seem to regulate endothelial permeability assuring the restriction to the periphery by the BBB [3]. The response of pericytes to an ischemic insult is poorly understood.

Using immunofluorescence we aimed to investigate the fate and dynamics of pericytes/mural cells up to 28 days after MCAo. Shortly after cerebral ischemia pericytes undergo apoptosis as shown by increased numbers of $CC3^+$ $CD13^+$ pericytes 3 days after MCAo. Similar, in a model of superior mesenteric artery occlusion pericytes were shown to be sensitive to anoxia [122]. Romeo et al. described NF-κB activation going along with pericyte apoptosis [123]. A correlation of NF-κB nuclear translocation and $CC3^+$ positive pericytes was also shown by our group after cerebral ischemia [124].

Increased levels of Ki67 at 3 days after MCAo indicates an onset of proliferation of pericytes positive for $CD13^+$ [125]. Proliferation of pericytes was also observed after spinal cord injury by Göritz et al. They further showed that the proliferating pericytes lose contact with the vessels and invade the surrounding tissue giving rise to stromal cells and participating in scar formation [126]. Others discovered detachment of pericytes from the blood vessels after MCAo [127]. Additional experiments in our lab suggest that proliferating pericytes indeed differentiate into stromal cells and are involved in scar formation after cerebral ischemia [124].

It has to be considered that stromal cells are immunocompetent cells and potentially suppress neuroinflammation [128]. Hence it is of high interest, if an expanding stromal cell population in the CNS affects stroke outcome. Further examination should clarify, whether therapeutic strategies modulating brain pericytes/stromal cells after cerebral ischemia are an option to mediate neuroregenerative consequences.

6.4 Conclusion

To sum up, we showed the feasibility of depleting *Ikk2* specifically in the myeloid cell population using the LysM-Cre $Ikk2^{fl/fl}$ mouse. Overall, expected consequences were detected at the DNA, mRNA, and protein as well as at the functional level regarding inhibited NF-κB activation and subsequent remodelling of gene expression. However, neither in microglia nor in

peripheral macrophages ablation of IKK2 was complete, indicating both leakiness and variance of the Cre/loxP system in this model. Furthermore, *in vitro* observations might not fully reflect the situation *in vivo*. Thus, for the future use and interpretation of the outcome of the LysM-Cre Ikk2$^{fl/fl}$ mouse in disease models like MCAo or experimental autoimmune encephalomyelitis (EAE), extended *in vivo* characterization of the naïve mouse is required. This is also requisite to explain splenomegaly and the exact role of the combined phenotype regarding the lack of *Ikk2* and *LysM* in the LysM-Cre$^{+/+}$ Ikk2$^{fl/fl}$ mouse. Besides, we demonstrated in this study that transplantation of mixed splenocytes does not affect infarct size and immunodepression in a model of focal cerebral ischemia. Beyond doubt transplantation of isolated splenic subpopulations in this context is outstanding. Finally, we affirmed that brain pericytes are highly sensitive to cerebral ischemia. However, further examinations will have to clarify, whether these cells influence the passage of peripheral immune cells into the brain after stroke.

7 REFERENCES

1. Carson, M.J., et al., *CNS immune privilege: hiding in plain sight.* Immunol Rev, 2006. **213**: p. 48-65.
2. Guillemin, G.J. and B.J. Brew, *Microglia, macrophages, perivascular macrophages, and pericytes: a review of function and identification.* J Leukoc Biol, 2004. **75**(3): p. 388-97.
3. Armulik, A., et al., *Pericytes regulate the blood-brain barrier.* Nature. **468**(7323): p. 557-61.
4. Owens, T., I. Bechmann, and B. Engelhardt, *Perivascular spaces and the two steps to neuroinflammation.* J Neuropathol Exp Neurol, 2008. **67**(12): p. 1113-21.
5. Hara, H., et al., *Identification of astrocyte-derived immune suppressor factor that induces apoptosis of autoreactive T cells.* J Neuroimmunol, 2011. **233**(1): p. 135-146.
6. Koedel, U., et al., *Acute brain injury triggers MyD88-dependent, TLR2/4-independent inflammatory responses.* Am J Pathol, 2007. **171**(1): p. 200-13.
7. Dirnagl, U., C. Iadecola, and M.A. Moskowitz, *Pathobiology of ischaemic stroke: an integrated view.* Trends Neurosci, 1999. **22**(9): p. 391-7.
8. Kriz, J. and M. Lalancette-Hebert, *Inflammation, plasticity and real-time imaging after cerebral ischemia.* Acta Neuropathol, 2009. **117**(5): p. 497-509.
9. Salminen, A., P.K. Liu, and C.Y. Hsu, *Alteration of transcription factor binding activities in the ischemic rat brain.* Biochem Biophys Res Commun, 1995. **212**(3): p. 939-44.
10. Schneider, A., et al., *NF-kappaB is activated and promotes cell death in focal cerebral ischemia.* Nat Med, 1999. **5**(5): p. 554-9.
11. O'Neill, L.A. and C. Kaltschmidt, *NF-kappa B: a crucial transcription factor for glial and neuronal cell function.* Trends Neurosci, 1997. **20**(6): p. 252-8.
12. Zheng, Z. and M.A. Yenari, *Post-ischemic inflammation: molecular mechanisms and therapeutic implications.* Neurol Res, 2004. **26**(8): p. 884-92.
13. Wang, Q., X.N. Tang, and M.A. Yenari, *The inflammatory response in stroke.* J Neuroimmunol, 2007. **184**(1-2): p. 53-68.
14. Jin, R., G. Yang, and G. Li, *Inflammatory mechanisms in ischemic stroke: role of inflammatory cells.* J Leukoc Biol, 2010. **87**(5): p. 779-89.
15. Meisel, C., et al., *Central nervous system injury-induced immune deficiency syndrome.* Nat Rev Neurosci, 2005. **6**(10): p. 775-86.

16. Prass, K., et al., *Stroke-induced immunodeficiency promotes spontaneous bacterial infections and is mediated by sympathetic activation reversal by poststroke T helper cell type 1-like immunostimulation.* J Exp Med, 2003. **198**(5): p. 725-36.
17. Longa, E.Z., et al., *Reversible middle cerebral artery occlusion without craniectomy in rats.* Stroke, 1989. **20**(1): p. 84-91.
18. O'Neill, M.J. and J.A. Clemens, *Rodent models of focal cerebral ischemia.* Curr Protoc Neurosci, 2001. **Chapter 9**: p. Unit9 6.
19. Engel, O., et al., *Modeling stroke in mice - middle cerebral artery occlusion with the filament model.* J Vis Exp, 2011. **6**(47): p. e2423, DOI: 10.3791/2423.
20. Howells, D.W., et al., *Different strokes for different folks: the rich diversity of animal models of focal cerebral ischemia.* J Cereb Blood Flow Metab, 2010. **30**(8): p. 1412-31.
21. Perkins, N.D., *Integrating cell-signalling pathways with NF-kappaB and IKK function.* Nat Rev Mol Cell Biol, 2007. **8**(1): p. 49-62.
22. Karin, M., Y. Yamamoto, and Q.M. Wang, *The IKK NF-kappa B system: a treasure trove for drug development.* Nat Rev Drug Discov, 2004. **3**(1): p. 17-26.
23. Hayden, M.S. and S. Ghosh, *Signaling to NF-kappaB.* Genes Dev, 2004. **18**(18): p. 2195-224.
24. Terai, K., et al., *Enhancement of immunoreactivity for NF-kappa B in human cerebral infarctions.* Brain Res, 1996. **739**(1-2): p. 343-9.
25. Nurmi, A., et al., *Nuclear factor-kappaB contributes to infarction after permanent focal ischemia.* Stroke, 2004. **35**(4): p. 987-91.
26. Ridder, D.A. and M. Schwaninger, *NF-kappaB signaling in cerebral ischemia.* Neuroscience, 2009. **158**(3): p. 995-1006.
27. Huang, C.Y., et al., *SOD1 down-regulates NF-kappaB and c-Myc expression in mice after transient focal cerebral ischemia.* J Cereb Blood Flow Metab, 2001. **21**(2): p. 163-73.
28. Xu, L., et al., *Recombinant adenoviral expression of dominant negative IkappaBalpha protects brain from cerebral ischemic injury.* Biochem Biophys Res Commun, 2002. **299**(1): p. 14-7.
29. Zhang, W., et al., *Neuronal activation of NF-kappaB contributes to cell death in cerebral ischemia.* J Cereb Blood Flow Metab, 2005. **25**(1): p. 30-40.
30. Herrmann, O., et al., *IKK mediates ischemia-induced neuronal death.* Nat Med, 2005. **11**(12): p. 1322-9.

31. Regnier, C.H., et al., *Identification and characterization of an IkappaB kinase.* Cell, 1997. **90**(2): p. 373-83.
32. Bonizzi, G. and M. Karin, *The two NF-kappaB activation pathways and their role in innate and adaptive immunity.* Trends Immunol, 2004. **25**(6): p. 280-8.
33. Israel, A., *The IKK complex, a central regulator of NF-kappaB activation.* Cold Spring Harb Perspect Biol, 2010. **2**(3): p. a000158.
34. Perkins, N.D. and T.D. Gilmore, *Good cop, bad cop: the different faces of NF-kappaB.* Cell Death Differ, 2006. **13**(5): p. 759-72.
35. Chu, W.M., et al., *JNK2 and IKKbeta are required for activating the innate response to viral infection.* Immunity, 1999. **11**(6): p. 721-31.
36. Hu, Y., et al., *Abnormal morphogenesis but intact IKK activation in mice lacking the IKKalpha subunit of IkappaB kinase.* Science, 1999. **284**(5412): p. 316-20.
37. Schmid, J.A. and A. Birbach, *IkappaB kinase beta (IKKbeta/IKK2/IKBKB)--a key molecule in signaling to the transcription factor NF-kappaB.* Cytokine Growth Factor Rev, 2008. **19**(2): p. 157-65.
38. Chen, L.F. and W.C. Greene, *Shaping the nuclear action of NF-kappaB.* Nat Rev Mol Cell Biol, 2004. **5**(5): p. 392-401.
39. Sakurai, H., et al., *Tumor necrosis factor-alpha-induced IKK phosphorylation of NF-kappaB p65 on serine 536 is mediated through the TRAF2, TRAF5, and TAK1 signaling pathway.* J Biol Chem, 2003. **278**(38): p. 36916-23.
40. Li, Z.W., et al., *The IKKbeta subunit of IkappaB kinase (IKK) is essential for nuclear factor kappaB activation and prevention of apoptosis.* J Exp Med, 1999. **189**(11): p. 1839-45.
41. Rudolph, D., et al., *Severe liver degeneration and lack of NF-kappaB activation in NEMO/IKKgamma-deficient mice.* Genes Dev, 2000. **14**(7): p. 854-62.
42. Senftleben, U., et al., *Activation by IKKalpha of a second, evolutionary conserved, NF-kappa B signaling pathway.* Science, 2001. **293**(5534): p. 1495-9.
43. Gerondakis, S., et al., *Unravelling the complexities of the NF-kappaB signalling pathway using mouse knockout and transgenic models.* Oncogene, 2006. **25**(51): p. 6781-99.
44. Beg, A.A., et al., *Embryonic lethality and liver degeneration in mice lacking the RelA component of NF-kappa B.* Nature, 1995. **376**(6536): p. 167-70.
45. Doi, T.S., et al., *Absence of tumor necrosis factor rescues RelA-deficient mice from embryonic lethality.* Proc Natl Acad Sci U S A, 1999. **96**(6): p. 2994-9.

46. Alcamo, E., et al., *Targeted mutation of TNF receptor I rescues the RelA-deficient mouse and reveals a critical role for NF-kappa B in leukocyte recruitment.* J Immunol, 2001. **167**(3): p. 1592-600.

47. Kuhn, R. and F. Schwenk, *Advances in gene targeting methods.* Curr Opin Immunol, 1997. **9**(2): p. 183-8.

48. Sternberg, N. and D. Hamilton, *Bacteriophage P1 site-specific recombination. I. Recombination between loxP sites.* J Mol Biol, 1981. **150**(4): p. 467-86.

49. Hoess, R.H., M. Ziese, and N. Sternberg, *P1 site-specific recombination: nucleotide sequence of the recombining sites.* Proc Natl Acad Sci U S A, 1982. **79**(11): p. 3398-402.

50. Sauer, B., *Functional expression of the cre-lox site-specific recombination system in the yeast Saccharomyces cerevisiae.* Mol Cell Biol, 1987. **7**(6): p. 2087-96.

51. Sauer, B. and N. Henderson, *Site-specific DNA recombination in mammalian cells by the Cre recombinase of bacteriophage P1.* Proc Natl Acad Sci U S A, 1988. **85**(14): p. 5166-70.

52. Clausen, B.E., et al., *Conditional gene targeting in macrophages and granulocytes using LysMcre mice.* Transgenic Res, 1999. **8**(4): p. 265-77.

53. Cross, M., et al., *Mouse lysozyme M gene: isolation, characterization, and expression studies.* Proc Natl Acad Sci U S A, 1988. **85**(17): p. 6232-6.

54. Faust, N., et al., *Insertion of enhanced green fluorescent protein into the lysozyme gene creates mice with green fluorescent granulocytes and macrophages.* Blood, 2000. **96**(2): p. 719-26.

55. Sinha, P., et al., *Mouse lysozyme-M knockout mice reveal how the self-determinant hierarchy shapes the T cell repertoire against this circulating self antigen in wild-type mice.* J Immunol, 2004. **173**(3): p. 1763-71.

56. Gu, H., et al., *Deletion of a DNA polymerase beta gene segment in T cells using cell type-specific gene targeting.* Science, 1994. **265**(5168): p. 103-6.

57. Goren, I., et al., *A transgenic mouse model of inducible macrophage depletion: effects of diphtheria toxin-driven lysozyme M-specific cell lineage ablation on wound inflammatory, angiogenic, and contractive processes.* Am J Pathol, 2009. **175**(1): p. 132-47.

58. Prinz, M., et al., *Distinct and nonredundant in vivo functions of IFNAR on myeloid cells limit autoimmunity in the central nervous system.* Immunity, 2008. **28**(5): p. 675-86.

59. Pasparakis, M., et al., *TNF-mediated inflammatory skin disease in mice with epidermis-specific deletion of IKK2.* Nature, 2002. **417**(6891): p. 861-6.

60. Schwenk, F., U. Baron, and K. Rajewsky, *A cre-transgenic mouse strain for the ubiquitous deletion of loxP-flanked gene segments including deletion in germ cells.* Nucleic Acids Res, 1995. **23**(24): p. 5080-1.

61. Pasparakis, M., M. Schmidt-Supprian, and K. Rajewsky, *IkappaB kinase signaling is essential for maintenance of mature B cells.* J Exp Med, 2002. **196**(6): p. 743-52.

62. Schmidt-Supprian, M., et al., *Mature T cells depend on signaling through the IKK complex.* Immunity, 2003. **19**(3): p. 377-89.

63. Greten, F.R., et al., *NF-kappaB is a negative regulator of IL-1beta secretion as revealed by genetic and pharmacological inhibition of IKKbeta.* Cell, 2007. **130**(5): p. 918-31.

64. Ruocco, M.G., et al., *I{kappa}B kinase (IKK){beta}, but not IKK{alpha}, is a critical mediator of osteoclast survival and is required for inflammation-induced bone loss.* J Exp Med, 2005. **201**(10): p. 1677-87.

65. Park, J.M., et al., *Macrophage apoptosis by anthrax lethal factor through p38 MAP kinase inhibition.* Science, 2002. **297**(5589): p. 2048-51.

66. Park, J.M., et al., *Signaling pathways and genes that inhibit pathogen-induced macrophage apoptosis--CREB and NF-kappaB as key regulators.* Immunity, 2005. **23**(3): p. 319-29.

67. Greve, B., et al., *I kappa B kinase 2/beta deficiency controls expansion of autoreactive T cells and suppresses experimental autoimmune encephalomyelitis.* J Immunol, 2007. **179**(1): p. 179-85.

68. van Loo, G., et al., *Inhibition of transcription factor NF-kappaB in the central nervous system ameliorates autoimmune encephalomyelitis in mice.* Nat Immunol, 2006. **7**(9): p. 954-61.

69. Cho, I.H., et al., *Role of microglial IKKbeta in kainic acid-induced hippocampal neuronal cell death.* Brain, 2008. **131**(Pt 11): p. 3019-33.

70. Chen, L.W., et al., *The two faces of IKK and NF-kappaB inhibition: prevention of systemic inflammation but increased local injury following intestinal ischemia-reperfusion.* Nat Med, 2003. **9**(5): p. 575-81.

71. Luedde, T., et al., *Deletion of IKK2 in hepatocytes does not sensitize these cells to TNF-induced apoptosis but protects from ischemia/reperfusion injury.* J Clin Invest, 2005. **115**(4): p. 849-59.

72. Greten, F.R., et al., *IKKbeta links inflammation and tumorigenesis in a mouse model of colitis-associated cancer.* Cell, 2004. **118**(3): p. 285-96.

73. Lin, W.W. and M. Karin, *A cytokine-mediated link between innate immunity, inflammation, and cancer.* J Clin Invest, 2007. **117**(5): p. 1175-83.
74. Mantovani, A., *Cancer: Inflaming metastasis.* Nature, 2009. **457**(7225): p. 36-7.
75. Maeda, S., et al., *IKKbeta couples hepatocyte death to cytokine-driven compensatory proliferation that promotes chemical hepatocarcinogenesis.* Cell, 2005. **121**(7): p. 977-90.
76. Bollrath, J. and F.R. Greten, *IKK/NF-kappaB and STAT3 pathways: central signalling hubs in inflammation-mediated tumour promotion and metastasis.* EMBO Rep, 2009. **10**(12): p. 1314-9.
77. Burgess, A.W., et al., *Purification of two forms of colony-stimulating factor from mouse L-cell-conditioned medium.* J Biol Chem, 1985. **260**(29): p. 16004-11.
78. Mosmann, T., *Rapid colorimetric assay for cellular growth and survival: application to proliferation and cytotoxicity assays.* J Immunol Methods, 1983. **65**(1-2): p. 55-63.
79. Dirnagl, U., *Standard operating procedures (SOP) in experimental stroke research: SOP for middle cerebral artery occlusion in the mouse.* Nature Precedings, 2010 (<http://dx.doi.org/10.1038/npre.2010.3492.2>)
80. Endres, M., et al., *DNA methyltransferase contributes to delayed ischemic brain injury.* J Neurosci, 2000. **20**(9): p. 3175-81.
81. Endres, M., et al., *Neuroprotective effects of gelsolin during murine stroke.* J Clin Invest, 1999. **103**(3): p. 347-54.
82. Hirsh, J., *Progress review: the relationship between dose of aspirin, side-effects and antithrombotic effectiveness.* Stroke, 1985. **16**(1): p. 1-4.
83. Schwaninger, M., I. Inta, and O. Herrmann, *NF-kappaB signalling in cerebral ischaemia.* Biochem Soc Trans, 2006. **34**(Pt 6): p. 1291-4.
84. Voll, R.E., et al., *NF-kappa B activation by the pre-T cell receptor serves as a selective survival signal in T lymphocyte development.* Immunity, 2000. **13**(5): p. 677-89.
85. Jimi, E., et al., *Activation of NF-kappaB promotes the transition of large, CD43+ pre-B cells to small, CD43- pre-B cells.* Int Immunol, 2005. **17**(6): p. 815-25.
86. Boillee, S., et al., *Onset and progression in inherited ALS determined by motor neurons and microglia.* Science, 2006. **312**(5778): p. 1389-92.
87. Jung, S., et al., *Analysis of fractalkine receptor CX(3)CR1 function by targeted deletion and green fluorescent protein reporter gene insertion.* Mol Cell Biol, 2000. **20**(11): p. 4106-14.
88. Araki, K., et al., *Efficiency of recombination by Cre transient expression in embryonic stem cells: comparison of various promoters.* J Biochem, 1997. **122**(5): p. 977-82.

89. Akinbi, H.T., et al., *Bacterial killing is enhanced by expression of lysozyme in the lungs of transgenic mice.* J Immunol, 2000. **165**(10): p. 5760-6.

90. Ganz, T., et al., *Increased inflammation in lysozyme M-deficient mice in response to Micrococcus luteus and its peptidoglycan.* Blood, 2003. **101**(6): p. 2388-92.

91. Cole, A.M., et al., *Decreased clearance of Pseudomonas aeruginosa from airways of mice deficient in lysozyme M.* J Leukoc Biol, 2005. **78**(5): p. 1081-5.

92. Shimada, J., et al., *Lysozyme M deficiency leads to an increased susceptibility to Streptococcus pneumoniae-induced otitis media.* BMC Infect Dis, 2008. **8**: p. 134.

93. Kanters, E., et al., *Inhibition of NF-kappaB activation in macrophages increases atherosclerosis in LDL receptor-deficient mice.* J Clin Invest, 2003. **112**(8): p. 1176-85.

94. Gerber, J.S. and D.M. Mosser, *Reversing lipopolysaccharide toxicity by ligating the macrophage Fc gamma receptors.* J Immunol, 2001. **166**(11): p. 6861-8.

95. Mosser, D.M. and J.P. Edwards, *Exploring the full spectrum of macrophage activation.* Nat Rev Immunol, 2008. **8**(12): p. 958-69.

96. Mosser, D.M., *The many faces of macrophage activation.* J Leukoc Biol, 2003. **73**(2): p. 209-12.

97. Hagemann, T., et al., *"Re-educating" tumor-associated macrophages by targeting NF-kappaB.* J Exp Med, 2008. **205**(6): p. 1261-8.

98. Bruey, J.M., et al., *Bcl-2 and Bcl-XL regulate proinflammatory caspase-1 activation by interaction with NALP1.* Cell, 2007. **129**(1): p. 45-56.

99. Greenberg, S. and S. Grinstein, *Phagocytosis and innate immunity.* Curr Opin Immunol, 2002. **14**(1): p. 136-45.

100. Aderem, A. and D.M. Underhill, *Mechanisms of phagocytosis in macrophages.* Annu Rev Immunol, 1999. **17**: p. 593-623.

101. Underhill, D.M., et al., *The Toll-like receptor 2 is recruited to macrophage phagosomes and discriminates between pathogens.* Nature, 1999. **401**(6755): p. 811-5.

102. Weih, F., et al., *Multiorgan inflammation and hematopoietic abnormalities in mice with a targeted disruption of RelB, a member of the NF-kappa B/Rel family.* Cell, 1995. **80**(2): p. 331-40.

103. Sunderkotter, C., et al., *Subpopulations of mouse blood monocytes differ in maturation stage and inflammatory response.* J Immunol, 2004. **172**(7): p. 4410-7.

104. Geissmann, F., et al., *Development of monocytes, macrophages, and dendritic cells.* Science, 2010. **327**(5966): p. 656-61.

105. Swirski, F.K., et al., *Identification of splenic reservoir monocytes and their deployment to inflammatory sites.* Science, 2009. **325**(5940): p. 612-6.

106. Gordy, C., et al., *Regulation of steady-state neutrophil homeostasis by macrophages.* Blood. **117**(2): p. 618-29.

107. Jiang, D., J. Liang, and P.W. Noble, *Hyaluronan as an immune regulator in human diseases.* Physiol Rev, 2011. **91**(1): p. 221-64.

108. Huebener, P., et al., *CD44 is critically involved in infarct healing by regulating the inflammatory and fibrotic response.* J Immunol, 2008. **180**(4): p. 2625-33.

109. Teder, P., et al., *Resolution of lung inflammation by CD44.* Science, 2002. **296**(5565): p. 155-8.

110. Walker, P.A., et al., *Progenitor cells as remote "bioreactors": Neuroprotection via modulation of the systemic inflammatory response.* World J Stem Cells, 2011. **3**(2): p. 9-18.

111. Fischer, U.M., et al., *Pulmonary passage is a major obstacle for intravenous stem cell delivery: the pulmonary first-pass effect.* Stem Cells Dev, 2009. **18**(5): p. 683-92.

112. Schrepfer, S., et al., *Stem cell transplantation: the lung barrier.* Transplant Proc, 2007. **39**(2): p. 573-6.

113. Lee, R.H., et al., *Intravenous hMSCs improve myocardial infarction in mice because cells embolized in lung are activated to secrete the anti-inflammatory protein TSG-6.* Cell Stem Cell, 2009. **5**(1): p. 54-63.

114. Chua, J.Y., et al., *Intra-arterial injection of neural stem cells using a microneedle technique does not cause microembolic strokes.* J Cereb Blood Flow Metab, 2011. **31**(5): p. 1263-71.

115. Scheibe, F., et al., *Immune effects of Mesenchymal Stomal Cells in Experimental Stroke.* Submitted, 2011.

116. Hauben, E., et al., *Vaccination with dendritic cells pulsed with peptides of myelin basic protein promotes functional recovery from spinal cord injury.* J Neurosci, 2003. **23**(25): p. 8808-19.

117. Butovsky, O., et al., *Activation of microglia by aggregated beta-amyloid or lipopolysaccharide impairs MHC-II expression and renders them cytotoxic whereas IFN-gamma and IL-4 render them protective.* Mol Cell Neurosci, 2005. **29**(3): p. 381-93.

118. Moalem, G., et al., *Production of neurotrophins by activated T cells: implications for neuroprotective autoimmunity.* J Autoimmun, 2000. **15**(3): p. 331-45.

119. Kipnis, J., et al., *Neuroprotective autoimmunity: naturally occurring CD4+CD25+ regulatory T cells suppress the ability to withstand injury to the central nervous system.* Proc Natl Acad Sci U S A, 2002. **99**(24): p. 15620-5.

120. Vendrame, M., et al., *Cord blood rescues stroke-induced changes in splenocyte phenotype and function.* Exp Neurol, 2006. **199**(1): p. 191-200.

121. Ajmo, C.T., Jr., et al., *The spleen contributes to stroke-induced neurodegeneration.* J Neurosci Res, 2008. **86**(10): p. 2227-34.

122. Yu, X., et al., *Heparin-binding EGF-like growth factor increases intestinal microvascular blood flow in necrotizing enterocolitis.* Gastroenterology, 2009. **137**(1): p. 221-30.

123. Romeo, G., et al., *Activation of nuclear factor-kappaB induced by diabetes and high glucose regulates a proapoptotic program in retinal pericytes.* Diabetes, 2002. **51**(7): p. 2241-8.

124. Fernández-Klett, F., et al., *Early loss of pericytes and tissue scarring by perivascular stromal cells after stroke.* Submitted, 2012.

125. Kunz, J., et al., *The 140-kDa protein of blood-brain barrier-associated pericytes is identical to aminopeptidase N.* J Neurochem, 1994. **62**(6): p. 2375-86.

126. Goritz, C., et al., *A pericyte origin of spinal cord scar tissue.* Science, 2011. **333**(6039): p. 238-42.

127. Melgar, M.A., et al., *Postischemic reperfusion: ultrastructural blood-brain barrier and hemodynamic correlative changes in an awake model of transient forebrain ischemia.* Neurosurgery, 2005. **56**(3): p. 571-81.

128. Jones, S., et al., *The antiproliferative effect of mesenchymal stem cells is a fundamental property shared by all stromal cells.* J Immunol, 2007. **179**(5): p. 2824-31.

8 APPENDIX

8.1 List of figures

8.2 List of tables

8.3 Abbreviations

ANOVA	analysis of variance
AC	acetylcholine
AMPA	α-amino-3-hydroxy-5-methyl-4-isoxazolepropionic acid
ATP	adenosine triphosphate
BBB	blood brain barrier
BMDM	bone marrow derived macrophages
BrdU	5-bromo-2'-deoxyuridine
BSA	bovine serum albumin
CA	catecholamine
CC3	cleaved caspase 3
CCD	charge-coupled device
cDNA	complementary DNA
cfu	colony forming units
CNS	central nervous system
COX	cyclooxygenase
DAMPs	danger-associated molecular patterns

DAPI	4',6-diamidino-2-phenylindole
DEPC	diethylpyrocarbonate
DNA	deoxyribonucleic acid
EAE	experimental autoimmune encephalomyelitis
ECL	enhanced chemoluminescence substrate
EDTA	ethylenediaminetetraacetic acid
ELISA	enzyme-linked immunosorbent assay
EMSA	electrophoretic mobility shift assay
ES cells	embryonic stem cells
FACS	fluorescent activated cell sorting
FCS	fetal calf serum
g	gravity
Gapdh	Glyceraldehyde 3-phosphate dehydrogenase
GCs	glucocorticoids
GFAP	glial fibrillary acidic protein
GM-CSF	granulocyte macrophage-colony stimulating factor
GTP	guanosine-5'-triphosphate
HA	hyaluronan
HCl	hydrochloric acid
HLH	helix-loop-helix
HPA	hypothalamo-pituitary-adrenal
HRP	horseradish peroxidase
ICC	immunocytochemistry
ICA	internal carotid artery
ICAM	intercellular adhesion molecule
Ifnar	IFN type I receptor
IHC	immunohistochemistry
IKK	IκB kinase
IL	interleukin
INF	interferon
iNOS	inducible nitric oxide synthase
IκB	inhibitor of κB
kg	kilogram

l	liter
LB	lysogeny broth
LZ	leucine zipper
LPS	lipopolysaccharide
LysM	Lysozyme M
MACS	magnetic cell sorting
MCA	middle cerebral artery
MCAo	middle cerebral artery occlusion
MCP	macrophage chemoattractant protein
MIP	macrophage inflammatory protein
ml	milliliter
MMP	matrix metalloproteinases
MSCs	mesenchymal stromal cells
MTT	3-(4,5-dimethylthiazol-2-yl)-2,5-diphenyltetrazolium bromide
Myd88	myeloid differentiation primary response gene 88
NBD	NEMO-binding domain
NEMO	NF-κB essential modulator
NF-κB	nuclear factor κB
NDS	normal donkey serum
NGS	normal goat serum
NK	natural killer cells
NLS	nuclear localization sequence
NSAID	non-steroidal anti-inflammatory drug
NO	nitric oxide
PAMPs	pathogen-associated molecular patterns
PAGE	SDS-polyacrylamide gel electrophoresis
PBS	Dulbecco´s phosphate buffered saline
PCR	polymerase chain reaction
PFA	paraformaldehyde
PI3	phosphatidylinositol 3
PBMC	peripheral blood mononuclear cells
PNS	parasympathetic nervous system
PVDF	polyvinylidene fluorid

TAE	tris acetate
TBS	tris buffered saline
TBS-t	tris buffered saline-Tween
TCR	T cell receptor
TEMED	tetramethylethylenediamine
TGF	transforming growth factor
T_H1/2/17	T helper cells 1/2
TLR	toll-like receptors
TNF	tumor necrosis factor
TNFR	TNF receptor
TRAF	TNF-receptor associated factors
RHD	Rel homology domain
RIPA	radioimmunoprecipitation assay
RNA	ribonucleic acid
ROS	reactive oxygen species
Rpm	revolutions per minute
SD	standard deviation
SDS	sodium dodecyl sulphate
SNS	sympathetic nervous system
SR	super-repressor
VCAM	vascular cell adhesion molecule
µl	micro liter

8.4 Acknowledgements

I would like to thank my doctoral adviser Prof. Dr. Josef Priller for giving me the opportunity to do my PhD thesis in his lab, and for his advice and support.

A special thank goes to Dr. Helena Radbruch, Dr. Juliane Ladhoff, Dr. Jens-Uwe Peter and Dr. Maik Grohman for supervising and supporting me with my experiments and my thesis and for fruitful discussions on my PhD topic.

Beside the already mentioned postdocs I would like to thank Francisco Fernández-Klett, Peggy Mex, Christian Böttcher, Jasmin Jamal El-Din, Marco Foddis, Mihovil Mladinov, Simone Rolfes, Nadine Gladow, Melanie Lange and Susanne Müller for their experimental assistance.

Many thanks go to Grietje Tessmann and the lab of Prof. Kettenmann for sharing with me their knowledge about culturing primary microglia.

I thankfully acknowledge the DFG Research Training School 1258 “Neuroinflammation” for mentoring and financial support, and the International Graduate Program Medical Neuroscience.

I am very grateful to Dr. Chotima Böttcher, who accompanied me during my whole PhD time with experimental and theoretical advice, and for being a friend inside and outside of the lab.

I want to thank everybody from the Priller-lab for the pleasant working atmosphere.

I am thankfully appreciating the support of Dr. Dorette Freyer and the whole Experimental Neurology Department for technical advice and for many joyful moments.

Finally many thanks to Juan Morello and all my friends for their support, understanding and patience during my PhD time.

8.5 Curriculum Vitae

Mein Lebenslauf wird aus datenschutzrechtlichen Gründen in der elektronischen Version meiner Arbeit nicht veröffentlicht.

8.6 Publications and posters

Publications:

Scheibe F., Ladhoff J., Huck J., Grohmann M., **Blazej K.**, Oersal A., Seifert M. & Priller J.
Immune effects of mesenchymal stromal cells in experimental stroke
Submitted (2011)

Fernández-Klett F., Potas J., Hilpert D., **Blazej K.**, Radke J., Huck J., Stenzel W., Genové G., Priller J.
Early loss of pericytes and tissue scarring by perivascular stromal cells after stroke
Submitted (2012)

Radbruch H., **Blazej K.**, Peter J.-U., Bardua M., Ladhoff J., Fernández-Klett F., Infante-Duarte C., Prinz M., Priller J.
Mice with myeloid-specific deletion of the *Ikk2* gene are resistant to experimental autoimmune encephalomyelitis
In preparation

Posters:

Blazej K., Ladhoff J., Radbruch H., Gladow N., Fernández-Klett F., Priller J. (2010)
Characterization of the LysM-Cre Ikk2$^{fl/fl}$ mouse
Best poster at *Berlin Brain Days 2010,* Berlin (Germany)

Blazej K., Peter J.-U., Fernández-Klett F., Priller J. (2009)
Microglia- and macrophage-specific *Ikk2* knock-out reduces survival rate after experimental stroke in mice
Kyushu Brain Days 2009, Fukuoka (Japan)

Blazej K., Peter J.-U., Grohmann M., Priller J. (2008)
Inhibition of nuclear factor-κB signaling in microglia derived from LysM-Cre Ikk2$^{fl/fl}$ mice
Berlin Brain Days 2008, Berlin (Germany)

8.7 Selbständigkeitserklärung

Ich, Katja Blazej, erkläre, dass ich die vorgelegte Dissertation mit dem Thema:

"Role of inflammatory cells in cerebral ischemia"

selbst verfasst und keine anderen als die angegebenen Quellen und Hilfsmittel benutzt, ohne die (unzulässige) Hilfe Dritter verfasst und auch in Teilen keine Kopien anderer Arbeiten dargestellt habe.

Berlin, 22. Februar 2012 Katja Blazej